UCSF
UC San Francisco Electronic Theses and Dissertations

Title
Engineering Therapeutic Biomaterials for Medical Implants

Permalink
https://escholarship.org/uc/item/1xd1n7kn

Author
Cao, Yiqi

Publication Date
2019

Peer reviewed|Thesis/dissertation

eScholarship.org Powered by the California Digital Library
University of California

Engineering Therapeutic Biomaterials for Medical Implants

by

Yiqi Cao

DISSERTATION

Submitted in partial satisfaction of the requirements for degree of

DOCTOR OF PHILOSOPHY

in

Bioengineering

in the

GRADUATE DIVISION

of the

UNIVERSITY OF CALIFORNIA, SAN FRANCISCO
AND
UNIVERSITY OF CALIFORNIA, BERKELEY

Approved:

DocuSigned by:
Tejal Desai
5D917BC35F4B4A0...

Tejal Desai

Chair

DocuSigned by:
Phillip Messersmith
D2D5A6E4F4...

Phillip Messersmith

DocuSigned by:
Michael Conte
62F3CB5892124BF...

Michael Conte

Committee Members

Copyright 2019

by

Yiqi Cao

Dedication and Acknowledgments

This dissertation is made possible by the support of so many individuals, to whom I give my most sincere gratitude.

First and foremost, my deepest gratitude goes to my advisor, Prof. Tejal Desai, for training me to become an independent researcher, and for teaching me by example what it means to be a great leader. As a new graduate student, I was drawn to the Desai lab for the opportunity to work on translational research with therapeutic potential, and this was made possible by Prof. Desai's dedication to developing technologies that have clinical impact. Over the past few years, Prof. Desai has provided me with invaluable strategic advice, opportunities for scientific leadership, and also the freedom to pursue my ideas and interests. This enabled an incredibly multifaceted graduate education, in which I not only trained as a critical thinker and scientist, but also as a thoughtful communicator and leader. In the lab, Prof. Desai has skillfully fostered a collaborative and collegial environment, where I built meaningful collaborations and friendships while developing scientifically and professionally. I am eternally grateful for Prof. Desai's guidance as I chart a course for how to pursue my passion for developing technologies that improve human health.

I also thank my former teachers and mentors, without whom I would not have had this opportunity to earn my Ph.D. Thank you to Mr. Larry Hawkins, my high school AP Biology teacher, for introducing me to the wonders of biology—how nature has created intricate machinery that allow us to function and thrive. Thank you to Prof. Shayn Peirce-Cottler and Dr. Scott Seaman, who first guided me in the world of biomedical engineering research as an undergraduate student at the University of Virginia. I would not be here without your guidance and mentorship. Thank you to Dr. Matt Hall at the National Institutes of Health, whose

leadership during my summer internship instilled in me an excitement and confidence in research at a graduate level. And thank you to Prof. Dana Elzey, who taught me that engineers should solve problems, not just problem sets. This I will remember for the rest of my life.

Thank you to the professors on my qualifying exam and dissertation committees: Prof. Phil Messersmith, Prof. Michael Conte, Prof. Tamara Alliston and Prof. Zev Gartner. Your insights and feedback were instrumental to improving the quality of my qualifying exam proposal and dissertation research. Discussions with you all have challenged my thinking and helped me grow as a scientist.

I thank my coauthors and team mates: Dr. Jean Kim, Dr. Karen Samy, Dr. Daniel Bernards, Prof. Robert Bhisitkul, Dr. Nina Rosa Konichi da Silva, Audrey Phone. It has been an honor to work with each of you on the ocular drug delivery projects. Working with you all has shown me the incredible power of a good team.

To my current and former lab mates in the Desai Lab, thank you for creating a wonderful place for carrying out my graduate research. To Long and Jean: thank you for being my mentors throughout my years in graduate school. You showed me what it means to be mentors who make an indelible influence in the lives of others. Earning a Ph.D. has many ups and downs. I cannot understate the impact of your guidance, advice, reassurance, and encouragement throughout my journey. Will and Liz, I hope we continue to have “third year meetings” for years to come. Priya, thank you for always stepping up to the plate to help out in lab, and for all of your efforts to plan lab outings and checking off lists on the whiteboard to keep us sane and happy outside the lab. Cameron, thank you for helping me get my start in lab as my rotation mentor, and also for being our local boardgame guru. Thank you to Joel, for always being up for chatting about ideas and offering scientific and general life advice. To current and former lab managers at the Desai Lab,

Daniel Johengen, Gauree Chendkee, Initha Setiady: thank you for keeping the lab running smoothly, helping us track down reagents and orders, and making sure we have everything we need to succeed in lab.

To my fellow bioengineering students in the program, Katie Cabral and Kayla Wolf. Thank you for always being enthusiastic about sharing your scientific expertise in vascular biology and mechanobiology. Your advice, suggestions, and insights over the past several years have been invaluable.

Thank you to Katherine Krebs for tirelessly scheduling meetings with Tejal when we needed it, to Hilary Smith-Mahon for years of seamless paperwork, and to SarahJane Taylor and Kristin Olson for all of your support of the BioE program.

I give thanks to the NSF Graduate Research Fellowship and the Alfred Mann Institute for funding and for allowing me to maintain my focus on research productivity.

Of course, none of this would be possible without my parents, Dianjun Cao and Yanliu Kong, who taught me from an early age the value of a hard work, perseverance, and creativity. Thank you for giving me the freedom to explore and for always supporting me.

And thank you, Matt, for making me believe that I can do anything I set my mind to. Your love and support mean the world to me.

Contributions

Elements of this dissertation have been published elsewhere or are in submission or preparation for publication in a peer-reviewed journal.

Chapter 1 is adapted from "TiO_2 nanotube arrays as smart platforms for biomedical applications," a textbook chapter published in Smart Nanoparticles for Biomedicine (1st Edition), and authored by Giada Graziana Genchi, Yiqi Cao, and Tejal A. Desai. Chapter 2 is adapted from "TiO_2-based nanotopographical cues attenuate the restenotic phenotype in primary human vascular endothelial and smooth muscle cells," a research article submitted for publication and authored by Yiqi Cao and Tejal A. Desai. Chapter 3 is adapted from "Recent advances in intraocular sustained-release drug delivery devices," a review article published in Drug Delivery Today in 2018 and authored by Yiqi Cao, Karen Samy, Daniel Bernards, and Tejal Desai. Chapter x is adapted from "Co-delivery of Timolol and Brimonidine with a Polymer Thin-film Intraocular Device," a research article published in Journal of Ocular Pharmacology and Therapeutics in 2019 and authored by Karen E. Samy*, Yiqi Cao*, Jean Kim*, Nina Rosa Konichi da Silva, Audrey Phone, Michele M. Bloomer, Robert B. Bhisitkul, Tejal A. Desai (*Equal Contribution).

Abstract

Engineering Therapeutic Biomaterials for Medical Implants

Yiqi Cao

Understanding material-host interactions is critical to designing and characterizing biomaterials for use in medical implants. From joint replacements, to pacemakers, to artificial hearts, all surfaces that contact the body require thorough characterization and optimization to elicit an appropriate response in the body. This dissertation discusses the applications of biomaterials for two distinct clinical needs: ocular drug delivery, and vascular stenting.

The first half of this dissertation discusses the surface engineering of titanium implants by fabricating TiO_2 nanotube coatings. First, Chapter 1 provides an overview of the uses of TiO2 nanotubes for applications in tissue engineering, smart drug release platforms, and biosensing. Then, Chapter 2 is a mechanistic study of titania nanotube topography as a surface coating for vascular stents. In this study, we investigated how nanotopographical cues on the stent surface can modulate vascular phenotype, with the goal of developing an alternative strategy to drug-eluting stents (DES) for decreasing restenosis. We demonstrated that nanotube topography can decrease SMC surface coverage without affecting endothelialization. In addition, to our knowledge, this is the first study reporting that TiO_2 nanotube topography dampens the response to inflammatory cytokine stimulation in endothelial and smooth muscle cells.

The second part of this work addresses the clinical need for long-acting intraocular drug delivery implants. Chapter 3 is a survey of recent advances in long-acting, sustained-release intraocular implants, highlighting the recent developments spanning the pre-clinical, clinical, and post-FDA approval stages. Then, Chapter 4 is a report of the design, characterization, and *in vivo* validation of a drug delivery implant for the treatment of glaucoma. Eye drop administration is

the current gold standard, but patient noncompliance is an obstacle to efficacious treatment. We designed a polymeric implant to co-deliver two hypotensive agents, achieving independently controlled zero-order release of timolol maleate and brimonidine tartrate. We also demonstrated IOP-lowering effects of the implant for three months *in vivo*. Taken together, these projects seek to contribute to the continued expansion and development of the biomaterials field and its applications in medicine.

Table of Contents

List of Figures

List of Tables

TiO2 nanotube arrays as smart platforms for biomedical applications

1.1 Abstract

TiO_2 nanotube arrays (NTAs) have met increasing interest in the scientific community due to their extraordinary properties, including responsivity to UV light and biocompatibility. These properties have motivated their application in many fields ranging from energy to environmental remediation and regenerative medicine. This chapter briefly reports on their most recent biomedical applications by citing significant examples of works that exploit TiO_2 NTAs, alone or in association with other nanomaterials, for remote control through many physical sources. In particular, the focus is on TiO_2 NTAs as active devices for interaction with biological environments in tissue engineering, drug delivery and biosensing.

1.2 Introduction

Titanium is a material extensively used for many biomedical applications due to its corrosion resistance, light weight, and biocompatibility. Recent advances in nanotechnology have offered significant opportunities to tune surface features by development of several kinds of nanostructures, most notably TiO_2 nanotubes.

Over the last two decades, many straightforward and inexpensive fabrication methods have been developed, including hydrothermal and electrochemical synthesis [1, 2, 3]. By simple variations of fabrication parameters such as electrolyte composition, reaction temperature and anodization voltage, these methods enable the formation of TiO_2 nanotube arrays (TiO_2 NTAs) with different characteristics such as length, diameter, density, wall thickness *etc.* Nanotube surface morphology can be easily improved, for instance, by ultrasonication procedures at the end

of the fabrication process, or even by sequential anodizations [4, 5]. Typical products of electrochemical anodization are amorphous nanotubes, which can be later converted into crystalline materials by thermal treatment, with improvement in nanotube purity [6]. Annealing temperature and nanotube diameter are critical in obtaining anatase TiO_2 (300-500°C), rutile TiO_2 (above 500°C), or combinations thereof, all characterized by different conductivity properties (in the 10^{-1} Ω cm range for anatase, and 10^2 Ω cm for rutile). Moreover, if amorphous nanotubes exhibit a band gap of ~3.3 eV, anatase ones have a band gap of 3.2, whereas rutile nanotubes have an even narrower band gap of 3.0 eV. These crucial properties are at the base for the application of TiO_2 NTAs as smart materials for many biomedical applications. In these semiconductors sensitive to UV light, electrons promoted from the valence band to the conduction band can reach the material interface, where they react with environmental redox species [1]. Generation of highly reactive species occurs and results in oxidation of biomolecules, with important microbial control effects [7].

In this chapter, studies on the application of TiO_2 NTAs to tissue engineering, drug delivery and biosensing are presented. When possible, focus will be on the "smart" properties of these materials, and thus on the tunability of their effects on biological environments through remote control. The auspice is to stimulate the discussion on these fascinating materials in the scientific community, and to open novel pathways for challenging biomedical applications of TiO_2 NTAs.

1.3 Tissue engineering based on TiO_2 nanotube arrays

Nanostructured materials are increasingly used in biomedical research in order to modulate biological responses and eventually direct cellular behavior towards a desired phenotype [3, 8, 9]. The ultimate goal is often the faster recovery of structural and functional integrity in tissues compromised by degenerative conditions of disparate etiology, including trauma. Interest in TiO_2

NTAs for affecting cell response and influencing cell fate is largely due to the possibility to tune their geometry and composition by straightforward adjustments of fabrication parameters. Among these, anodization voltage can for instance be easily changed to produce arrays of nanotubes with strikingly different diameters, wall thicknesses and lengths.

Over the latest two decades, several *in vitro* studies have focused on the interaction of TiO_2 NTAs with different kinds of cells, such as chondrocytes [10], endothelial cells [11, 12], smooth muscle cells [11], macrophages [13], mesenchymal stem cells [8, 14, 15, 16], neural progenitors [17], osteoblasts [18], periodontal ligament stem cells [19], platelets and leucocytes [20]. Most studies have investigated the biological effects of nanotube diameter, often in association with nanotube chemistry (by doping during fabrication/annealing, or by modification with wet chemistry and plasmochemical routes). Only recently, there have been studies that exploit TiO_2 NTAs as active devices for delivering physical stimulation to cells and tissues. In the following, a few significant examples of both approaches will be discussed, implying future perspectives for these versatile nanomaterials.

Relevant studies on the potential of TiO_2 NTAs to influence cell behavior have been conducted since 2007 [8, 10, 14, 15, 18, 21]. These works have demonstrated the critical role of urface topography in influencing events like adhesion, apoptosis, proliferation and even differentiation, and have suggested how the surface chemistry may synergistically rather than additively work to affect specific biological responses.

For instance, Tejal Desai's group investigated the effects of long-term interaction of arrays of 80 nm diameter nanotubes with rat mesenchymal stem cell (MSCs), finding enhanced alkaline phosphatase activity and calcium content in the cultures. No adverse immune response was detected after subcutaneous implantation of TiO_2 NTAs in a healthy murine model [15].

Furthermore, TiO_2 NTAs were demonstrated to be substrates suitable for decreased adhesion of *Staphylococcus epidermidis* and for MC3T3-E1 pre-osteoblast differentiation after nanotubes were loaded with gentamycin [21]. In another study, arrays of TiO_2 nanotubes with 30 nm diameter were found to be improving bovine aortic endothelial cell (EC) proliferation, while maintaining mouse aortic smooth muscle cell in their differentiated status. Also, ECs secreted more prostaglandin I2 on TiO_2 NTAs compared to flat titanium surfaces, thus demonstrating suitability of the array for coating of vascular stents [11]. Based on these findings, whole genome analysis was performed on the cultures, and confirmed again this divergent behavior of ECs and SMCs with respect to proliferation and migration [22]. Further, the study demonstrated that TiO_2 NTAs led to downregulation of genes involved in inflammation and coagulation, processes related to restenosis and thrombosis in both cell types.

A study from Park and coworkers provides a good example of investigation of the biological effects of array topography and chemistry. In this study, arrays of TiO_2 nanotubes with 15 nm and 100 nm diameter were used for MSC culture either in the presence or in the absence of bone morphogenetic protein-2 (BMP-2), a growth factor stimulating both chondro- and osteogenic differentiation [10]. Chondrogenic differentiation of MSCs was enhanced by BMP-2 coated nanotubes of 100 nm in diameter, but not on coated 15 nm diameter nanotubes, where spreading and de-differentiation occurred. Conversely, osteogenic differentiation was promoted by BMP-2 coated 15 nm diameter nanotubes, but not by 100 nm diameter nanotubes. Coating with BMP-2 was also effective at preventing apoptosis found on 100 nm diameter nanotubes. The observed differences in MSC behavior on arrays of TiO_2 nanotubes with different diameter were ascribed to integrin clustering.

TiO_2 NTAs-coated devices also interact with soft tissues. In a pilot investigation, TiO_2 NTAs were tested with C2C12 myoblasts, aiming at skeletal muscle tissue engineering and stimulation [6]. Arrays with increasing nanotube diameters were fabricated and annealed to anatase; then, they were either coated with laminin or not, and used for supporting both cell proliferation and differentiation. The synergic effect of surface topography and chemistry was demonstrated, pointing to laminin-coated arrays with 10 nm diameter nanotubes as the most beneficial substrates for myoblast adhesion and differentiation.

In another study, plain arrays of TiO_2 nanotubes with 100 nm diameter were tested for implantation in rat abdominal wall, where they significantly reduced fibrotic capsule formation and exerted a more pronounced nitric oxide scavenging activity in comparison to planar titanium surfaces [23]. Recent studies conducted on vascular titanium stents coated with 100 nm diameter TiO_2 nanotubes confirmed that the coating improved long term stent integration in the iliofemoral artery of a rabbit model by decreasing neointima formation and accelerating recovery of functional endothelium. This resulted in a 30% lower in-stent restenosis compared to controls, and promises application of TiO_2 NTAs in drug-free vasculature prosthetics [24].

A very recent study from Park and coworkers proposes the use of 15 nm diameter TiO_2 NTAs for promoting osteodifferentiation of MSCs by electric field (EF) stimulation, in the absence of pro-differentiative soluble factors [25]. In this study, a low voltage was applied to the arrays, which served as anodal electrodes during long-term electric field stimulation. EF application increased Ca^{2+} levels and connexin 43 (Cx43) localization at the plasma membrane protrusions. It also determined intercellular spreading of Ca^{2+} fluxes through gap junctions, that resulted in downstream signaling activation (including calcineurin/CAMKII phosphorylation and NFAT dephosphorylation). Overexpression of osteogenic differentiation markers like osteocalcin and

osterix was found at a transcriptional and translational level, as well as enhanced mineralization upon EF application to TiO_2 NTAs. The latter were therefore found suitable to electric field application for osteodifferentiation induction.

As suggested by the studies presented above, the role of TiO_2 nanotube diameter in arrays for tissue engineering is well recognized and to date is still the focus of intense debate. This field is growing in breadth due to innovative methods for enriching array properties during synthesis by doping, or at fabrication endpoint by surface modification with other nanoparticles and functional groups of biological relevance [3, 26]. Investigations on array features such as crystallinity and related conductivity may provide further advances in tissue engineering applications of TiO_2 NTAs in the near future, eventually turning them from passive vehicles of bioinstructive cues to intrinsically active and multifunctional interfaces (microbial control, electrical stimulation, *etc.*) for dynamic, tunable interaction with biological environments.

1.4 Drug delivery from TiO_2 nanotube arrays

Drug-releasing implants represent a promising strategy for achieving therapeutic concentrations of drugs to a target site with minimal or no systemic effects. Titanium is a material of common use for implants, due to its biocompatibility and mechanical stability, and provides a resistant platform for shape and surface modifications. Indeed, titanium medical devices can be surface-coated with vertically aligned nanotube arrays for drug loading and release, including bone screws [27], titanium stents [24], and wires [28, 29]. The main advantages provided by TiO_2 nanotube arrays (NTAs) are their simple and inexpensive fabrication procedures (for instance, through electrochemistry), and their tunable features (length, diameter, conductivity, *etc.*) [1, 29, 30, 31, 32]. These properties have motivated many orthopedics, dental, and vascular surgery

applications [11, 25, 33, 34]. In the following section, relevant properties of TiO_2 NTAs will be briefly recalled and examples of studies exploiting the extraordinary properties of these materials as smart platforms for drug delivery purposes will be reported.

The kinetics of drug release from plain TiO_2 nanotubes is based on desorption and diffusion. Drug release depends on factors including nanotube surface chemistry, surface area and pore size, along with molecule size, charge, drug solubility, and diffusion coefficient. The Desai group fabricated nanotubes with varying heights and diameters to explore the release rates of model proteins (albumin and lysozyme) and antibiotics (sirolimus and paclitaxel) [34, 35], changing from burst release, where the majority of drug is eluted in a few hours, to prolonged release over a week. To achieve prolonged release profiles, recent studies proposed biodegradable films for nanotube capping [36, 37], and polymeric micelles for drug encapsulation [38]. Other studies focused on the photocatalytic properties of the nanotubes for drug release modulation, aiming at turning TiO_2 NTAs into active "smart" devices. Indeed, TiO_2 nanotubes are semiconductors with photocatalytic properties so they are able to induce redox reactions when irradiated by light of suitable wavelength [39]. This peculiar characteristic of TiO_2 NTAs has also been exploited in association with properties of other nanomaterials, thus making drug delivery devices based on TiO_2 NTAs responsive to many external stimuli, including magnetic fields, radiofrequencies and ultrasounds.

Among the first studies on light-induced drug release from TiO_2 NTAs, there is that one from Song and coworkers. TiO_2 NTAs were coated with (3-aminopropyl)triethoxysilane, APTES, a siloxane linker, then loaded with horseradish peroxidase, a model drug, and with octadecylphosphonic acid (ODPA) for nanotube capping. Amphiphilic drug release platforms were obtained by two sequential anodizations [4]. Upon UV-light irradiation, the ODPA cap underwent UV-induced chain scission, which exposed the loaded drug and allowed its diffusion

into the aqueous environment. The APTES linker also underwent UV-induced chain scission, thus contributing to controlled drug release after irradiation. In another study, a fluorescent molecule was used as a model drug, and was attached to TiO_2 nanotubes using a siloxane cross-linker. Upon illumination by UV light, hole generation in the valance band of the titanium oxide led to chain scission of the siloxane linker, triggering drug release from the nanotubes. This platform was also compatible with magnetic nanoparticle filling, so that the location of the implant could be controlled by application of a static magnetic field [40].

To overcome limitations inherent to UV light irradiation, including payload degradation or poor tissue penetration *in vivo*, hybrid drug delivery systems based on TiO_2 NTAs were developed to allow drug release upon exposure to visible or infrared light. An interesting example of drug release induced by visible light is represented by a study on a dual device, where the first nanotube layer was used for capping and the second one for antibacterial drug loading through silane. The first layer was decorated with gold nanoparticles (Au NPs), and it was then coated with a hydrophobic cap. By visible light irradiation, gold surface plasmon resonance occurred that photocatalytically induced chain scission of the cap. This resulted in silane degradation along with sustained ampicillin release. Antibacterial effect of the device was also demonstrated on *Escherichia coli* cultures [41].

On-demand drug release systems using TiO_2 NTAs have also been demonstrated with near infrared light, which has the additional advantage of higher tissue penetration (1-2 cm under the skin). In order to make devices responsive to infrared light, gold nanorods (GNRs) were grafted onto TiO_2 nanotubes *via* thiolactic acid treatment by Moon and coworkers [42]. Tetracycline, an antibiotic, was then loaded into TiO_2 nanotubes. GNRs exhibited photothermal effects upon IR-irradiation, leading to a local heating effect that increased drug diffusion. The photothermal effect

was shown to increase the release of tetracycline from the arrays, which exerted antibacterial effects on *Streptococcus mutans* cultures.

The association of TiO_2 NTAs with gold nanomaterials also enables drug release upon local heating induction by radiofrequency. In a study from Bariana and coworkers, nanotubes anodized on the surfaces of a titanium wire were loaded with AuNPs, and coated by tocopheryl-poly(ethylene glycol)-succinate micelles for release of indomethacin, an anti-inflammatory drug [43]. Radiofrequency (RF) stimulation of different durations modulated payload release after immersion in saline solution. A release of 80-100% of the drug was obtained by a short-term RF stimulation at 20W for 5 min, achieving a dosage of 100-250 μg (much higher that that allowed by oral administration). This study shows promise for enabling non-invasive, on-demand release of high drug dosages.

TiO_2 NTAs provide an excellent platform for remote controlled drug delivery also through magnetic field upon combination with magnetic nanoparticles. In a study from Aw and coworkers, magnetic iron oxide nanoparticles coated with dopamine were loaded into titanium nanotubes, followed by indomethacin-loaded micelles [44]. Without magnetic stimulation, drug release exhibited near zero-order kinetics, as expected from drug release out of micelles. When a magnetic field was applied, the magnetic particles were dragged out of the tubes, allowing 100% drug release within 1-1.5 h.

In another study from Aw and coworkers, TiO_2 nanotubes were again loaded with drug-encapsulated polymeric micelles, but drug release was triggered with the aid of ultrasounds (US) [45]. Different US parameters (including pulse length, time, amplitude, and power intensity) were finely explored to trigger the release of micelles from the nanotubes. Optimal stimulation led to

100% drug release within 5-50 min from US application, very likely due to processes including cavitation and temperature increase that deserve further studies.

TiO_2 nanotube arrays are promising surface coatings for drug-eluting implants. These nanostructures can be obtained on existing titanium implants through a simple and inexpensive process. TiO_2 nanotubes can serve as reservoirs for small molecule and protein therapeutics, as well as drug-encapsulating micelles, for achieving desired rates of drug release. Thanks to the inherent smart properties of TiO_2 nanotube arrays themselves or arising upon interaction with other nanomaterials, these devices demonstrate on-demand drug release in response to an external trigger, such as light, radiofrequency, magnetic field, and ultrasounds. While many of these platforms still require further *in vivo* validation, they are promising for local, controlled drug delivery in many applications ranging from orthopedics to cancer treatment.

1.5 Biosensing mediated by TiO_2 nanotube arrays

Titanium dioxide nanotube arrays (TiO_2 NTAs) represent excellent substrates for the quantification of several typologies of biomolecules, by working as probe-free analytical devices, or as immobilization platforms of biorecognition elements. In most applications, they mediate the detection of events involving antibodies [46, 47], antioxidants [48, 49], metabolites [51, 52, 53, 54, 55, 56, 57], neurotransmitters [58], peptides/proteins (regulatory [59, 60], or not [61]), and even xenobiotics [62]. The extraordinary physical properties of TiO_2 NAs can be exploited *per se* [46], or they can be improved by association to low-cost metal nanoparticles, such as Cu_2O [55], or to noble metal nanoparticles, such as Ag [63], Au [49, 53, 54, 56, 61, 64], Pt [57] and combinations thereof [52]. Over the last two decades, TiO_2 NAs have been used for quantification of analytes mainly through amperometric methodologies [48, 51, 52, 54, 63] and by taking advantage of their intrinsic photocatalytic properties [56, 57, 58, 60, 61, 62, 63]. Other techniques

have also been used, including immunochemistry [47, 53], interferometry [46], and spectroscopy [56, 57, 60], providing increasing evidences of the high versatility of TiO_2 nanotube arrays even in biosensing applications.

The main reasons for the continued interest in TiO_2 NTAs lie in their simple and inexpensive fabrication procedures, in their photocatalytic properties (exhibited over a wide active surface), their facile tunability by doping/surface decoration (see for instance [63]), and in their high biocompatibility, that enables the full retention of the biological activity of biorecognition elements also after immobilization. Indeed, chemical reactions can occur at the nanoscale on the nanotube surface and even within nanotube channels, deeply affecting biosensing outcomes. Moreover, TiO_2 NTAs are semiconductors where electrons can be promoted from the valence band to the conduction band by light (typically UV) of energy higher than the band-gap (3 eV for rutile and 3.2 eV for anatase), thus generating holes in the valence band. Electrons and holes can react with environmental acceptor and donor species, thus allowing analyte quantification upon photocurrent determination. Arrays of TiO_2 nanotubes possess high electron conduction properties that can be enhanced when an external electric field is applied. The latter can promote deposition of metal nanoparticles on the array surface, resulting in efficient electron transfer due to improved charge separation. TiO_2 NTAs provide electron percolation pathways, show large capacitance in solution, and have defined, controllable reflectance spectra [1, 2].

Biosensors based on the simple electron conductivity of TiO_2 nanotube arrays have been proposed for the quantification of glucose [51, 54, 55], hydrogen peroxide [50, 52, 53, 55], ascorbic acid [48], glutathione [49] and immunoglobulin G [46]. Of the cited examples of TiO_2 NTA-based devices, only biosensors that were reported to have very high performances in terms of detection limit, sensitivity, response time and analytic range will be concisely presented in the following.

Among the studies on photoelectrochemical biosensors, there is that one performed by An and coworkers on α-synuclein [61]. In this study, TiO_2 NTAs were obtained by electrochemistry, photoelectrochemically decorated by Au nanoparticles (Au NPs) and then with primary antibodies against α-synuclein. Complexes of Au NPs with secondary antibodies and with glucose oxidase were also immobilized on the surface for signal amplification. In the presence of glucose, the enzyme produced hydrogen peroxide, which acted as a sacrificial electron donor for scavenging of UV light-generated holes in the valence band of the arrays, thus improving charge separation. Higher photocurrents were obtained when the arrays were decorated by Au NPs on both sides. The obtained immunosensor exhibited linear response in the 50 pg/ml - 100 μg/ml analyte range, and a detection limit of 34 pg/ml, denoting high sensitivity.

Biosensors that are molecularly imprinted with the analyte can provide enhanced sensitivity and photocurrents due to improved electron transfer. In a study from Wang and coworkers, this was shown for the quantification of a pesticide, chlorphyrifos [62]. In this study, TiO_2 NTAs were electrochemically obtained and decorated with Au NPs, and then coated with poly (O-phenylenediamine) (PoPD) and chlorpyrifos as template molecule. Typically, TiO_2 nanotube arrays do not show photocurrent unless exposed to UV light, whereas molecularly imprinted PoPD/Au nanoparticle-coated TiO_2 NTAs demonstrate photocurrent generation in the visible light range of 400-540 nm. Indeed, PoPD generates photoelectrons under visible light and supports HOMO to LUMO electron transitions, whereas Au NPs increase the rate of electron injection into the conduction band of TiO_2 nanotubes, thus contributing to the overall photocurrents. The resulting biosensor had a fast response time (10 s) and a linear behavior in the 0.05-10 μmol/l range, with a detection limit of 0.96 nmol/l.

In another study from Xin and coworkers, adsorption of dopamine on TiO_2 NTAs enabled the achievement of highly sensitive and selective biosensors and the neurotransmitter detection in mouse brain [58]. Dopamine supported spatial separation of photogenerated charges, with holes localizing on dopamine, and electrons on TiO_2 NTs. By drastically reducing charge recombination, the obtained biosensor demonstrated increased photocurrent and even self-cleaning behavior under solar light. It showed a linear response in the 0.001-25 μM dopamine range, with detection limit of 0.15 nM and a sensitivity of 1.343 $\mu A/cm^2$ μM. The biosensor also enabled detection of dopamine in mouse brain while demonstrating low sensitivity to a number of catechol derivatives. No interference occurred from ascorbic acid, uric acid, glucose, cysteine and glutathione.

Other interesting studies on the exploitation of the smart properties of TiO_2 NTAs will not be discussed in detail here for the sake of conciseness, but interested readers are encouraged to refer to works on acethylthiocholine [63], cystatin C [60], lactate [56], and rhodamine G or glucose [57]. The aforementioned examples demonstrate the great potential of both plain TiO_2 nanotube arrays and hybrid platforms based on TiO_2 NTAs in detecting very different types of analytes with high sensitivity and selectivity, thanks to the analyte molecular imprinting and to the mediation of biorecognition elements. However, for these devices to be provided to the patients in the future, more studies on analyte detection in complex matrices are necessary, as well as investigations on multianalyte detection.

1.6 Conclusions

TiO_2 nanotube arrays have proven to be highly versatile platforms for addressing/exploring biological responses in many *in vitro* contexts (biosensors included), and have also shown great potential in the fields of tissue engineering and drug delivery. To date, studies on complex

biological environments (such as whole organisms) are scarce yet highly desirable in order to make these devices available to the end point-of-care. In particular, future studies should take advantage of the large body of scientific evidences on the topic, and focus on the long-term stability and storage of these materials, as well as their long-term interaction with biological entities. Most importantly, further protocols for remote control of platforms based on TiO_2 NTAs (alone or in association with other nanomaterials) should be conducted in order to fully exploit their active properties for tissue shaping/stimulation, controlled release of therapeutic doses of pharmaceutical cargoes and quantification of chemical species, either alone or in combination. This will allow for the development of smart multifunctional biomedical devices that can ultimately improve diagnostics and therapeutics.

1.7 References

[1] P. Roy, S. Berger, P. Schmuki, TiO_2 Nanotubes: Synthesis and applications, Angew. Chemie Int. Ed.. 50 (2011) 2904–2939.

[2] I. Paramasivam, H. Jha, N. Liu, P. Schmuki, A review of photocatalysis using self-organized TiO_2 nanotubes and other ordered oxide nanostructures, Small 8 (2012) 3073–3103.

[3] M Kulkarni, A Mazare, E Gongadze, Š. Perutkova, V. Kralj-Iglič, I. Milošev, P. Schmuki, A. Iglič, M. Mozetič, Titanium nanostructures for biomedical applications, Nanotechnology 26 (2015) 062002.

[4] Y.Y. Song, F. Schmidt-Stein, S. Bauer, P. Schmuki, Amphiphilic TiO_2 nanotube arrays: An actively controllable drug delivery system, J. Am. Chem. Soc 131 (2009) 4230–4232.

[5] J. Xu, X. Zhou, Z. Gao, Y.-Y. Song, P. Schmuki, Visible-light-triggered drug release from TiO_2 nanotube arrays: A controllable antibacterial platform, Angew. Chemie Int. Ed. 55 (2016) 593–597.

[6] G.G. Genchi, H. Nuhn, I. Liakos, A. Marino, S. Marras, A. Athanassiou, V. Mattoli, T.A. Desai, Titanium dioxide nanotube arrays coated with laminin enhance C2C12 skeletal myoblast adhesion and differentiation, RSC Adv. 6 (2016) 18502–18514.

[7] R. Yin, T. Agrawal, U. Khan, G.K Gupta, V. Rai, Y.-Y. Huang, M.R Hamblin, Antimicrobial photodynamic inactivation in nanomedicine: small light strides against bad bugs, Nanomedicine (Lond.) 10 (2015) 2379–2404.

[8] J. Park, S. Bauer, K. von der Mark, P. Schmuki, Nanosize and vitality: TiO_2 nanotube diameter directs cell fate, Nano Lett. 7 (2007) 1686−1691.

[9] P.P. Lee, A. Cerchiari, T.A. Desai, Nitinol-based nanotubular coatings for the modulation of human vascular cell function, Nano Lett. 14 (2014) 5021−5028.

[10] J. Park, S. Bauer, A. Pittrof, M.S. Killian, P. Schmuki, K. von der Mark, Synergistic control of mesenchymal stem cell differentiation by nanoscale surface geometry and immobilized growth factors on TiO_2 nanotubes, Small 8 (2012) 98–107.

[11] L. Peng, M. L. Eltgroth, T. J. LaTempa, C. A. Grimes, T. A. Desai, The effect of TiO_2 nanotubes on endothelial function and smooth muscle proliferation, Biomaterials 30 (2009) 1268–1272.

[12] A. Flašker, M. Kulkarni, K. Mrak-Poljšak, I. Junkar, S. Čučnik, P. Žigon, A. Mazare, P. Schmuki, A. Iglič, S. Sodin-Semrl, Binding of human coronary artery endothelial cells to plasma-treated titanium dioxide nanotubes of different diameters, J. Biomed. Mater. Res. Part A 104A (2016) 1113–1120.

[13] P. Neacsu, A. Mazare, P. Schmuki, A. Cimpean, Attenuation of the macrophage inflammatory activity by TiO_2 nanotubes *via* inhibition of MAPK and NF-κB pathways, Int. J. Nanomedicine 10 (2015) 6455–6467.

[14] J. Park, S. Bauer, P. Schmuki, K. von der Mark, Narrow window in nanoscale dependent activation of endothelial cell growth and differentiation on TiO_2 nanotube surfaces, Nano Lett. 9 (2009) 3157-3164.

[15] K.C. Popat, L. Leoni, C.A. Grimes, T.A. Desai, Influence of engineered titania nanotubular surfaces on bone cells, Biomaterials 28 (2007) 3188–3197.

[16] D. Kim, B. Choi, J. Song, S. Kim, S. Oh, E.H. Jin, S.S. Kang, E.J. Jin, TiO_2 nanotube stimulate chondrogenic differentiation of limb mesenchymal cells by modulating focal activity, Exp. Mol. Med. 43 (2011) 455–461.

[17] J.A. Sorkin, S. Hughes, P. Soares, K.C. Popat, Titania nanotube arrays as interfaces for neural prostheses, Mater. Sci. Eng. C 49 (2015) 735–745.

[18] J. Park, S. Bauer, K.A. Schlegel, F.W. Neukam, K. von der Mark, P. Schmuki "TiO_2 nanotube surfaces: An optimal length scale of surface topography for cell adhesion and differentiation, Small 5 (2009) 666–671.

[19] H. Gao, B. Li, L. Zhao, Y Jin, Influence of nanotopography on periodontal ligament stem cell functions and cell sheet based periodontal regeneration, Int. J. Nanomedicine 10 (2015) 4009–4027.

[20] K. Bartlet, S. Movafaghi, A. Kota, K.C. Popat Superhemophobic titania nanotube array surfaces for blood contacting medical devices, RSC Adv. 7 (2017) 35466–35476.

[21] K.C. Popat, M. Eltgroth, T.J. Latempa, C. Grimes, T.A. Desai, Decreased Staphylococcus epidermis adhesion and increased osteoblast functionality on antibiotic-loaded titania nanotubes, Biomaterials 28 (2007) 4880–4888.

[22] L. Peng, A.J. Barczak, R.A. Barbeau, Y. Xiao, T.J. LaTempa, C.A. Grimes, T.A. Desai, Whole genome expression analysis reveals differential effects of TiO_2 nanotubes on vascular cells, Nano Lett. 10 (2010) 143–148.

[23] G.C. Smith, L. Chamberlain, L. Faxius, G.W. Johnston, S. Jin, L.M. Bjursten, Soft tissue response to titanium dioxide nanotube modified implants, Acta Biomater. 7 (2011) 3209–3215.

[24] H. Nuhn, C. E. Blanco, T.A. Desai, Nanoengineered stent surface to reduce in-stent restenosis *in vivo*, ACS Appl. Mater. Interfaces 9 (2017) 19677–19686.

[25] J. Park, A. Mazare, H. Schneider, K. von der Mark, M.J.M. Fischer, P. Schmuki, Electric field-induced osteogenic differentiation on TiO_2 Nanotubular Layer, Tissue Eng. C 22 (2016) 809−821.

[26] M. Li, Q. Liu, Z. Jia, X. Xu, Y. Shi, Y. Cheng, Y. Zheng, Polydopamine-induced

nanocomposite Ag/CaP coatings on the surface of titania nanotubes for antibacterial and osteointegration functions, J. Mater. Chem. B 3(2015) 8796−8805.

[27] C. Sukotjo, C. R. Friedrich, T. Shokuhfar, M. Kolati, T. Moser, Survivability of TiO_2 nanotubes on the surface of bone screws, Surf. Innov. 2 (2013) 1–22.

[28] K.Gulati, S. Maher, D.M. Findlay, D. Losic, Titania nanotubes for orchestrating osteogenesis at the bone–implant interface, Nanomedicine 11 (2016) 1847–1860.

[29] C.A. Grimes, Synthesis and application of highly ordered arrays of TiO_2 nanotubes, J. Mater. Chem. 17 (2007) 1451–1457

[30] J.M. Macak, H. Hildebrand, U. Marten-Jahns, P. Schmuki, Mechanistic aspects and growth of large diameter self-organized TiO_2 nanotubes, J. Electroanal. Chem. 621 (2008) 254–266.

[31] K. Gulati, S. Maher, S. Chandrasekaran, D.M. Findlay, D. Losic, Conversion of titania (TiO_2) into conductive titanium (Ti) nanotube arrays for combined drug-delivery and electrical stimulation therapy, J. Mater. Chem. B 14 (2015) 371–375.

[32] K. Gulati, M. Kogawa, M. Prideaux, D. M. Findlay, G. J. Atkins, D. Losic, Drug-releasing nano-engineered titanium implants: therapeutic efficacy in 3D cell culture model, controlled release and stability, Mater. Sci. Eng. C 69 (2016) 831–840.

[33] L.M. Bjursten, L. Rasmusson, S. Oh, G. C. Smith, K. S. Brammer, S. Jin, Titanium dioxide nanotubes enhance bone bonding *in vivo*, J. Biomed. Mater. Res. Part A 92 (2010) 1218–1224.

[34] K.C. Popat, M. Eltgroth, T.J. LaTempa, C.A. Grimes, T.A. Desai, Titania Nanotubes: a novel platform for drug-eluting coatings for medical implants? Small 3 (2007) 1878–1881.

[35] L. Peng, A.D. Mendelsohn, T.J. LaTempa, S. Yoriya, C.A. Grimes, T.A. Desai, Long-term

small molecule and protein elution from TiO_2 nanotubes, Nano Lett. 9 (2009) 1932–1936.

[36] T. Kumeria, H. Mon, M.S. Aw, K. Gulati, A. Santos, H.J. Griesser, D. Losic, Advanced biopolymer-coated drug-releasing titania nanotubes (TNTs) implants with simultaneously enhanced osteoblast adhesion and antibacterial properties, Colloids Surf. B 130 (2015) 255–263.

[37] M.S. Aw, K. Gulati, D. Losic, Controlling drug release from titania nanotube arrays using polymer nanocarriers and biopolymer coating, J. Biomater. Nanobiotechnol. 2 (2011) 477–484.

[38] M.S. Aw, S. Simovic, J. Addai-Mensah, D. Losic, L. Bazinet, I. Adini, E. Pravda, Y. Nahmias, S. Koirala, G. Corfas, R. J. D'Amato, J. Folkman, Polymeric micelles in porous and nanotubular implants as a new system for extended delivery of poorly soluble drugs, J. Mater. Chem. 21 (2011) 7082-7089.

[39] J. Schneider, M. Matsuoka, M. Takeuchi, J. Zhang, Y. Horiuchi, M. Anpo, D. W. Bahnemann, Understanding TiO_2 photocatalysis: Mechanisms and materials, Chem. Rev. 114 (2014) 9919–9986.

[40] N. Shrestha, J. Macak, F. Schmidt-Stein, R. Hahn, C. Mierke, B. Fabry, P. Schmuki, Magnetically guided titania nanotubes for site-selective photocatalysis and drug release, Angew. Chemie Int. Ed.48 (2009) 969–972.

[41] Z. Xu, Y. Lai, D. Wu, W. Huang, S. Huang, L. Zhou, J. Chen, Increased mesenchymal stem cell response and decreased *Staphylococcus aureus* adhesion on titania nanotubes without pharmaceuticals, BioMed Res. Int. (2015) 172898.

[42] K.S. Moon, J.-M. Bae, S. Jin, S. Oh, Infrared-mediated drug elution activity of gold nanorod-grafted TiO_2 nanotubes, J. Nanomater. 2014 (2014) 1–8.

[43] M. Bariana, M. S. Aw, E. Moore, N. H. Voelcker, D. Losic, Radiofrequency-triggered release for on-demand delivery of therapeutics from titania nanotube drug-eluting implants, Nanomedicine 9 (2014) 1263–1275.

[44] M.S. Aw, J. Addai-Mensah, D. Losic, Magnetic-responsive delivery of drug-carriers using titania nanotube arrays, J. Mater. Chem. 22 (2012) 6561-6563.

[45] M. S. Aw and D. Losic, Ultrasound enhanced release of therapeutics from drug-releasing implants based on titania nanotube arrays, Int. J. Pharm. 443 (2013) 154–162.

[46] K.S. Mun, S.D. Alvarez, W.Y. Choi, M.J. Sailor, A Stable, Label-free optical interferometric biosensor based on TiO_2 nanotube arrays, ACS Nano 4 (2010) 2070–2076.

[47] Y.Y. Song, F. Schmidt-Stein, S. Berger, P. Schmuki, TiO_2 Nano Test Tubes as a Self-Cleaning Platform for High-Sensitivity Immunoassays, Small 6 (2010) 1180–1184.

[48] T.G.S. Babu, P.V. Suneesh, T. Ramachandran, B. Nair, Gold nanoparticles modified titania nanotube arrays for amperometric detection of ascorbic acid, Anal. Lett. 43 (2010) 2809–2822.

[49] S.V.S. Mers, E.T.D. Kumar, V. Ganesh, Gold nanoparticles-immobilized, hierarchically ordered, porous TiO_2 nanotubes for biosensing of glutathione, Int. J. Nanomedicine 10 (2015) 171-182.

[50] P. Xiao, B. Batalla Garcia, Q. Guo, D. Liu, G. Cao, TiO_2 nanotube arrays fabricated by anodization in different electrolytes for biosensing, Electrochem. Commun. 9 (2007) 2441–2447.

[51] Y. Xie, L. Zhou, H. Huang, Bioelectrocatalytic application of titania nanotube array for molecule detection, Biosens. Bioelectron. 22 (2007) 2812–2818.

[52] Q. Kang, L. Yang, Q. Cai, An electro-catalytic biosensor fabricated with Pt–Au nanoparticle-decorated titania nanotube array, Bioelectrochemistry 74 (2008) 62–65.

[53] Z.D. Gao, F.F. Guan, C.Y. Li, H.F. Liu, Y.Y. Song, Signal-amplified platform for electrochemical immunosensor based on TiO_2 nanotube arrays using a HRP tagged antibody-Au nanoparticles as probe, Biosens. Bioelectron. 41(2013) 771–775.

[54] Z.D. Gao, Y. Qu, T. Li, N.K. Shrestha, Y.Y. Song, Development of amperometric glucose biosensor based on Prussian blue functionalized TiO_2 nanotube arrays, Sci. Rep. 4 (2014) 6891.

[55] M. Long, L. Tan, H. Liu, Z. He, A. Tang, Novel helical TiO_2 nanotube arrays modified by Cu_2O for enzyme-free glucose oxidation, Biosens. Bioelectron. 59 (2014) 243–250.

[56] J. Zhu, X. Huo, X. Liu, H. Ju, Gold nanoparticles deposited polyaniline-TiO_2 nanotube for surface plasmon resonance enhanced photoelectrochemical biosensing, ACS Appl. Mater. Interfaces 8 (2016) 341–349.

[57] J. Cai, J.Huang, M. Ge, J. Iocozzia, Z. Lin, K.-Q. Zhang, Y. Lai, Immobilization of Pt nanoparticles *via* rapid and reusable electropolymerization of dopamine on TiO_2 nanotube arrays for reversible SERS substrates and nonenzymatic glucose sensors, Small 13 (2017) 1604240.

[58] Y. Xin, Z. Li, W. Wu, B. Fu, H. Wu, Z. Zhang, Recognition unit-free and self-cleaning photoelectrochemical sensing platform onTiO_2 nanotube photonic crystals for sensitive and selective detection of dopamine release from mouse brain, Biosens. Bioelectron. 87 (2017) 396–403.

[59] P. Kar, A. Pandey, J.J. Greer, K. Shankar, Ultrahigh sensitivity assays for human cardiac troponin I using TiO_2 nanotube arrays, Lab Chip 12 (2012) 821–828.

[60] L. Mi, P. Wang, J. Yan, J. Qian, J. Lu, J. Yu, Y. Wang, H. Liu, M. Zhu, Y. Wan, S. Liu, A novel photoelectrochemical immunosensor by integration of nanobody and TiO_2 nanotubes for sensitive detection of serum cystatin C, Anal. Chim. Acta 902 (2016) 107–114.

[61] Y.R. An, L.L. Tang, X.L. Jiang, H. Chen, M.C. Yang, L.T. Jin, S.P. Zhang, C.G. Wang, W. Zhang, A photoelectrochemical immunosensor based on Au-doped TiO_2 nanotube arrays for the detection of α-synuclein, Chem. Eur. J. 16 (2010) 14439–14446.

[62] P. Wang, W. Dai, L. Ge, M. Yan, S. Ge, J. Yu, Visible light photoelectrochemical sensor based on Au nanoparticles and molecularly imprinted poly(o-phenylenediamine)-modified TiO_2 nanotubes for specific and sensitive detection chlorpyrifos, Analyst 138 (2013) 939–945.

[63] Q. Huang, H. Chen, L. Xu, D. Lu, L. Tang, L. Jin, Z. Xu, W. Zhang, Visible-light-activated photoelectrochemical biosensor for the study of acetylcholinesterase inhibition induced by endogenous neurotoxins, Biosens. Bioelectron. 45 (2013) 292–299.

[64] G. Wang, X. He, G. Xu, L. Chen, Y. Zhu, X. Zhang, L. Wang, Detection of T4 polynucleotide kinase activity with immobilization of TiO_2 nanotubes and amplification of Au nanoparticles, Biosens. Bioelectron. 43 (2013) 125–130.

TiO2-based nanotopographical cues attenuate the restenotic phenotype in primary human vascular endothelial and smooth muscle cells

2.1 Abstract

Coronary and peripheral stents are implants that are inserted into blocked arteries to restore blood flow. After stent deployment, the denudation of the endothelial cell layer and the resulting inflammatory cascade can lead to restenosis, the renarrowing of the vessel wall due to the hyperproliferation and excess matrix secretion of smooth muscle cells. Despite advances in drug-eluting stents (DES), restenosis remains a clinical challenge, and can require repeat revascularizations. In this study, we investigated how vascular cell phenotype can be modulated by nanotopographical cues on the stent surface, with the goal of developing an alternative strategy to DES for decreasing restenosis. We fabricated TiO_2 nanotubes and demonstrated that this topography can decrease SMC surface coverage without affecting endothelialization. In addition, to our knowledge, this is the first study reporting that TiO_2 nanotube topography dampens the response to inflammatory cytokine stimulation in endothelial and smooth muscle cells. We observed that compared to flat titanium surfaces, nanotube surfaces attenuated TNFα-induced VCAM-1 expression in ECs by 1.8-fold, and decreased TNFα-induced SMC growth by 42%. Further, we find that the resulting cellular phenotype is sensitive to changes in nanotube diameter, and that 90 nm diameter nanotubes leads to the greatest magnitude in cell response compared to 30 nm or 50 nm nanotubes.

2.2. Introduction

Coronary stenting is a procedure for opening blocked arteries. Post-procedure, the renarrowing of the artery through restenosis is a persisting complication that requires revascularizations[1]. Restenosis is caused by injury to the vessel wall during stent deployment, which denudes the endothelium and triggers an inflammatory cascade due to the release of proinflammatory cytokines, chemokines, and the expression of adhesion molecules [2], [3]. Subsequently, the inflammation recruits smooth muscle cells (SMC) to migrate to the vessel lumen, where the cells hyperproliferate and secrete excess extracellular matrix [4], [5]. This leads to the formation of the restenotic lesion, which renarrows the vessel and causes the failure of stents to maintain patency. Restenosis can present as recurrent angina or acute myocardial infarction in some patients, and may require repeat revascularization.

Drug-eluting stents (DES) inhibit the proliferation of SMCs and decrease restenosis, thus reducing the risk for repeat vascularizations [6], [7]. However, they also inhibit endothelial cell (EC) function and delay endothelial healing, leading to an increased risk of thrombosis [8]. Moreover, a meta-analysis of randomized clinical trials suggested that there is an increased mortality rate following application of paclitaxel-coated balloons and stents in patients with peripheral arterial disease (PAD) [9]. This study led the FDA to issue a warning letter to health care providers, cautioning them to weigh the relative risks and benefits of paclitaxel-coated stents and balloons for their patients. The risks of DES motivate the development of an alternative strategy to decrease restenosis in a safe and effective manner. The ideal stent surface would allow for rapid and functional reendothelialization and the suppression of SMC proliferation, in order to minimize the risks of restenosis and thrombosis [10].

Nanomaterials have been widely explored as therapeutic agents for many biomedical applications, including drug delivery and regenerative medicine [11]–[17]. In particular, nanoscale topographical cues have been engineered to modulate vascular cell adhesion and function for cardiovascular applications [18]–[21]. Titanium, a common material used in medical devices and implants, can be patterned into a vertically oriented, highly ordered nanotubes through a simple process of electrochemical anodization [22]. Studies have shown that TiO_2 nanotube surfaces can promote bovine aortic endothelial cell adhesion and proliferation, while also downregulating murine vascular smooth muscle cell proliferation [23]. In an *in vivo* rabbit iliac artery model, titanium stents coated with 90 nm nanotubes led to a 17% decrease in restenosis rates as compared to flat titanium stents [24]. This study demonstrated proof of concept that TiO_2 nanotube coatings can decrease restenosis *in vivo*, but the mechanism through which TiO_2 nanotubes decreases restenosis is not yet fully understood.

Therefore, we sought to investigate the effect of nanotube topography on primary human vascular cell phenotype on a cellular level, to explain the tissue-level responses observed *in vivo.* We cultured primary human coronary artery ECs and SMCs, and quantified their relative coverage on the surface as well as responses to inflammation. To our knowledge, this is the first study that quantifies the effect of TiO_2 nanotube topography on the inflammatory responses in primary human vascular cells. We also investigated the cell-interface interactions by quantifying focal adhesion kinase expression and phosphorylation. Lastly, we compared EC and SMC response to varying nanotube diameters, to determine whether cellular responses were dependent on the size and spacing of the surface features. The information revealed in this study can guide the design of new stent surfaces to decrease restenosis.

2.3 Materials and Methods

2.3.1 TiO_2 Nanotube Anodization

Titanium foil sheets (0.127 mm thickness, 99.7% trace metals basis), aluminum fluoride (Ammonium fluoride, =99.99% trace metals basis), glycerol (ACS reagent, >=99.5%), and ethylene glycol (ReagentPlus) were purchased from Sigma-Aldrich (Milwaukee, WI). Titanium foil sheets were cut into 2 cm by 2 cm squares and cleaned by sonication in a sequential bath of

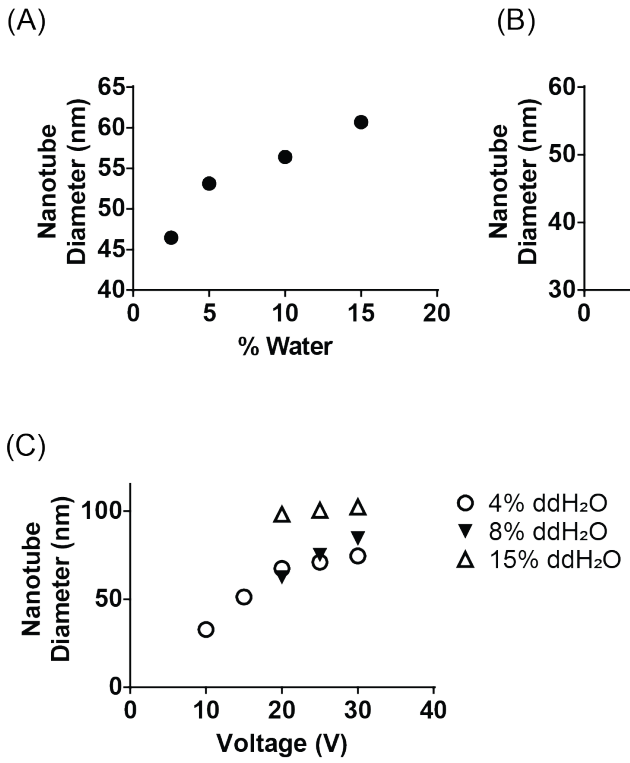

Figure 2.1 Voltage and electrolyte composition were adjusted to determine the optimal anodization parameters to achieve the target nanotube dimensions of 30, 50, and 90 nm. (A) Anodization voltage was kept constant at 15V, while the water content in the electrolyte was adjusted between 2.5 wt% to 15 wt%. The electrolyte contained 3 g/L ammonium fluoride, and between 97.5 wt% and 85 wt% ethylene glycol, adjusting for the changes in water content. (B) Anodization voltage was tuned from 5 V to 15 V. The electrolyte composition remained constant, containing 3 g/L ammonium fluoride, 10 wt% distilled water, and 90wt% ethylene glycol. Nanotube diameter increases as voltage increases. (C) Voltage was tuned between 10 V and 30 V for anodizing TiO_2 foil in a glycerol electrolyte solution. The electrolytes contained 1.4 wt% ammonium fluoride, the indicated wt% of water, and the remaining wt% as glycerol.

Micro-90 solution (International Products Corporation), 100% acetone, and 70% ethanol. To fabricate titanium nanotubes, the titanium foil and an equal-sized piece of platinum foil were secured in a custom-made, 3D-printed holder (Figure 2.1A). The titanium and platinum foils were maintained parallel to each other and 19 mm apart. The foils were connected to electrodes using platinum wire, where the titanium foil served as the anode and the platinum as the cathode. The foils in the holder were submerged in an electrolyte solution, containing 90 wt% ethylene glycol, 9.1 wt% DI water, and 0.9 wt% ammonium fluoride. An anodic voltage of 30 V was applied for 60 minutes in order to fabricate the titanium nanotube coating. The nanotube surfaces were then annealed in a furnace at 450℃ for 2 hours and stored in a vacuum chamber until use.

For fabricating 30 nm and 50 nm nanotubes (NT30 and NT50), the electrolyte solution was composed of 94.3 wt% glycerol, 4.3 wt% water, and 1.4 wt% ammonium fluoride. Figure 2.2 shows the optimization of anodization parameters for achieving the target nanotube diameters. A 10 V or 15 V voltage was applied for 120 min for the NT30 and NT90 surfaces, respectively. To fabricate NT90* nanotubes, the electrolyte solution was composed of 90.6 wt% glycerol, 8 wt% water, 1.4 wt% ammonium fluoride. A voltage of 30V was applied for 120 minutes. Following anodization, the foils were rinsed in DI water, then sonicated briefly in 70% ethanol to clean off the residual electrolyte solution. The foils were then annealed in a furnace at 350℃ for 1 h.

2.3.2 Helium Ion Microscopy

Anodized nanotube surfaces were imaged using a Zeiss Helium Ion Microscope (HIM) at the University of California Berkeley Biomolecular Nanotechnology Center (Berkeley, California). Foils were sputter coated with gold-palladium at 10 mA for 45 s prior to imaging.

Cells cultured for 2 days on 90 nm-diameter nanotubes (NT90) and flat foils were fixed in glutaraldehyde SEM fixation buffer overnight (2.7% (v/v) glutaraldehyde, 0.1 M sodium cacodylate buffer), then washed 3x with 0.1M sodium cacodylate for 10 minutes each. The sample was then dehydrated in serial baths of 35%, 50%, 70%, 85%, 90%, 95%, and 100% ethanol, for at least 10 minutes each. The foils were then dried using a critical point dryer in 100% ethanol. The cells were sputter coated with the same settings as above, and then imaged using HIM.

2.3.3 Atomic Force Microscopy

AFM was performed using a NanoWizard Ultra Speed A AFM in soft tapping mode, using a BudgetSensors All-In-One probe (BudgetSensors, Sofia, Bulgaria). Scans were performed in three different fields of view, and root mean squared roughness values were calculated using the Gwyddion software (Czech Metrology Institute, Jihlava, Czechia).

2.3.4 Cell Culture and Cell Proliferation Assays

Primary human coronary artery endothelial cells (EC) and primary human coronary artery smooth muscle cells (SMC) were purchased from PromoCell (Heidelberg, Germany). SMCs were maintained in smooth muscle growth medium-2 (SMGM-2) (PromoCell), and ECs were maintained in endothelial cell growth medium-2 (EGM-2) (PromoCell). ECs used for cell area measurements were cultured in endothelial cell growth medium-2 MV (EGM-2 MV).

Cells were seeded onto NT90 or flat surfaces to measure the effect of surface topography on cell behavior. To measure cell proliferation, ECs were seeded on foils at 8,000 cells/cm^2 and cultured for 1, 2, or 3 days. SMCs were seeded on foils at 10,000 cells/cm^2 and cultured for 1, 3, or 5 days. Cell numbers were quantified using a CyQUANT proliferation assay (Molecular

Probes, USA), using DNA content as a measurement of cell number. Experiments were performed in triplicate.

2.3.5 Cell staining and immunofluorescence

Cells were then fixed with 4% paraformaldehyde for 10 minutes at room temperature, washed three times with PBS for 5 minutes each, then permeabilized with 0.1% Triton X-100 for 5 minutes.

For immunofluorescence, fixed and permeabilized samples were blocked for 1 hour at room temperature with 10% goat serum, then incubated with primary antibody overnight at 4℃. Either anti-paxillin [ab32084] (Abcam, Burlingame, CA) or anti-vinculin [V9131] (Thermo-Fisher, Waltham, MA) antibodies was used to visualize focal adhesions. The antibodies were used at 1:250 and 1:400 dilutions, respectively. Cells were then washed and incubated with secondary antibodies for 30 minutes at room temperature. Lastly, cells were counterstained with Alexa Fluor 488-tagged phalloidin (Invitrogen, Carlsbad, CA) at a 1:500 dilution, and with DAPI at a 1:1000 dilution. Microscopy images were acquired using a Nikon 6D optical microscope (NIKON Instruments, Inc., Melville, NY) with 4–20x magnification. All image quantification was performed using ImageJ.

2.3.6 Cell Area Measurements

To measure cell area, EC and SMC were cultured for 24 h on NT90 or flat surfaces. The cells were fixed, permeabilized, and stained with phalloidin and DAPI as described previously. Cell area quantification was performed using ImageJ. The images were thresholded, individual cells were selected, and their areas was measured. Measurements were taken from at three foils per condition, with at least three fields of view measured per foil.

2.3.7 Quantitative Real-Time PCR

To measure gene expression, the cells were cultured on NT90 or flat surfaces for 24 h. For ECs, the cells were then stimulated with 2 ng/mL of human TNFα (R&D Systems, Minneapolis, MN) for 4 h. mRNA was extracted using the RNEasy Mini Kit (Qiagen). Reverse transcription was performed using the iScript™ cDNA Synthesis Kit (Bio-Rad Laboratories, Hercules, CA). qPCR was performed using Fast SYBR Green Mastermix (Life Technologies, Grand Island, NY) and a Viia7 qPCR machine (Life Technologies, Carlsbad, CA). The relative transcript quantities were calculated using the ΔΔCt method and normalized to the housekeeping gene encoding RPL19. Custom-made DNA primers were purchased from Integrated DNA Technologies (Coralville, IA) and the sequences are shown in Table 2.1.

Table 2.1 Primer sequences used for qPCR

Gene	Primer Sequence
RPL-19	Fwd: TCGCCTCTAGTGTCCTCCG Rev: GCGGGCCAAGGTGTTTTTC
VCAM-1	Fwd: GGGAAGATGGTCGTGATCCTT Rev: TCTGGGGTGGTCTCGATTTTA
CCL-2	Fwd: CAGCCAGATGCAATCAATGCC Rev: TGGAATCCTGAACCCACTTCT

2.3.8 ELISA

Collagen production was measured using the Human Pro-Collagen I alpha 1 ELISA Kit (Abcam, Cambridge, UK). SMCs were cultured on NT90 or flat surfaces for 24 h. The conditioned media was collected to measure secreted pro-collagen I concentration, and the cell extract was collected to measure pro-collagen I concentration within the cells. Cell extracts were

prepared using the extraction buffer and enhancer provided in the kit, following manufacturer instructions.

To measure MCP-1 secretion, SMCs were cultured on NT90 or flat surfaces for 24 h. Cells were treated with either 1 ng/mL of TNFα, or an equal volume of PBS as a vehicle control. All cells were incubated for an additional 24 hours. The conditioned media was then removed and MCP-1 concentration was measured using a Human CCL2/MCP-1 Quantikine ELISA Kit (R&D Systems) according to manufacturer instructions.

To measure FAK and pFAK expression, SMCs or ECs were cultured on TiO_2 nanotube and flat surfaces for 24 hours. The foils were washed with PBS, and cells were lysed with Cell Extraction Buffer (Invitrogen, Waltham, MA, USA) supplemented with Pierce Protease and Phosphatase Inhibitor Mini Tablets (Thermo Scientific, Waltham, MA, USA) for 10 minutes on ice. Cells were then scraped off the surface, transferred to centrifuge tubes, and spun down at 10,000 RPM for 10 minutes at 4℃. The supernatant was removed and cell lysates were analyzed using the FAK (Total) Human ELISA Kit and FAK (Phospho) [pY397] Human ELISA Kit (Invitrogen, Waltham, MA, USA). Total FAK concentration was normalized to total protein concentration of the same sample, as measured using a BCA assay. pFAK concentration was normalized to total FAK concentration of the same sample. Experiments were performed in triplicate or quadruplicate.

2.3.7 Statistical Analysis

Experiments were performed in triplicate or quadruplicate, and are reported as mean ± standard deviation (SD). Statistical analysis was performed using GraphPad Prism 6. Student's t-tests were used to compare cell responses on flat versus NT90 surfaces. For the cell number

assays over 3 time points, a multiple t-test was performed using the Holm-Sidak method for multiple comparisons correction.

For experiments comparing flat, NT30, NT50, and NT90 surfaces, One-Way ANOVA was performed followed by Tukey's method for multiple comparisons correction. For the cell number assays comparing cell numbers on these surfaces, a Two-Way ANOVA was performed, followed by Tukey's method for multiple comparisons correction.

2.4. Results

2.4.1 Nanotube surface characterization and cell morphology

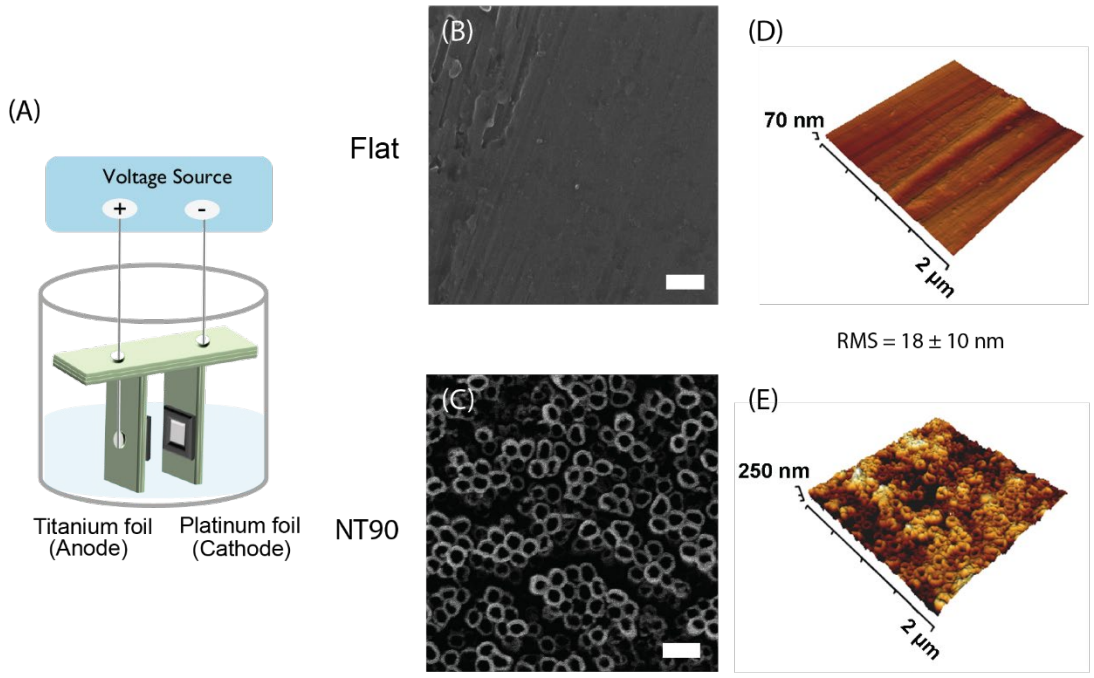

Figure 2.2 (A) A schematic of the electrochemical anodization of TiO_2 nanotube coatings on titanium foil using a custom 3D printed holder. Helium ion microscopy (HIM) images of (B) flat and (C) NT90 surfaces. Atomic Force Microscopy (AFM) projections of (D) flat and (E) NT90 surfaces. D=Diameter; RMS=Root-mean-squared roughness. Scale bar = 200 nm.

Helium ion microscopy images revealed that TiO_2 nanotube surfaces with 90 nm diameters (NT90) were successfully fabricated (Figure 2.1). The average nanotube diameter (Figure 2.1C) and root-mean-squared roughness (RMS) (Figure 2.1E) are reported.

Ridges can be observed on flat surfaces, likely due to draw marks formed during the process of casting the titanium sheets. AFM revealed that NT90 surfaces have greater roughness than the flat surfaces, with an RMS value of 55 nm as compared to 18 nm for flat (Figure 2.1). EC and SMC both adhere to the surfaces and can form cytoplasmic projections including filopodia on both the flat and NT90 surfaces (Figure 2.3).

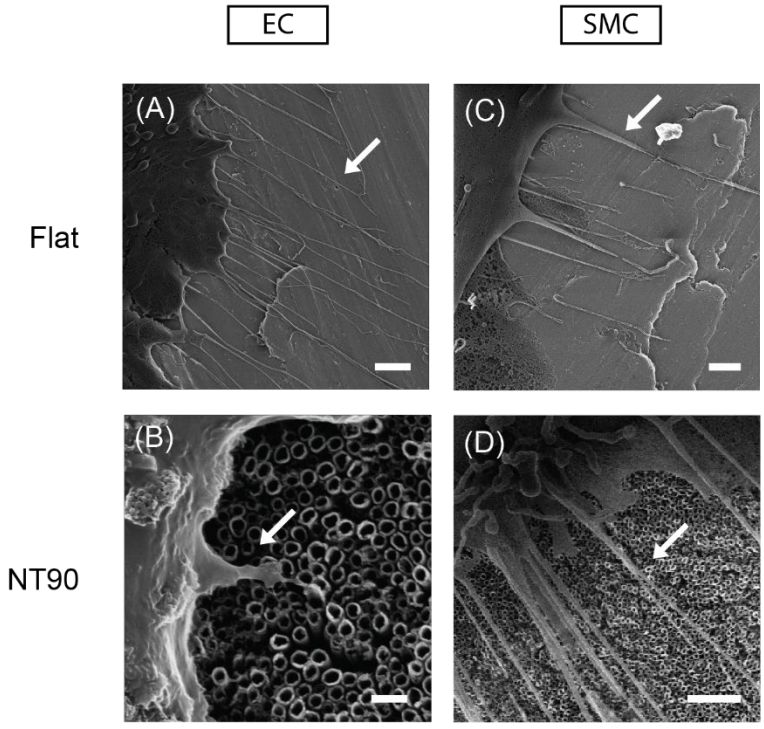

Figure 2.3 Representative HIM images of primary human coronary endothelial muscle cells on (A) flat (scale bar = 2 μm) and (B) NT90 surfaces (scale bar = 200 nm). Representative HIM images of primary human coronary smooth muscle cells on (C) flat (scale bar = 1 μm) and (D) NT90 surface (scale bar = 2 μm). Cells were fixed after 2 days of culture. Filopodia are indicated by white arrows.

2.4.2 NT surface decreases SMC cell coverage without affecting EC coverage

The cell number and cell area of ECs cultured on flat and NT90 surfaces were measured over the course of 3 days (Figure 2.4A, B). For both NT90 and flat surfaces, cell growth was negligible between days 1 and 2, before increasing after day 2. This delay may be due to the time

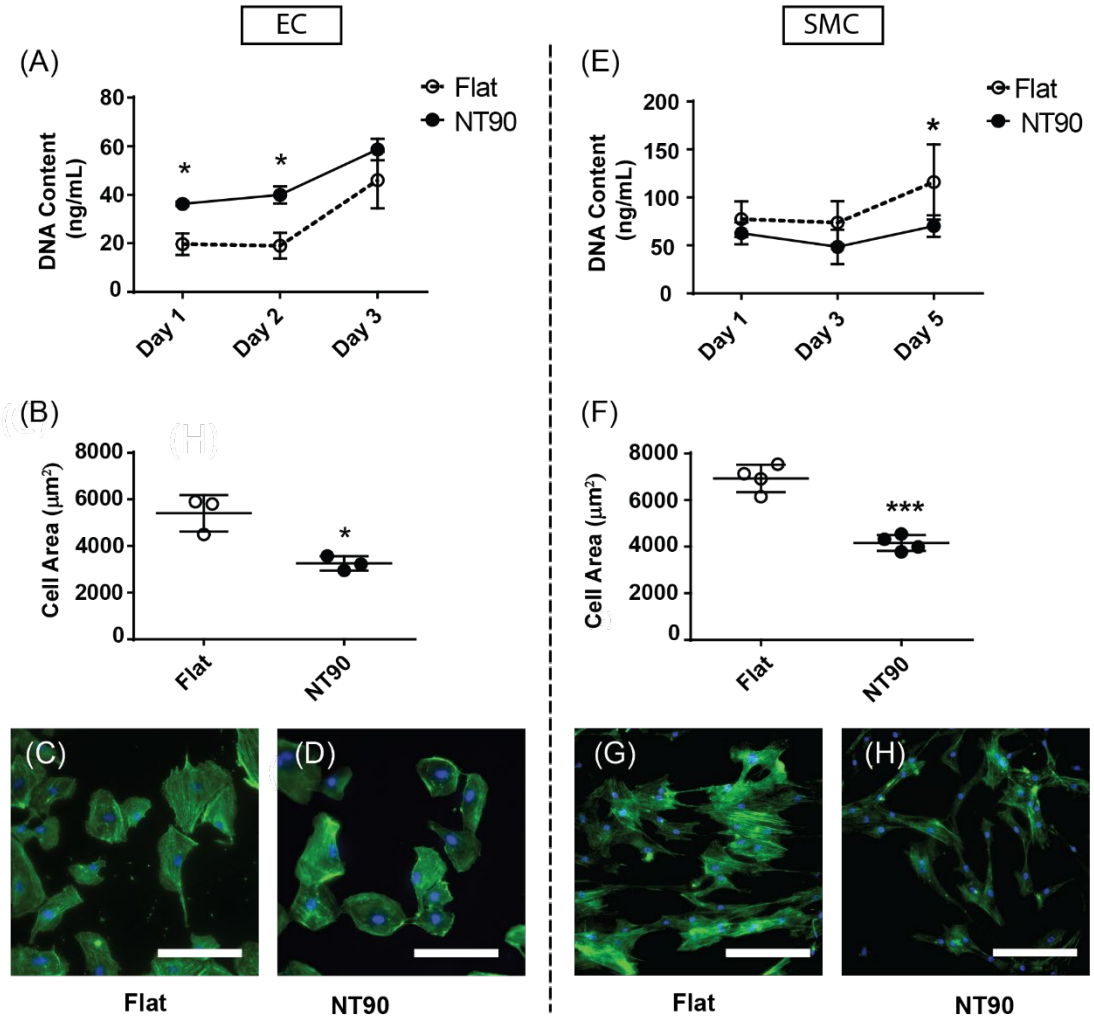

Figure 2.4 EC and SMC cell coverage on flat and NT surfaces. (A) EC and (E) SMC cell numbers on flat and NT surfaces were measured using a CyQUANT assay, which quantifies DNA content in cell lysates. (B) EC and (F) SMC area were quantified using fluorescence microscopy and ImageJ. Representative images of (C, D) ECs and (G, H) SMCs stained with phalloidin (green) and DAPI (blue) cultured on flat and NT surfaces are shown. Scale bar: 150 μm.

needed for sufficient serum protein to adsorb onto the surface and allow for cell attachment and spreading. For ECs, the number of cells is about 1.5-fold greater on NT90 than flat surfaces after 1 day. By day 3, cell numbers were more similar between the two surfaces (Figure 2.4A). When we quantified EC spreading on NT90 surfaces, we found that the cell area decreased by about 40% on NT90 surfaces. We then quantified overall cell coverage by calculating the percent of the foil surface covered by EC cellular material to gauge the effect of nanotubes on endothelialization (Figure 2.5). We found that when accounting for both cell number and cell area, the overall cell coverage on flat and NT90 surfaces are similar over the course of 7 days (Figure 2.5.) Further, in confluent endothelial cell layers, we observed staining for circumferential actin bundles along cell-cell junctions on both flat and NT90 surfaces (Figure 2.8B, D, F, H). The accumulation of polymerized actin at cell-cell contacts have been shown to contribute to VE-cadherin stabilization [25]. Therefore, our results suggest that intact endothelial layers can be formed on both flat and NT90 surfaces. In summary, NT90 surfaces increases the number of ECs compared to flat surfaces, but decreases the average cell area, leading to a similar extent of endothelialization as compared to flat titanium.

The number of adherent SMCs on day 1 is similar on both flat and NT90 surfaces (Figure 2.4B). After 3 days, the is a trend of fewer SMCs on NT90 than flat surfaces. By day 5, there are 40% fewer SMCs on NT90 than flat surfaces ($p<0.05$). In addition to the differences in cell number, we observed that SMCs are also approximately 40% smaller surface areas on NT90 as compared to flat surfaces (Figure 2.4C, D). This suggests that the cells are less spread on NT90 as compared to flat surfaces. For SMCs, the decrease in both cell number and cell area of SMCs on NT90 surfaces leads to a substantial decrease in overall SMC coverage (Figure 2.4G, H). In

summary, we observe that NT90 surfaces can decrease SMC coverage without adversely affecting endothelialization.

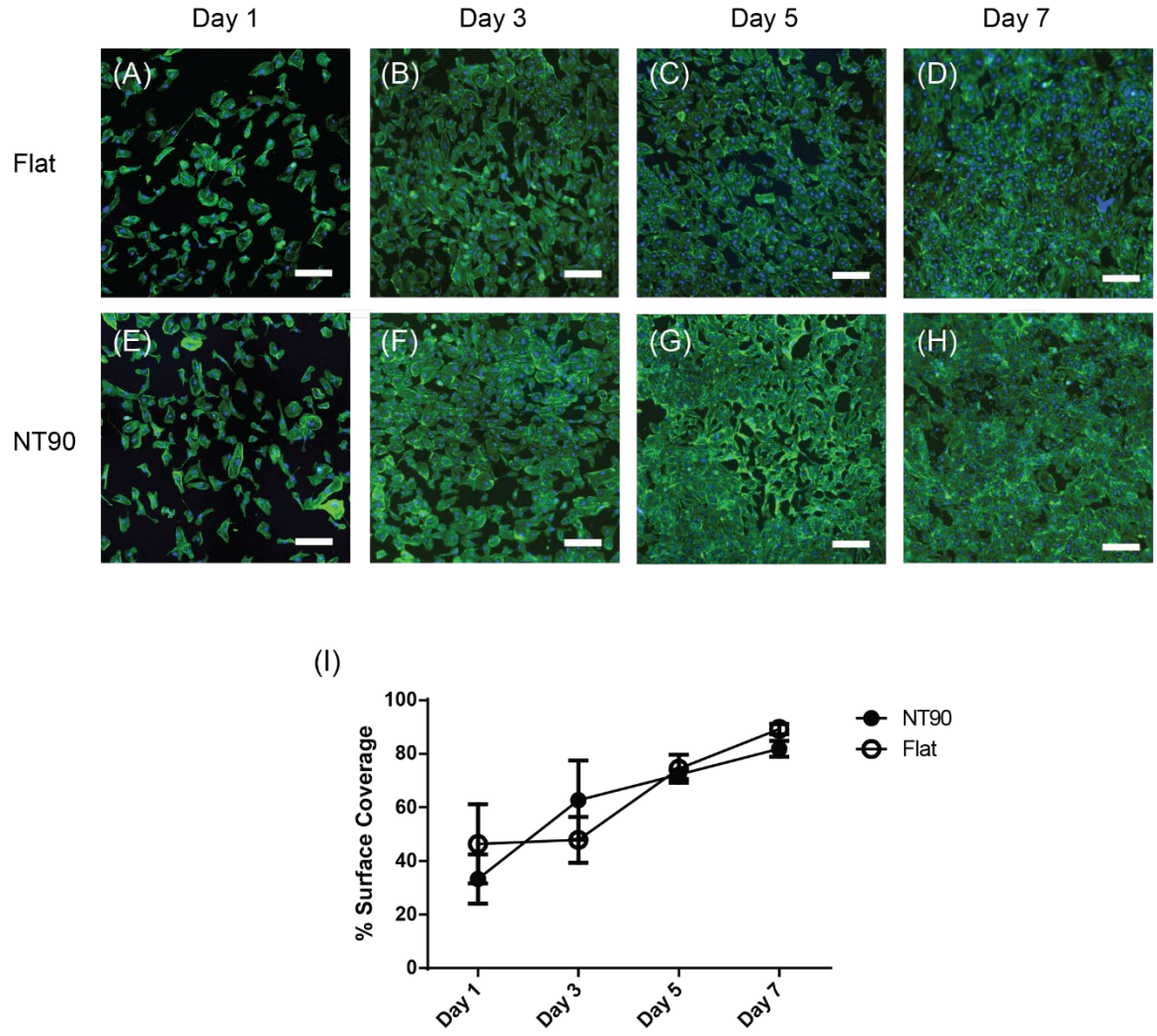

Figure 2.5 ECs were cultured on (A-D) flat and (E-H) NT90 surfaces for 1, 3, 5 or 7 days. At the end of each time point, the cells were fixed with 4% paraformaldehyde, permeabilized with 0.1% Triton X-100, and stained with phalloidin (green) and DAPI (blue). Cells were imaged fluorescence microscopy. Cell coverage shown in (I) was quantified cell coverage by thresholding the images in ImageJ and measuring the percentage of the field of view covered by endothelial cells. Scale bar: 200 μm.

2.4.3 NT surfaces decrease the inflammatory responses in endothelial and smooth muscle cells.

Several cytokines are implicated in the development of restenosis, including MCP-1 [26], IL-6 [26], [27] and TNFα [28]. We chose TNFα as a model cytokine to simulate an inflammatory environment in our *in vitro* cultures. We assessed how vascular ECs and SMCs cultured on flat and NT90 surfaces responded to TNFα stimulation.

To probe the effect of NT90 surfaces on the inflammatory response in ECs, we measured the gene expression of VCAM-1, which encodes an adhesion molecule that mediates immune cell binding and tissue inflammation [29], [30]. Increased levels of VCAM-1 expression is correlated with patients who develop restenosis [31], [32]. We used qPCR to measure the expression of VCAM-1 in ECs cultured on NT90 and flat surfaces, and found that NT90 decreased VCAM-1 expression by 1.8-fold (Figure 2.6A). This result suggests that NT90 has a protective effect against the stimulation of the inflammatory molecule TNFα

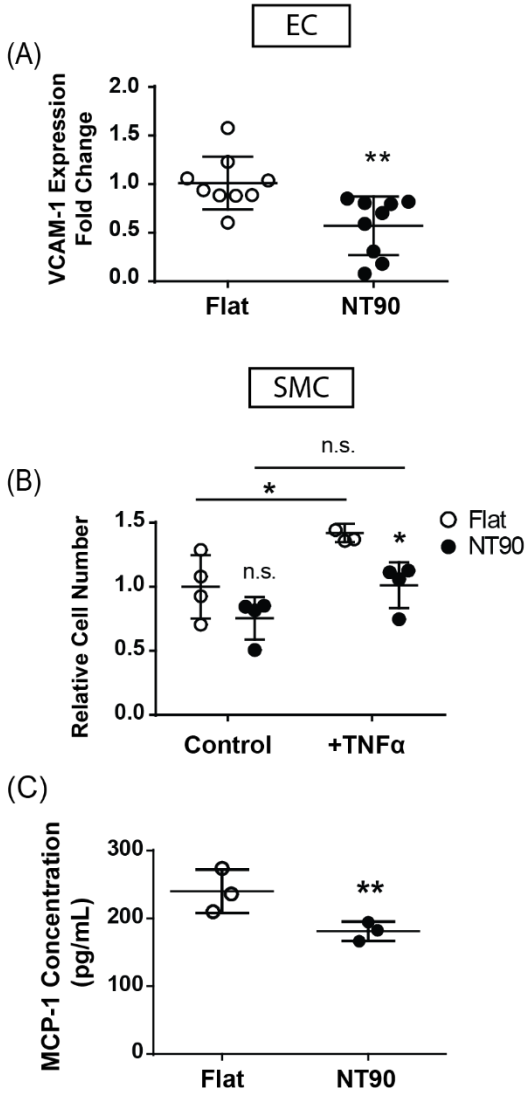

Figure 2.6 The effect of nanotube topography on inflammatory response. (A) VCAM-1 gene expression in ECs. (B) SMC cell numbers when cultured on flat or NT90 surfaces in control media or under stimulation with 2 ng/mL TNFα, an inflammatory cytokine and known mitogen for SMCs. (C) MCP-1 secretion by SMCs cultured on flat or NT surfaces was measured in conditioned media using ELISA. Data are expressed as mean ± SD

on ECs. The decreased expression of adhesion molecules may dampen the inflammatory cascade and attenuate overall tissue inflammation in the area of stent deployment.

NT90 has a similar anti-inflammatory effect in SMCs stimulated with TNFα. This effect was seen in two ways: inflammation-induced cell growth and cytokine production. Firstly, during the pathogenesis of restenosis, inflammatory cytokines induce the hyperproliferation of SMCs. TNFα is one of the mitogens that stimulates SMC proliferation [33], [34]. As expected, we observed that TNFα increases cell number on both flat and NT90 surfaces after 48 hours, as compared to control media that does not contain TNFα. When cultured on flat surfaces, SMC

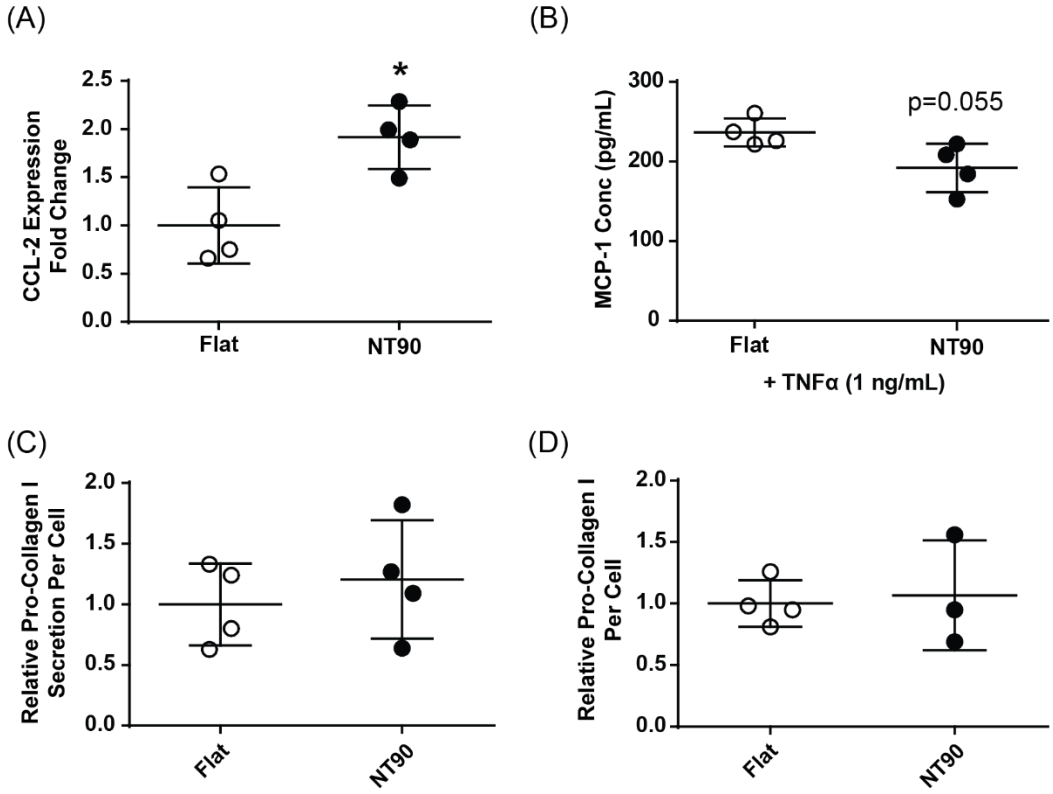

Figure 2.7 (A) SMCs cultured on NT surfaces increases the gene expression of CCL-2, which encodes the protein MCP-1. (B) Secretion of MCP-1 from SMCs cultured on flat or NT surfaces, in the presence of inflammatory cytokine stimulation (1 ng/mL TNFα). Pro-collagen I content of SMCs cultured on flat or NT90 surfaces was quantified using ELISA. Pro-collagen I concentration in (C) conditioned media, (D) cell extract. Data are expressed as mean ± SD.

numbers increased by 42% when stimulated with TNFα (Figure 2.6B). However, when cultured on NT90, SMC numbers increased by only 34%. In the presence of TNFα, there were 29% fewer SMCs on NT90 than those cultured on flat surfaces. These data indicate that NT90 may be protective against the mitogenic effects of TNFα. Secondly, SMCs also respond to inflammation by producing their own cytokines, including MCP-1. We observed that the gene expression of CCL-2, the gene that encodes MCP-1, increased when SMCs were cultured on NT90 (Figure 2.7A). However, we found the opposite trend in protein secretion, which is likely due to the decrease in total cell number. Under standard media conditions, we observed that SMC cultured on NT90 secreted 39% less MCP-1 than those cultured on flat surfaces (Figure 2.6C). When stimulated with 1 ng/mL TNFα, SMCs secrete 18% less MCP-1 when cultured on NT90 ($p=0.055$) (Figure 2.7B). These results indicate that nanotube surfaces can dampen the pathogenesis of restenosis by decreasing the inflammatory response of SMCs.

2.4.4 Focal Adhesion Kinase (FAK) expression and phosphorylation

Changes in focal adhesion kinase activity likely mediates other downstream signaling processes. Focal adhesions and the actin cytoskeleton in ECs cultured on flat and NT90 surfaces can be seen in Figure 2.8. We observe via vinculin staining that punctate focal adhesions can be formed on both flat and NT90 surfaces. We quantified FAK expression and phosphorylation via ELISA, and found that ECs cultured on NT90 had a similar level of total FAK and pFAK protein levels as compared to flat surfaces (Figure 2.9A, B). This result suggests that FAK total expression and phosphorylation is not a mechanism that mediates the differences that we observe in EC behavior on NT90 surfaces.

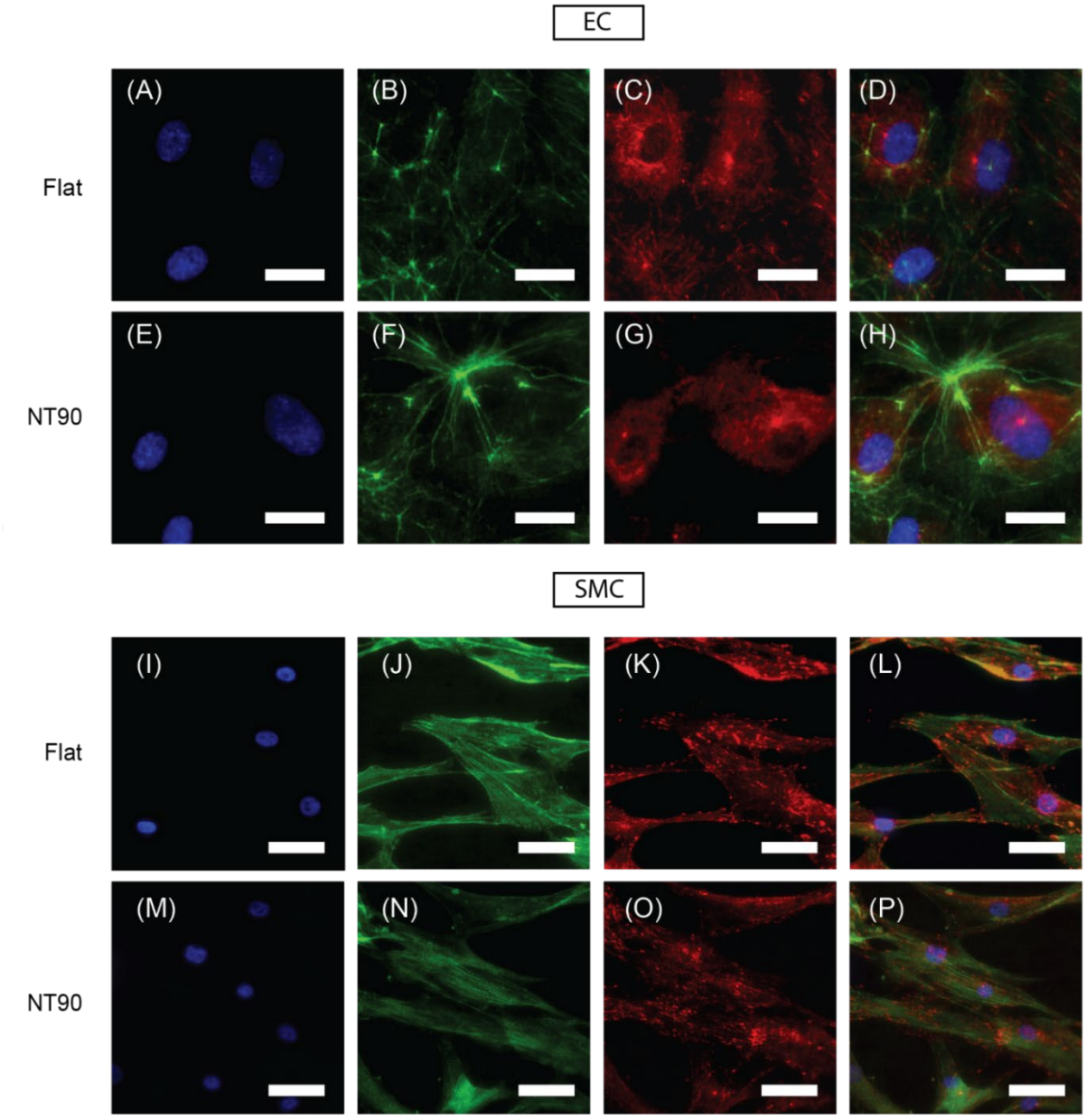

Figure 2.8 (A-H) ECs were cultured on on (A-D) flat or (E-H) NT90 surfaces for 1 day, and then the cells were fixed with 4% paraformaldehyde, permeabilized with 0.1% Triton X-100, and stained with (A, E) DAPI (blue), (B,F) phalloidin (green), (C, G) anti-vinculin (red). Merged images are shown in (D, H). (I-P) HCASMCs were cultured on (I-L) flat or (M-P) NT90 surfaces for 1 day, then fixed and permeabilized as described for HCAECs. SMCs were then stained with (I, M) DAPI (blue), (J,N) phalloidin (green), (K, O) anti-paxillin (red). Merged images are shown in (L, P). (A-H) scale bar: 25 μm. (I-P) scale bar: 50 μm.

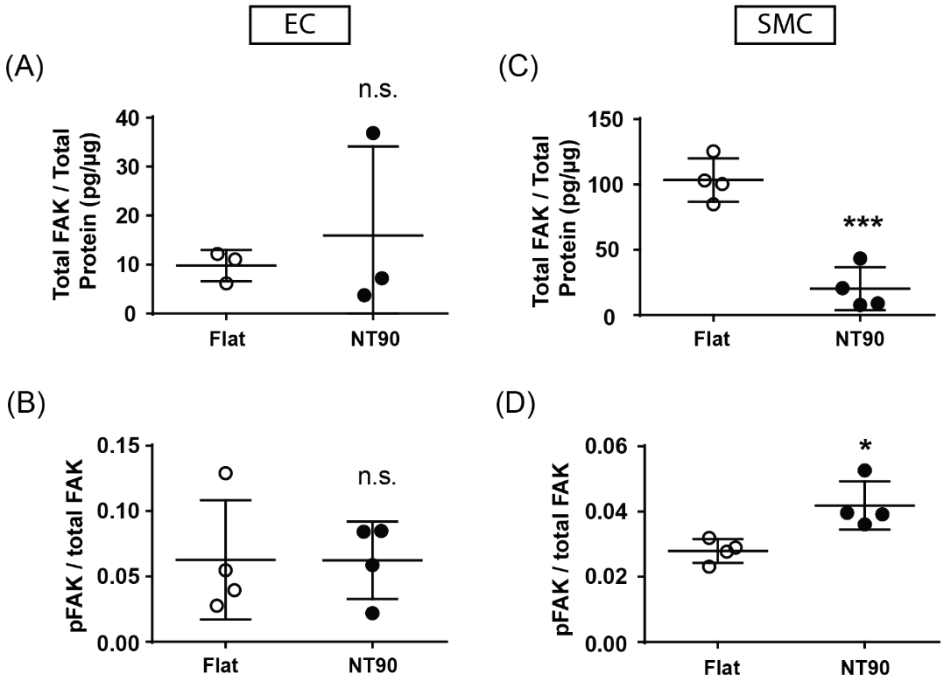

Figure 2.9 Total FAK and pFAK were quantified by ELISA using cell lysates from (A), (B) ECs and (C), (D) SMCs cultured on flat and NT90 surfaces. Total FAK concentration was normalized to total protein content. pFAK concentration was normalized to total FAK concentration. Data are expressed as mean ± SD.

SMCs cultured on both flat and NT90 surfaces were able to form punctate focal adhesions, as shown in Figure 2.8 with paxillin staining. We also observed a 5-fold decrease in total FAK expression, as quantified by ELISA, when the cells are cultured on NT90 ($p<0.001$) (Figure 2.9C). This was as expected because nanotube surfaces have decreased available adhesive area compared to flat surfaces. Interestingly, there was an increase in the ratio of phosphorylated FAK on SMCs cultured on NT90 compared to those cultured on flat surfaces (Figure 2.9D). This could be a mechanism for the cells to compensate for traction forces lost due to the decrease in total FAK expression.

2.4.5 Nanotube effects on EC and SMC response is diameter-dependent

We fabricated TiO_2 nanotubes with 30 nm and 50 nm diameters to investigate whether tuning TiO_2 nanotube diameter has an effect on cell responses. To fabricate these smaller diameters, the electrolyte base was switched from ethylene glycol to glycerol, a more viscous liquid that changes the kinetics of the anodization process to result in different nanotube features. Anodization parameters including electrolyte content and voltage were tuned to achieve these specified diameters, and the optimization of the parameters are shown in Figure 2.2. These surfaces were characterized using HIM and AFM as indicated above and representative images are shown (Figure 2.10).

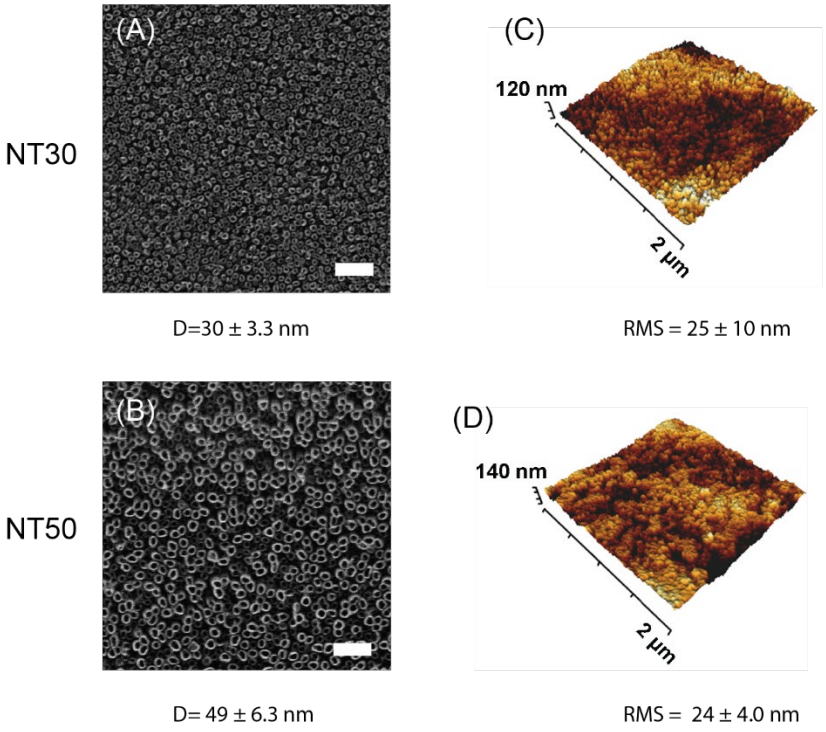

Figure 2.10 Fabrication and characterization of (A, C) NT30 and (B, D) NT50 surfaces. (A, B) HIM images and (C, D) AFM 3D-projections are shown. D = diameter; RMS = root-mean-squared roughness. Scale bar = 200 nm.

The number of ECs on all NT surfaces, regardless of diameter, was increased as compared to flat surfaces on day 1 (Figure 2.11A). All nanotube surfaces increased EC cell numbers over 3 days. For SMC, all nanotube surfaces decreased SMC cell numbers compared to flat, but only NT90 led to a statistically significant decrease in cell number by day 5 (Figure 2.11C).

Next, we measured how response to inflammation changes with nanotube diameter. All NT surfaces led to a decrease in VCAM-1 expression in ECs cultured with 2 ng/mL of TNFα (Figure 2.11B). There was a trend of greater reduction in VCAM-1 expression correlating to the larger NT diameters, with NT90 leading to the greatest reduction in adhesion molecule gene expression.

For SMCs under standard media conditions, all NT surfaces led to slight reductions in cell number as compared to flat, with the greatest magnitude of cell number reduction on NT90 (Figure 2.11D). These results agree with cell number results in Figure 2.6C. In the presence of 2 ng/mL TNFα, all NT surfaces led to decreased cell numbers as compared to flat surfaces.

When measuring SMC MCP-1 secretion, we observed that NT30 and NT50 led to similar levels of MCP-1 secretion as flat surfaces, and only NT90 led to a statistically significant decrease ($p<0.01$) as compared to all other NT or flat surfaces (Figure 2.11E). These data demonstrate that NT90 led to the greatest reduction in anti-inflammation markers for both ECs and SMCs compared to flat and NT surfaces with smaller diameters.

We noted that nanotube surfaces with smaller diameters, also had decreased overall surface roughness, possibly because the different electrolytes and voltages used led to varying growth rates of the nanotubes on the surface. NT90 surfaces have an RMS of 58 nm, whereas NT30 and NT50 have a root-mean-squared roughness (RMS) of 24 nm and 29 nm respectively

(Figures 1, 6) Therefore, we set out to change the roughness independently from the diameter to investigate whether roughness or diameter is the primary driving force behind these observed changes in cellular response. We fabricated NT90*, a nanotube surface with 90 nm diameter

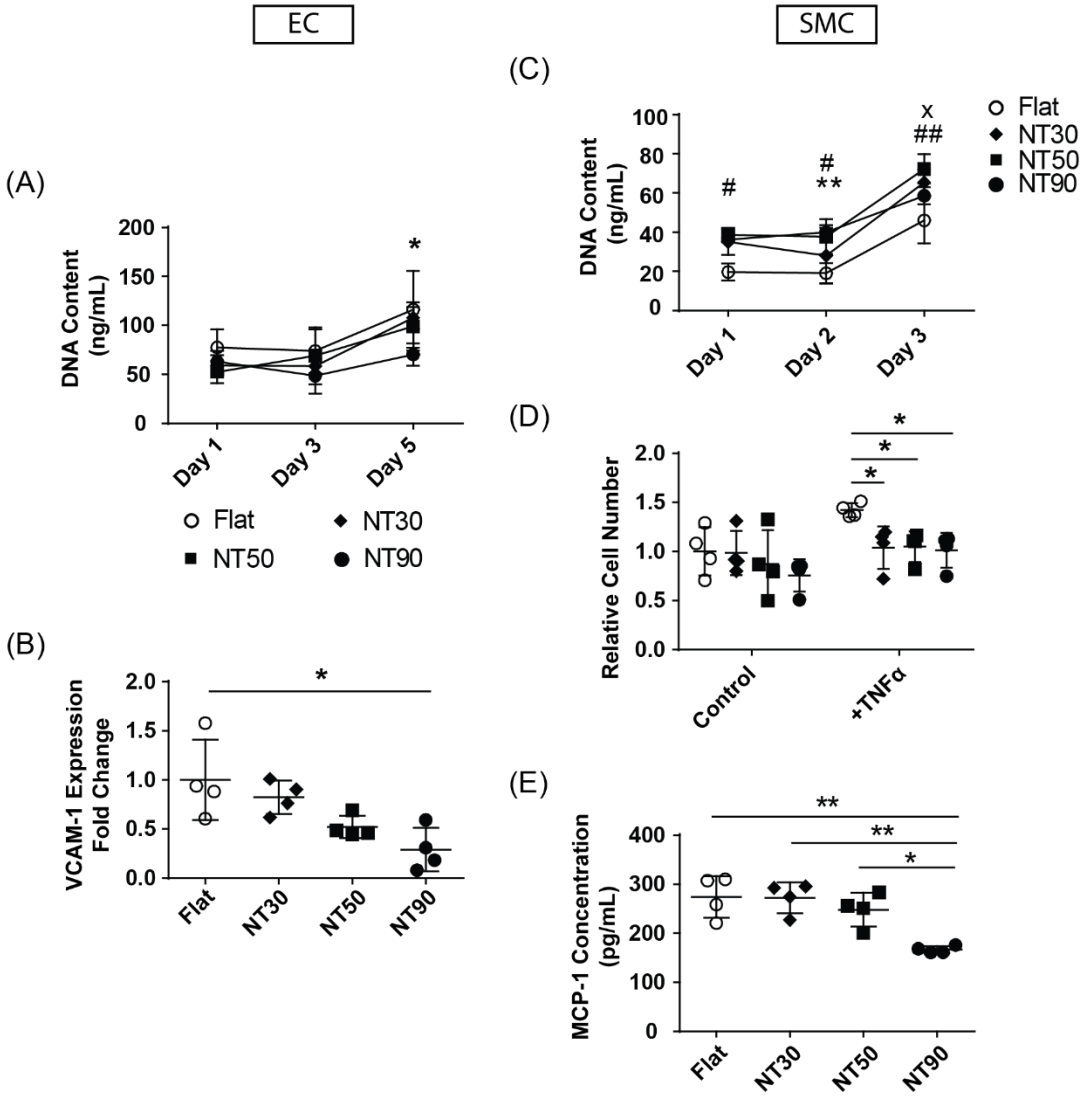

Figure 2.11 The effect of varying NT diameter on EC and SMC response. Cell growth rates on flat and NT surfaces using (A) ECs and (D) SMCs. Significance values are represented as follows: x NT30; # NT50; *NT90. One symbol: $p<0.05$; two symbols: $p<0.01$. (B) VCAM-1 mRNA expression in ECs cultured on flat and NT surfaces. Values are normalized to mRNA expression on flat surfaces. (D) SMC cell numbers cultured on flat and NT surfaces, in control media and in media containing 2 ng/mL TNFα. (E) MCP-1 secretion by SMCs cultured on flat and NT surfaces. Note: Data shown here for flat and NT90 surfaces are identical as those in previous figures. They are shown here as a reference for comparison purposes.

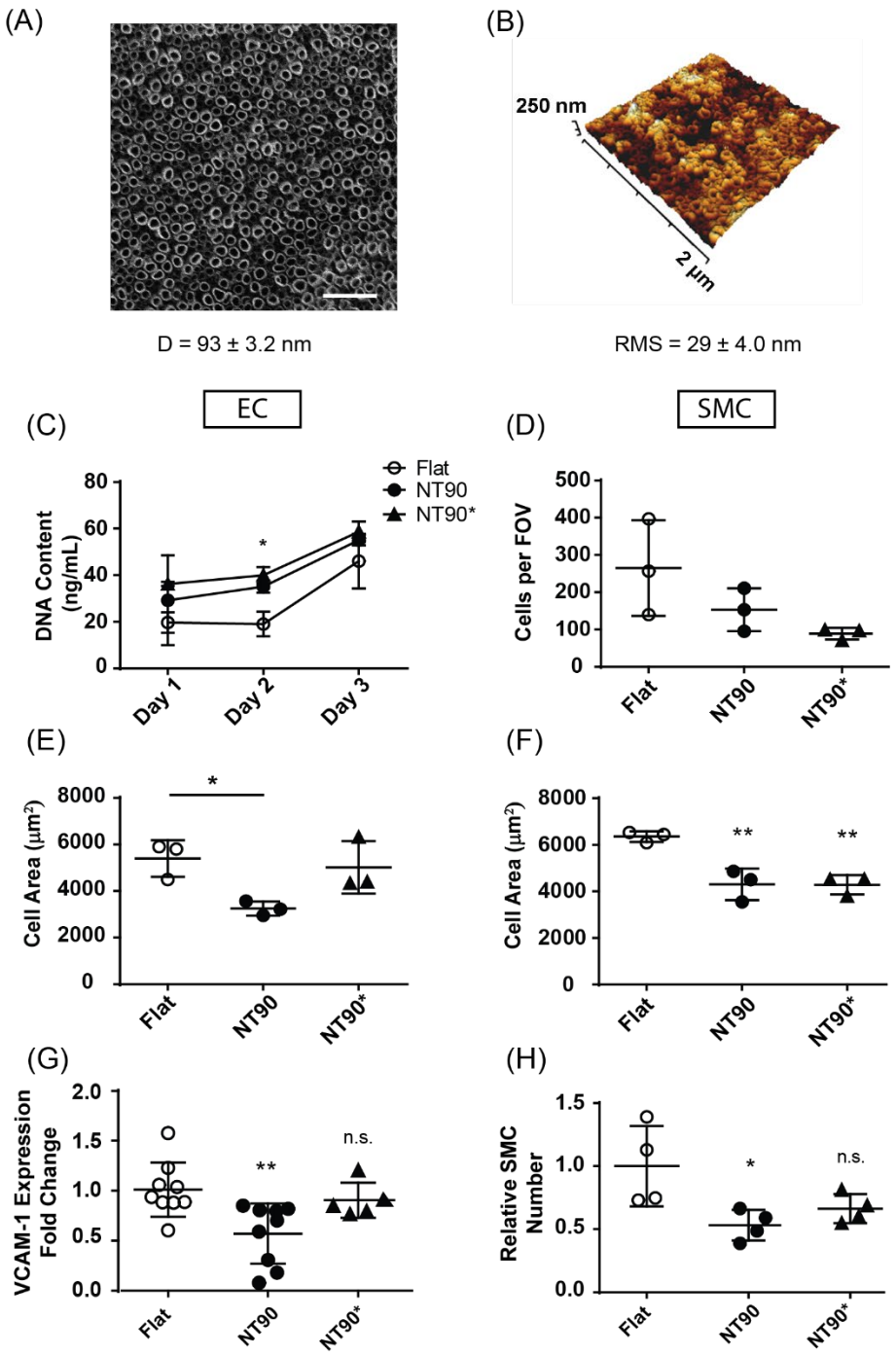

Figure 2.12 The effect of varying TiO_2 nanotube surface roughness EC and SMC phenotype. NT90* surfaces were characterized using (A) helium ion microscopy and (B) AFM. (C) EC surface coverage was measured using CyQUANT over 3 days. (D) SMC cell number on day 1 was quantified by fluorescence microscopy and ImageJ. (E) EC and (F) SMC cell area were quantified by fluorescence microscopy and ImageJ. (G) EC VCAM-1 expression after 2 ng/mL TNFα stimulation was measured by qPCR. (H) SMC numbers after stimulation with 2 ng/mL TNFα was measured by CYQUANT.

nanotubes (Figure 2.12A), but 33 nm RMS roughness (Figure 2.12B), which was more similar to the roughness of NT30 and NT50 surfaces. We observed that SMC cultured on NT90* surfaces had similar cell adhesion and cell area to those cultured on NT90 surfaces (Figure 2.12D, S5F). ECs cultured on NT90* surfaces had similar cell numbers as compared to those cultured on NT90 (Figure 2.12C), but cell area on NT90* was increased relative to NT90, and more closely resembled cell areas of ECs cultured on flat surfaces (Figure 2.12E). This suggests while roughness did not change SMC response, EC response were affected by changes in surface roughness. When we then assayed the effect of NT90* on inflammatory responses in terms of EC VCAM-1 expression and cytokine-induced SMC growth, we found no differences compared to flat surfaces (Figure 2.12G, H). Therefore, while a decrease in roughness in the NT90* surfaces may potentially improve EC surface coverage, the anti-inflammatory effects were diminished.

2.5. Discussion

Tuning cell behavior on the stent surface using nanotube topography has several advantages: 1) The anodization process for patterning surfaces is simple and compatible with metallic substrates, 2) the surface topography can be modified without altering the bulk mechanical properties of the stent, and 3) it avoids the use of the toxic drugs commonly used in DES. In this study, we investigated how TiO_2 nanotube topography can affect the responses of vascular endothelial and smooth muscle cells, with respect to their roles in restenosis. We quantified three major hallmarks of restenosis: EC coverage, SMC coverage, and inflammatory responses.

2.5.1 TiO2 nanotube decrease SMC coverage without changing endothelialization

When SMCs were cultured on NT surfaces, we found that cell numbers were 40% less on NT90 by day 5. We also found that cell area was 40% smaller on NT90. This results in an overall decrease in cell coverage when SMCs were cultured on nanotube surfaces. This result agrees with previous literature reporting that NT surfaces decrease cell mouse aortic vascular smooth muscle cells (MOVAS) proliferation [23] and decrease SMC coverage [35]. A decrease in SMC coverage on the stent surface could lead to a decrease in restenosis *in vivo*.

For endothelial cells, we found that NT surfaces resulted in a similar rate and extent of endothelialization compared to flat surfaces (Figure 2.5). While the cell number increased, cell area decreased (Figure 2.4). Previous work has also shown that NT surfaces increase HUVEC cell number as compared to flat [35], which agrees with our results shown here. However, the study also shows that HUVEC cell spreading is not affected by NT surfaces, thus leading to an increase in total cell coverage attributed to the increase in cell number. The difference in our results may be due to different cell types used, or due to distinctions in the fabrication of NT surfaces. In our study, we found that the endothelialization was comparable on both NT90 and flat surfaces for primary human coronary artery endothelial cells.

Since the restenotic lesion is composed of both cellular material and secreted matrix proteins, we also measured pro-collagen I secretion from SMCs. Collagen I is one of the major components of the restenotic lesion [36], and pro-collagen I is the un-crosslinked precursor to the crosslinked, insoluble collagen I. As shown in Figure 2.7C and 2.7D, SMCs cultured on flat and NT90 surfaces have similar pro-collagen I content per cell, as measured both internally in the cell lysate, and externally in the conditioned media. This suggests that tissue-level changes in

collagen I content would likely be driven by total cell number, and not the level of production per cell.

2.5.2 Response to inflammation

Inflammation plays a significant role in the development of restenosis [27], [37], [38]. Therefore, we set out to assess how NT surfaces affect the responses of ECs and SMCs to the inflammatory cytokine TNFα, which is implicated in restenosis [28].

Our data demonstrates that NT topography decreases the gene expression of VCAM-1 by 1.8-fold. VCAM-1 encodes adhesion molecules that contribute to the inflammation within the vessel wall. Their expression is induced by inflammation, and in turn, they increase endothelial cell activation and mediate immune cell binding and extravasation [29], [30]. In particular, the implication of VCAM-1 in restenosis has been previously reported, and its blockade can lead to decreased restenosis. For example, blocking VCAM-1 using monoclonal antibodies was demonstrated to reduce neointimal formation after periadventitial carotid artery injury in genetically hypercholesterolemic mice [39]. In addition, siRNA inhibition of VCAM-1 reduced neointimal formation after surgical mechanical injury of the carotid artery in a rat model [40]. Taken together, the decrease in VCAM-1 expression is likely a mechanism through which NT topography can decrease tissue-level inflammation and attenuate restenosis.

We also found that when SMCs are cultured on NT90, TNFα induced a smaller degree of hyperproliferation as compared to SMCs cultured on flat surfaces. This indicates that in an inflammatory environment, there is a significant decrease in SMC number when cells are cultured on NT90 surfaces. NT90 surfaces may act in concert with TNFα receptor signaling to attenuate SMC coverage on the surface, since cell numbers on the two surface types are not statistically significantly different without the presence of TNFα.

NT90 also affects SMC response to inflammation by decreasing levels of MCP-1 produced. MCP-1 mediates monocyte recruitment and activation, which is a necessary contributor to restenosis [41]. MCP-1 is produced by many cell types, including macrophages, endothelial cells, fibroblasts, and smooth muscle cells. MCP-1 production is induced by other growth factors and cytokines, causing the cell to amplify the inflammatory cascade. We found that under both normal and inflammatory conditions, the total amount of secreted MCP-1 is lower on NT90 surfaces as compared to flat. This difference is likely due to the decreased numbers of SMC on NT surfaces contributes to the decrease in total MCP-1 concentration.

Our study indicates that TiO_2 nanotubes can curb the inflammatory cascade surrounding restenosis in several ways: 1) decreasing EC expression of adhesion molecules, 2) decreasing SMC mitogenesis in response to inflammatory cytokines like TNFα, and 3) decreasing the production of inflammatory cytokines such as MCP-1 by SMC.

2.5.3 The effect of NT surfaces on focal adhesion expression and phosphorylation

Cells sense mechanical signals via integrins, which physically engage the ECM and can become the nucleation points for focal contacts, and subsequently focal adhesions. Integrins also trigger intracellular signals that regulate remodeling of the actin cytoskeleton and other downstream activities. Focal adhesion kinase (FAK), as well as Src, paxillin, and several other adaptor proteins are associated with integrins on the membrane [42], and affect many physiological responses including proliferation, migration, and growth factor signaling.

We investigated how NT surfaces affect FAK expression and phosphorylation. For endothelial cells, we found that NT90 surfaces does not cause significant difference in FAK expression or levels of phosphorylation. However, because ECs do demonstrate different behavior on NT90 surfaces, as evidenced by smaller surface area, differences in cell numbers,

and decreased VCAM-1 expression, we believe that the nanotube topography is regulating cell phenotype in a different mechanism. Some potential examples include the regulation of focal adhesion localization, composition of the plaque components, and focal adhesion size [43].

In smooth muscle cells, nanotube topography led decreased total FAK expression, but an increased ratio of phosphorylated FAK. Increased FAK expression is correlated with increased traction forces and cell spreading area [44], [45], which agrees with our data illustrating that cells on flat surfaces, which had higher FAK expression, also had greater spreading area compared to NT90 surfaces. The decreased FAK expression could be explained by the decreased amount of available surface area on TiO_2 nanotube surface, since cells can likely only adhere to the walls of the tubes and not the void space in the middle of the nanotube. This means that there is less area for cells to attach and form focal adhesions. Despite the decrease in FAK protein expression, there is an increase in the ratio of phosphorylated FAK. This could be a compensatory mechanism through which the cells try to exert enough traction force despite the decreased number of focal adhesions. Further, there is a well-documented cross-talk between growth factor receptor and integrin-mediated signaling in cells [46], [47]. The formation and phosphorylation of FAK is likely to affect growth-factor signaling and other downstream cellular processes, which likely contributes to the differences we observed in SMC response to TNFα stimulation when cultured on NT90 versus flat surfaces.

2.5.4 Vascular cell responses to TiO2 nanotubes are diameter-dependent

Cellular response to topography can be influenced by the size and density, and regularity of the features [48], [49] , and the response is often cell-type dependent [50]. Cells attach to substrates via integrins, and several studies have shown that ECM ligand and integrin spacing affect focal adhesion formation, growth factor signaling, proliferation, and more [43], [48], [51].

The geometric constraints of the TiO_2 nanotube surfaces affect the possible patterns of integrin clustering, focal adhesion activation, and subsequent downstream signaling events. Further, TiO_2 nanotubes with varying diameters have been shown to exert different effects on cells. However, conflicting reports exist regarding the diameters that are optimal for eliciting the desired cellular response for a stent material. For example, Park *et al* found that TiO_2 nanotubes of 15-30 nm in diameter can increase endothelial cell adhesion, whereas nanotubes of 100 nm in diameter caused increased apoptosis [20]. On the other hand, Zhong *et al* reported that TiO_2 nanotubes of 110 nm increased endothelial cell proliferation [35]. We tuned nanotube diameter to study how it affects cell-substrate interactions and changes in cell growth and inflammation.

In terms of endothelial cell number, we found that there is no statistically significant difference in cell number amongst any of the TiO_2 nanotube surfaces. This data suggests that while the presence of nanotubes has an effect on cell number, changing the nanotube size does not significantly affect EC cell adhesion and growth. For SMC cells, the largest nanotubes, NT90 resulted in the greatest decrease in SMC cell number compared to flat and smaller-diameter nanotube surfaces. Our findings with endothelial cells are agree with previous studies on the effect of RGD ligand density on cell adhesion and cell area. Le Saux *et al* fabricated surfaces with controlled RGD ligand density and size, and measured endothelial cell adhesion and cell area[48]. The study reported that with decreased RGD density, cell adhesion increased significantly until a certain threshold, and then began to decrease. In our study, nanotube surfaces can be comparable to surfaces with decreased ligand density, since the nanotube geometry constrains the available adhesive area for cells to attach. We found that nanotube surfaces affect cell spreading area in both cell types, but the effect was cell type-dependent. Whereas nanotubes increased EC number, they decreased SMC number. This differential

response observed once again illustrates that the response to changing feature sizes depends on the cell type, and we can take advantage of this differential cell response to engineer material surfaces to have specific therapeutic outcomes.

We measured functional outputs in response to TiO_2 nanotubes of varying diameters. In some cases, the presence of nanotubes of any diameter led to significant changes in cell behavior. For instance, SMC growth in response to TNFα stimulation was significantly decreased on all nanotube surfaces compared to flat titanium. In other cases, the response to diameter is a graded response. For example, increasing nanotube diameters led to greater decreases in VCAM-1 expression in ECs. Lastly, there are other cases in which only the largest NT90 surfaces had an effect on cell phenotype, while NT30 and NT50 cause no change compared to flat surfaces. This was the case of MCP-1 production in SMCs. Given these observations, it is possible that there also exists a threshold of ligand spacing and density that is necessary to elicit a specific response, and that this difference is dependent on the cell type and the signaling pathways involved.

We also found that changing surface roughness independently of nanotube diameter led to changes in EC surface area, but not affect SMC area and cell number. Moreover, while NT90* surfaces with decreased surface roughness could potentially increase EC coverage, the anti-inflammation effects were diminished compared to NT90 surfaces. Thus, surface roughness is another important parameter to tune for modulating cell response, including cell spreading and response to inflammation. Our results show that NT90 surfaces are a promising combination of nanotube diameter and surface roughness to achieve an anti-restenotic phenotype in vascular endothelial and smooth muscle cells.

2.6 Conclusion

In this study, we fabricated TiO_2 nanotubes with 90 nm diameters to investigate how the presence of nanotube geometry affects endothelial and smooth muscle cell response, with the goal of designing a surface coating for bare metal stents that can decrease restenosis. We observed that nanotube surfaces decreased SMC coverage by decreasing both cell adhesion and cell spreading area. In addition, we found significant reductions in the inflammatory responses of both cell types cultured on nanotubes compared to unmodified surfaces: TiO_2 nanotube surfaces attenuated TNFα-induced SMC proliferation, as well as TNFα-induced EC adhesion molecule expression. Further, we compared the 90 nm nanotubes with 30 nm and 50 nm nanotubes and found that 90 nm nanotubes led to the greatest decrease in SMC coverage and inflammatory response. Taken together, we show that TiO_2 nanotube surface coatings on stents are a promising alternative to DES for decreasing restenosis.

2.7 Acknowledgements, and Disclosures

We acknowledge research support from the Alfred Mann Institute, the National Institutes of Health, and the National Science Foundation Graduate Research Fellowship.

Thank you to Dr. Frances Allen at the UC Berkeley Biomolecular Nanotechnology center for advice and assistance with helium ion microscopy data acquisition. Thank you to the staff at the UC Berkeley Electron Microscope Laboratory for assistance with sample preparation. We gratefully acknowledge the use of the JPK Instruments AFM and supporting equipment at SF State. The JPK Instruments AFMs and supporting facilities were obtained under NSF MRI award # NSF MRI award #1626611. We would also like to thank Kayla Wolf and Katie Cabral for their scientific input and advice during this study.

2.8 References

[1] C. P. Regan *et al.*, "Molecular mechanisms of decreased smooth muscle differentiation marker expression after vascular injury," *J. Clin. Invest.*, vol. 106, no. 9, pp. 1139–1147, Nov. 2000.

[2] V. J. Dzau, R. C. Braun-Dullaeus, and D. G. Sedding, "Vascular proliferation and atherosclerosis: New perspectives and therapeutic strategies," *Nat. Med.*, vol. 8, no. 11, pp. 1249–1256, Nov. 2002.

[3] A. Cuneo and M. Autieri, "Expression and Function of Anti-Inflammatory Interleukins: The Other Side of the Vascular Response to Injury," *Curr. Vasc. Pharmacol.*, vol. 7, no. 3, pp. 267–276, Jul. 2009.

[4] L. Denes, L. Entz, and V. Jancsik, "Restenosis and therapy.," *Int. J. Vasc. Med.*, vol. 2012, p. 406236, 2012.

[5] I.-M. . Chung, H. K. Gold, S. M. Schwartz, Y. Ikari, M. A. Reidy, and T. N. Wight, "Enhanced extracellular matrix accumulation in restenosis of coronary arteries after stent deployment," *J. Am. Coll. Cardiol.*, vol. 40, no. 12, pp. 2072–2081, Dec. 2002.

[6] C. Kaiser *et al.*, "Drug-Eluting versus Bare-Metal Stents in Large Coronary Arteries," *N. Engl. J. Med.*, vol. 363, no. 24, pp. 2310–2319, Dec. 2010.

[7] M. Sabate *et al.*, "Everolimus-eluting stent versus bare-metal stent in ST-segment elevation myocardial infarction (EXAMINATION): 1 year results of a randomised controlled trial," *Lancet*, vol. 380, no. 9852, pp. 1482–1490, Oct. 2012.

[8] G. Nakazawa *et al.*, "Delayed arterial healing and increased late stent thrombosis at culprit sites after drug-eluting stent placement for acute myocardial infarction patients: an autopsy study.," *Circulation*, vol. 118, no. 11, pp. 1138–45, Sep. 2008.

[9] K. Katsanos, S. Spiliopoulos, P. Kitrou, M. Krokidis, and D. Karnabatidis, “Risk of Death Following Application of Paclitaxel-Coated Balloons and Stents in the Femoropopliteal Artery of the Leg: A Systematic Review and Meta-Analysis of Randomized Controlled Trials.,” *J. Am. Heart Assoc.*, vol. 7, no. 24, p. e011245, Dec. 2018.

[10] M. Shuchman, “Trading Restenosis for Thrombosis? New Questions about Drug-Eluting Stents,” *N. Engl. J. Med.*, vol. 355, no. 19, pp. 1949–1952, Nov. 2006.

[11] K. R. Kam, L. A. Walsh, S. M. Bock, J. D. Ollerenshaw, R. F. Ross, and T. A. Desai, “The effect of nanotopography on modulating protein adsorption and the fibrotic response.,” *Tissue Eng. Part A*, vol. 20, no. 1–2, pp. 130–8, Jan. 2014.

[12] L. A. Walsh, J. L. Allen, and T. A. Desai, “Nanotopography applications in drug delivery.,” *Expert Opin. Drug Deliv.*, vol. 12, no. 12, pp. 1823–7, 2015.

[13] J. Kim, E. B. Schlesinger, and T. A. Desai, “Nanostructured materials for ocular delivery: nanodesign for enhanced bioadhesion, transepithelial permeability and sustained delivery.,” *Ther. Deliv.*, vol. 6, no. 12, pp. 1365–76, 2015.

[14] V. Uskoković and T. A. Desai, “Nanoparticulate drug delivery platforms for advancing bone infection therapies,” *Expert Opin. Drug Deliv.*, vol. 11, no. 12, pp. 1899–1912, Dec. 2014.

[15] C. R. Zamecnik, M. M. Lowe, D. M. Patterson, M. D. Rosenblum, and T. A. Desai, “Injectable Polymeric Cytokine-Binding Nanowires Are Effective Tissue-Specific Immunomodulators,” *ACS Nano*, vol. 11, no. 11, pp. 11433–11440, Nov. 2017.

[16] C. R. Zamecnik, E. S. Levy, M. M. Lowe, B. Zirak, M. D. Rosenblum, and T. A. Desai, “An Injectable Cytokine Trap for Local Treatment of Autoimmune Disease,” *Biomaterials*, p. 119626, Nov. 2019.

[17] M. K. Singh *et al.*, “Integrated biomimetic carbon nanotube composites for in vivo systems,” *Nanoscale*, vol. 2, no. 12, p. 2855, Dec. 2010.

[18] D. C. Miller, A. Thapa, K. M. Haberstroh, and T. J. Webster, “Endothelial and vascular smooth muscle cell function on poly(lactic-co-glycolic acid) with nano-structured surface features,” *Biomaterials*, vol. 25, no. 1, pp. 53–61, 2004.

[19] T.-W. Chung, D.-Z. Liu, S.-Y. Wang, and S.-S. Wang, “Enhancement of the growth of human endothelial cells by surface roughness at nanometer scale,” *Biomaterials*, vol. 24, no. 25, pp. 4655–4661, Nov. 2003.

[20] J. Park, S. Bauer, P. Schmuki, and K. von der Mark, “Narrow Window in Nanoscale Dependent Activation of Endothelial Cell Growth and Differentiation on TiO_2 Nanotube Surfaces,” *Nano Lett.*, vol. 9, no. 9, pp. 3157–3164, Sep. 2009.

[21] E. K. F. Yim, R. M. Reano, S. W. Pang, A. F. Yee, C. S. Chen, and K. W. Leong, “Nanopattern-induced changes in morphology and motility of smooth muscle cells.,” *Biomaterials*, vol. 26, no. 26, pp. 5405–13, Sep. 2005.

[22] P. Roy, S. Berger, and P. Schmuki, “TiO2 Nanotubes: Synthesis and Applications,” *Angew. Chemie Int. Ed.*, vol. 50, no. 13, pp. 2904–2939, Mar. 2011.

[23] L. Peng, M. L. Eltgroth, T. J. LaTempa, C. A. Grimes, and T. A. Desai, “The effect of TiO2 nanotubes on endothelial function and smooth muscle proliferation,” *Biomaterials*, vol. 30, no. 7, pp. 1268–1272, 2009.

[24] H. Nuhn, C. E. Blanco, and T. A. Desai, “Nanoengineered Stent Surface to Reduce In-Stent Restenosis *in Vivo*,” *ACS Appl. Mater. Interfaces*, vol. 9, no. 23, pp. 19677–19686, Jun. 2017.

[25] K. Noda, J. Zhang, S. Fukuhara, S. Kunimoto, M. Yoshimura, and N. Mochizuki,

"Vascular endothelial-cadherin stabilizes at cell-cell junctions by anchoring to circumferential actin bundles through alpha- and beta-catenins in cyclic AMP-Epac-Rap1 signal-activated endothelial cells.," *Mol. Biol. Cell*, vol. 21, no. 4, pp. 584–96, Feb. 2010.

[26] T. Suzuki *et al.*, "Stent-Based Delivery of Sirolimus Reduces Neointimal Formation in a Porcine Coronary Model," *Circulation*, vol. 104, no. 10, pp. 1188–1193, Sep. 2001.

[27] F. G. P. Welt and C. Rogers, "Inflammation and Restenosis in the Stent Era," *Arterioscler. Thromb. Vasc. Biol.*, vol. 22, no. 11, 2002.

[28] P. S. Monraats *et al.*, "Tumor necrosis factor-α plays an important role in restenosis development," *FASEB J.*, vol. 19, no. 14, pp. 1998–2004, Dec. 2005.

[29] C. Lawson and S. Wolf, "ICAM-1 signaling in endothelial cells.," *Pharmacol. Rep.*, vol. 61, no. 1, pp. 22–32.

[30] J. M. Cook-Mills, M. E. Marchese, and H. Abdala-Valencia, "Vascular Cell Adhesion Molecule-1 Expression and Signaling During Disease: Regulation by Reactive Oxygen Species and Antioxidants," *Antioxid. Redox Signal.*, vol. 15, no. 6, pp. 1607–1638, Sep. 2011.

[31] P. Heider, M. G. Wildgruber, W. Weiss, H. J. Berger, E. H. Henning, and O. Wolf, "Role of adhesion molecules in the induction of restenosis after angioplasty in the lower limb," *J. Vasc. Surg.*, vol. 43, no. 5, pp. 969–977, May 2006.

[32] S. Bayata, E. Arikan, M. Yesil, N. Postaci, A. Tas, and M. Koseoglu, "An important role for VCAM-1, but not for ICAM-1 in restenosis following coronary stent implantation," *Anadolu Kardiyol. Dergisi/The Anatol. J. Cardiol.*, vol. 10, no. 5, pp. 405–409, Oct. 2010.

[33] S. Choi *et al.*, "TNF-α elicits phenotypic and functional alterations of vascular smooth muscle cells by miR-155-5p-dependent down-regulation of cGMP-dependent kinase 1.,"

J. Biol. Chem., vol. 293, no. 38, pp. 14812–14822, Aug. 2018.

[34] R. Davis, S. Pillai, N. Lawrence, and S. P. Chellappan, "TNF-α-mediated proliferation of vascular smooth muscle cells involves Raf-1-mediated inactivation of Rb and transcription of E2F1-regulated genes," *Cell Cycle*, vol. 11, no. 1, pp. 109–118, Jan. 2012.

[35] S. Zhong *et al.*, "Effects of polydopamine functionalized titanium dioxide nanotubes on endothelial cell and smooth muscle cell," *Colloids Surfaces B Biointerfaces*, vol. 116, pp. 553–560, 2014.

[36] A. Farb *et al.*, "Extracellular matrix changes in stented human coronary arteries," *Circulation*, vol. 110, no. 8, pp. 940–947, 2004.

[37] R. Kornowski, M. K. Hong, F. O. Tio, O. Bramwell, H. Wu, and M. B. Leon, "In-Stent Restenosis: Contributions of Inflammatory Responses and Arterial Injury to Neointimal Hyperplasia," *J. Am. Coll. Cardiol.*, vol. 31, no. 1, pp. 224–230, Jan. 1998.

[38] A. Farb *et al.*, "Pathology of Acute and Chronic Coronary Stenting in Humans," *Circulation*, vol. 99, no. 1, pp. 44–52, Jan. 1999.

[39] S. Oguchi *et al.*, "Monoclonal Antibody Against Vascular Cell Adhesion Molecule-1 Inhibits Neointimal Formation After Periadventitial Carotid Artery Injury in Genetically Hypercholesterolemic Mice," *Arterioscler. Thromb. Vasc. Biol.*, vol. 20, no. 7, pp. 1729–1736, Jul. 2000.

[40] Y. Qu *et al.*, "VCAM-1 siRNA reduces neointimal formation after surgical mechanical injury of the rat carotid artery," *J. Vasc. Surg.*, vol. 50, no. 6, pp. 1452–1458, Dec. 2009.

[41] E. Mori *et al.*, "Essential Role of Monocyte Chemoattractant Protein-1 in Development of Restenotic Changes (Neointimal Hyperplasia and Constrictive Remodeling) After Balloon Angioplasty in Hypercholesterolemic Rabbits," *Circulation*, vol. 105, no. 24, pp. 2905–

2910, Jun. 2002.

[42] P. W. Bryant, Q. Zheng, and K. M. Pumiglia, “Focal adhesion kinase is a phospho-regulated repressor of Rac and proliferation in human endothelial cells.,” *Biol. Open*, vol. 1, no. 8, pp. 723–30, Aug. 2012.

[43] E. A. Cavalcanti-Adam, T. Volberg, A. Micoulet, H. Kessler, B. Geiger, and J. P. Spatz, “Cell Spreading and Focal Adhesion Dynamics Are Regulated by Spacing of Integrin Ligands,” *Biophys. J.*, vol. 92, no. 8, pp. 2964–2974, Apr. 2007.

[44] ‡ Cynthia A. Reinhart-King, § and Micah Dembo, and ‡ Daniel A. Hammer*, “Endothelial Cell Traction Forces on RGD-Derivatized Polyacrylamide Substrata†,” 2002.

[45] I. M. Tolić-Nørrelykke and N. Wang, “Traction in smooth muscle cells varies with cell spreading,” *J. Biomech.*, vol. 38, no. 7, pp. 1405–1412, Jul. 2005.

[46] F. Wang *et al.*, “Reciprocal interactions between beta1-integrin and epidermal growth factor receptor in three-dimensional basement membrane breast cultures: a different perspective in epithelial biology.,” *Proc. Natl. Acad. Sci. U. S. A.*, vol. 95, no. 25, pp. 14821–6, Dec. 1998.

[47] Z. Mostafavi-Pour, J. A. Askari, S. J. Parkinson, P. J. Parker, T. T. C. Ng, and M. J. Humphries, “Integrin-specific signaling pathways controlling focal adhesion formation and cell migration,” *J. Cell Biol.*, vol. 161, no. 1, p. 155, Apr. 2003.

[48] G. Le Saux *et al.*, “Spacing of Integrin Ligands Influences Signal Transduction in Endothelial Cells,” *Biophys. J.*, vol. 101, no. 4, pp. 764–773, Aug. 2011.

[49] G. Le Saux, A. Magenau, T. Böcking, K. Gaus, and J. J. Gooding, “The Relative Importance of Topography and RGD Ligand Density for Endothelial Cell Adhesion,” *PLoS One*, vol. 6, no. 7, p. e21869, Jul. 2011.

[50] W. Chen, Y. Shao, X. Li, G. Zhao, and J. Fu, “Nanotopographical Surfaces for Stem Cell Fate Control: Engineering Mechanobiology from the Bottom.,” *Nano Today*, vol. 9, no. 6, pp. 759–784, Dec. 2014.

[51] M. Arnold *et al.*, “Activation of Integrin Function by Nanopatterned Adhesive Interfaces,” *ChemPhysChem*, vol. 5, no. 3, pp. 383–388, Mar. 2004.

Recent advances in intraocular sustained-release drug delivery devices

3.1 Abstract

Topical eye-drop administration and intravitreal injections are the current standard for ocular drug delivery. However, patient adherence to the drug regimen and insufficient administration frequency are well-documented challenges to this field. In this review, we describe recent advances in intraocular implants designed to deliver therapeutics for months to years, in order to obviate the issues of patient adherence. We highlight recent advances in monolithic ocular implants in literature, the commercialization pipeline, and approved for the market. We describe design considerations based on material selection, active pharmaceutical ingredient, and implantation site.

3.2 Introduction

Elderly populations have increased incidences of ocular disease [1], [2], and as life expectancy increases, the burden of managing and treating ocular disease will become more prevalent [3]. Many ocular diseases have striking impacts to vision that significantly impact quality of life, eventually making everyday tasks difficult to impossible.

Therapeutic treatment of ocular disease falls into two primary modalities: topical drops or intravitreal injections. Topical drops have been a mainstay for decades. Specific to asymptomatic disease, such as glaucoma, compliance is a major challenge to efficacious therapy: a review across 5 studies showed an average of only 67% of glaucoma patients sustained their therapeutic schedule after one year [4].

Intraocular injections were the first effective back-of-the-eye therapy, most notably with the approval of ranibizumab (Lucentis®, Genentech, Inc.) and the subsequent approval of aflibercept (EYLEA®, Regeneron Pharmaceuticals) for treatment of wet age-related macular degeneration (wAMD). However, recent retrospective studies observed that real-world use and injection frequency did not replicate trial outcomes, largely due to insufficient administration frequency [5].

The first commercial examples of implantable intraocular devices were surgically implanted reservoir-based devices introduced via pars plana incision and sutured to the sclera for long-term residence within the eye. These devices (e.g. Vitrasert® for cytomegalovirus or Retisert® for non-infectious uveitis) release a small molecule therapeutic over the course of months to years [6], [7]. The subsequent generation of devices aimed to reduce the procedural invasiveness by introducing the device with a custom injector. Both degradable (e.g. Ozurdex®) and non-degradable (e.g. Iluvien®) versions became commercially available, where the rod-shaped implants are deployed by piston or fluid [8], [9]. To date, commercial intraocular devices have relied on small molecule therapeutics, leaving a significant opportunity in highly efficacious protein-based delivery technologies.

Despite some successes in device development, novel treatments that could supplant topical drops and intravitreal injection remain poised to advance treatment of ocular disease. External devices provide a means to maintain the minimally invasive advantage of topical drops, while providing a sustained release solution [10]. Alternatively, particle technologies are suitable for deployment via the familiar intravitreal injection, while providing an extended duration of therapeutic activity [11], [12]. In this review we will focus on a final class of sustained delivery devices that are monolithic and implanted intraocularly, which may be introduced via custom

injector or by surgical intervention. We will discuss recent advances in implantable intraocular devices, covering design considerations based on drug type, and means of delivering devices and final implantation site, as well as commercial and pipeline device development.

3.3 Material Selection

The material selection for long-acting, sustained release implants is critical for tuning the release kinetics, degradation rate, and biocompatibility. Both biodegradable and nonbiodegradable materials have been used for ocular drug delivery implants reported in literature and currently on the market. This section covers the commonly used materials for ocular drug delivery, including their tunability, biocompatibility, and degradation kinetics.

3.3.1 Non-biodegradable polymers

Non-biodegradable implants are commonly used for the first generation of ocular drug delivery implants. This includes Retisert® and Vitrasert®, which consist of drug tablets coated with non-biodegradable polymers. Commonly used non-degradable materials include polyvinyl alcohol (PVA), ethylene-vinyl acetate (EVA), and silicones. In Retisert®, the drug tablet is coated with a nonpermeable silicone featuring an orifice to allow drug release. Between the silicone orifice and the tablet, there is a permeable PVA membrane to control the rate of diffusion through the orifice. Vitrasert® employs a similar concept of diffusion-limited drug release through the orifice of a nonpermeable coating. Vitrasert® consists of a tablet first coated with PVA, followed by a nonpermeable, discontinuous EVA coating, which is then covered by a second coating of PVA. Other non-biodegradable implants in the market, such as Iluvien® (Alimera Sciences, Inc), consist of a polyimide tube loaded with a drug-PVA matrix, and capped on one end with a silicone adhesive. Another non-degradable material is crosslinked

poly(ethylene glycol) (PEG). For example, PEGDA, a photo-crosslinkable PEG hydrogel, has been reported to release triamcinolone acetonide and ovalbumin, a model protein [13].

Non-biodegradable implants have the advantage of achieving very long-term release and have demonstrated good biocompatibility [14]. However, upon drug depletion, the reservoir material either requires surgical removal or remains at the implantation site. In recent years, focus has shifted toward using biodegradable polymers for ocular implants.

3.3.2 Biodegradable polymers

Biodegradable or erodible polymers have been increasingly used in implants both in academic research and on the market. They have the advantage of eroding after drugs are released to avoid the need for surgical removal. Their degradation kinetics can also be tuned by material composition.

Commonly used biodegradable polymers include poly(lactic-co-glycolic acid) (PLGA) and poly(caprolactones) (PCL). The most widely used in both literature and commercially is PLGA. It can be engineered to achieve sustained release for several small molecules [15]–[17]. Commercially, PLGA is co-extruded with dexamethasone in Ozurdex® (Allergan) to achieve 6 months of drug delivery.

A limitation of PLGA is the formation of inflammatory degradation products. PLGA degrades into lactic acid and glycolic acid, which create a highly acidic environment [18] and cause local inflammatory reactions [19]. In one study, PLGA scaffolds were implanted subcutaneously into rats to observe host-tissue responses after 2 weeks. The authors observed significant host cell and macrophage accumulation near the PLGA scaffold, indicative of a severe inflammatory reaction [19]. These inflammatory effects are alleviated in implants that

release anti-inflammatory steroids, such as the case of Ozurdex® (described later). However, when releasing other drugs, the inflammatory responses may cause problematic reactions.

Polycaprolactone (PCL) is another biodegradable polymer that has been demonstrated in ocular drug delivery implants in literature. Like PLGA, PCL can be engineered to have highly tunable release kinetics and is easily fabricated into thin films by draw or spin casting polymer solutions. Studies of PCL in the eye have not elicited significant immunologic responses [20]–[22]. PCL degradation kinetics are slower than that of PLGA but can be tuned by adjusting the polymer molecular weight [23], [24].

While PEG itself is not degradable, it can be conjugated to and crosslinked by biodegradable linkers to form an absorbable material. In-situ forming PEG-based implants are under development by Ocular Therapeutix to deliver tyrosine kinase inhibitors (TKI) (NCT03630315). Polyorthoesters (POEs) and polyanhydrides are other materials used, though they have not been actively used commercially or in literature in recent years.

3.4 Design considerations based on drug type

3.4.1 Sustained delivery of small molecules

Most of the ophthalmic drug delivery technologies are currently targeted towards sustained delivery of small molecule therapeutics over the course of several months to years. Small molecules are conventionally delivered via eye drops and may require several administrations per day. A sustained-release implant would obviate the need for daily patient administration in favor of device implantation every few months or years. Drugs can also be co-extruded within polymer matrices to achieve long-term release with desired release kinetics. Release kinetics can be dissolution- [20] or solubility-limited [21] and depend on drug and

polymer properties, including partition coefficient, LogP, molecular weight, and drug solubility [25]. Both zero-order and first-order release profiles have been demonstrated [25]–[27], and release rate can be tuned by surface area and film thickness. The release duration is dependent on the amount of drug within the reservoir and the polymeric membranes degradation kinetics.

Within the past 2 years, PLGA has been used for the sustained release of small molecules including etoposide [16], lupeol [15], and clindamycin hydrochloride [17] (Table 3.1) with a release duration on the order of months. Since PLGA undergoes both bulk degradation and surface degradation [23], the release kinetics of long-acting implants may change during the course of polymer degradation. PLGA can also be formulated as a suspension with the drug of interest and a biocompatible solvent (e.g. N-methyl-2-pyrrolidone) that can be injected and formed *in situ*. *In situ* forming PLGA implants have been used to release triamcinolone acetonide [28] and dexamethasone [29], achieving 42 days and 1 week of sustained release respectively *in vitro*. In *in situ*-forming implants, polymer concentration can be tuned to achieve desired release kinetics. PCL thin-film ocular drug delivery devices have demonstrated *in vivo* release of rapamycin for 16 weeks [26] and omidenapag isopropyl (DE-117) for 24 weeks [30]. Since PCL degradation is much slower, drug release kinetics can be decoupled from polymer degradation kinetics.

Table 3.1 Recent developments in ocular implants for long-acting drug delivery in literature (2017-2018)

Material	Drug	Implantation Site	Release profile	Indication	Phase	Ref
Small Molecule Delivery Devices						
PLGA-NMP (in-situ forming PLGA)	Triamcinolone acetonide	N/A	42 days release	NA	*In vitro*	[28]
PLGA-NMP (in-situ forming PLGA)	Dexamethasone	N/A	Over ~1 week	AMD	*In vitro*	[29]
PLGA	Clindamycin hydrochloride	Intravitreal	6 weeks	Infection	*In vivo*	[17]
PLGA	Etoposide	Intravitreal	50 days	Retinoblastoma	*In vivo*	[16]
PLGA scleral plug	Curcumin	intravitreal	60 days	Posterior ocular diseases	*In vivo*	[42]
PLGA	Lupeol		7 days	Angiogenesis	*In vivo*	[15]
PCL	DE-117	Intracameral	24 weeks	Glaucoma	*In vivo*	[30]
PEGDA	Triamcinolone acetonide	N/A	21–28 days	AMD	*In vitro*	[13]
Protein Delivery Devices						
PDMS/PVA	Infliximab	Subconjunctival	3 months	Alkali Burns	*In vivo*	[35]
Hyaluronic acid, embedded with chitosan NP	Bevacizumab	N/A	60 days	Choroidal neovascularization (CNV)	*In vitro*	[34]

3.4.2 Sustained delivery of proteins and biologics

Biopharmaceuticals including proteins and peptides have shown great promise as novel therapeutics in the treatment of ocular diseases. Unlike small molecules, biologics have high potency and activity, low nonspecific binding, as well as lower toxicity and drug-drug interactions. With the approval of anti-VEGF therapeutics such ranibizumab (Lucentis®; Genentech, California), the market for ocular biopharmaceuticals is rapidly growing. However, patient compliance to monthly intravitreal injections has been a major hurdle with these treatments. In a recent study, 39.8% of AMD patients showed inadequate compliance to Lucentis treatment and follow-up [31]. Anti-VEGF therapies requiring less frequent injections are available (Aflibercept; Regeneron Pharmaceuticals), or under development (Abicipar; Allergan). Nevertheless, there is an urgent need for the development of suitable ocular delivery systems for biologics to alleviate patient compliance concerns. Biologics offer many delivery challenges due to their high molecular weight, hydrophilicity, degradation, short half-life, and poor permeability across epithelial barriers [32], [33]. Therefore, novel delivery systems are needed to enable the delivery of biologics to ocular tissues.

Much of the focus in protein drug delivery has been on gel-based formulations and reservoir systems. Gel-based formulations consist of liquid or injectable semi-solids with protein suspended in organic solvent that solidify upon injection [33]. The rate and duration of release is influenced by the gelling rate as well as implant porosity, polymer molecular weight, and solvent. Badiee *et al.* used chitosan nanoparticles embedded in a matrix of hyaluronic acid and zinc sulfate to provide long-term sustained release of becavizumab [34]. They showed this system enhanced sustained release compared to bevacizumab particles. Another study used a

porous polydimethylsiloxane/polyvinyl alcohol composite drug delivery system to deliver infliximab for 3 months in rabbits after an ocular burn [35].

For membrane-based reservoir systems, nonporous membranes used for delivering small molecules do not allow for the diffusion of larger proteins. Macroporous membranes fabricated by mixing porogens with a polymer would allow diffusion of proteins, but cannot achieve zero-order release. In order to achieve sustained, zero-order release of proteins, nanoporous PCL thin films were engineered with pore sizes on the order of the diffusing molecule size [36]. This nanoporous PCL thin film device was capable of delivering ranibizumab for 12 weeks in vivo without exhausting the initial drug payload [26]. Furthering thin film devices, a methodology was developed for design of such devices that utilized a PEG formulation to control protein solubility [37]. The corresponding devices can be engineered to achieve desired protein stability and release rate. The devices studied released aflibercept over the course of 11 weeks in vitro, and devices were well-tolerated in African green monkeys.

The Genentech/Forsight Vision 4 Port Delivery System is another reservoir device for delivering ranibizumab. The device is a scleral plug consisting of a reservoir, a semi-permeable, non-biodegradable membrane, and a port used to reload drug into the reservoir. Initial drug loading typically limits the total drug release duration and device lifetime and the refillable port was developed to address this challenge. The implant has been loaded with ranibizumab for the treatment of wAMD, and device is designed to last at least 6 months between refills [38].

With long-acting delivery systems for biologics, understanding the stability of the protein or biologic of interest at physiological temperature is essential. Proteins can undergo structural changes or degradation that lead to loss of biological activity over time. Biologics in long-acting implants can be engineered or formulated to be stable for the required release duration. In some

cases, using solubility-limiting excipients can improve protein stability, such as PEG in an aflibercept-eluting thin-film device [37]. However, due to the unique nature of each biologic, particularly antibodies, there is no single formulation that can effectively improve stability for all biologics [39]. Therefore, a thorough understanding of the possible degradation mechanisms for a particular biologic is necessary for their success in sustained-delivery systems.

Despite many advances, to date no ophthalmic biodegradable implant has been approved for biopharmaceutical drugs. With the large and growing numbers of protein and large molecule therapeutics under clinical trials, there remains an urgent need to develop new methods to deliver these highly potent biologics in a controlled and long-term manner.

3.4.3 Cells-based implants

Cell encapsulation is a novel way to deliver large compounds to tissues for an extended period of time. Neurotech Pharmaceuticals uses a unique customized NTC-200 cell line derived from normal human retinal pigment epithelial cells. These cells are engineered to have low metabolic activity, increasing likelihood of survival in the vitreous. The cells can also be genetically transfected to secrete therapeutics and growth factors. The cells are incorporated into a polymeric device that is surgically implanted in the vitreous, and the ocular implant enables continuous production and release of therapeutic proteins to the eye for over 2 years. The device isolates the cells from the vitreous while simultaneously allowing influx of nutrients. Their investigational treatment, NT-501 ECT, provides intravitreal sustained release of soluble ciliary neurotrophic factor (CNTF) receptor. The device was well-tolerated but achieved limited efficacy in treating retinitis pigmentosa (RP) [40], [41] and geographic atrophy (GA) [42]. Neurotech is now applying NT-501 in clinical studies for the treatment of glaucoma (NCT02862938) and macular telangectasia (MacTel) (NCT01949324). For glaucoma, Neurotech

has completed Phase I trials, and phase II studies are currently underway. Phase I trials of MacTel showed good tolerability and safety for the device [43].

3.5 Delivery and Implantation Site Considerations

Implantation site selection depends on the desired pharmacokinetics, biocompatibility, and clinical considerations. An implantation site closer to the target tissue can achieve a high concentration of drug in the target tissue. Drugs may diffuse from the anterior chamber to the posterior chamber by convection and normal movements, though the kinetics depend on the chemistry of the drug [44]. However, drug distribution between the anterior to the posterior segment may be hindered by aqueous flow, clearance to the blood, and the physical barrier of the iris, lens, and ciliary body. Pharmacokinetics of drug transport to various tissues in the eye must be tested for a particular drug and implantation location.

Common methods of implantation are intravitreal injection, subconjunctival delivery [45], and intracameral implantation via incision [27], [45].The most attractive route for delivery to the vitreous is via injection, as it duplicates the standard-of-care for existing anti-VEGF therapeutics. Implantable devices can be injected at the pars plana, which is located posterior to the lens and anterior to the retina. At this location in the vitreous, implant position can be controlled to be out of the visual axis. However, intravitreal implants can risk retinal detachment and endophthalmitis [46] as well as vitreous hemorrhage, cystoid macular edema, and formation of tenacious epiretinal membranes [47]. Placement is also critical for intracameral implants due to the risk of blocking vision. Development of cataracts due to contact with the lens, or damage to the corneal epithelium [27] are also potential risks. Subconjunctival implantation has also been

explored for Ozurdex®, and the implants were well-tolerated in the 2-month study in patients with open-angle glaucoma [48].

The injection needle also affects clinical outcomes. Standard intravitreal injections of Lucentis® or EYLEA® use 30-gauge needles, but drug delivery devices require larger gauge needles, such as 22- and 25-gauge for Ozurdex® and Iluvien®. Larger needles do not necessarily lead to more pain. A study showed that patients receiving 22-gauge injections had similar pain scores to those receiving 29-gauge injections [49]. The shape and size of the needle can also be optimized to improve clinical outcomes. An Ozurdex® study showed that optimizing needle shape can reduce required penetration force, improve the wound architecture, and increase ease of injection [50].

3.6 Implantable ocular drug delivery devices on the market or in the commercialization pipeline

3.6.1 Recently Approved Implants

The number of companies developing ocular drug delivery implants has skyrocketed over the past decade. Products in various stages of development are being investigated for indications such as glaucoma, macular degeneration, diabetic macular edema, and uveitis.

Vitrasert® and Retisert® have been widely reviewed since their approvals in 1996 and 2004. Since then, Ozurdex®, Iluvien®, Yutiq®, and DEXYCU® have been approved for sustained-release intraocular drug delivery (Table 3.2). Iluvien® (Alimera) is a non-erodible

Table 3.2 FDA approved intraocular drug delivery implants in the market

Implant	Approval Year	Material	Delivery method	Drug	Indication	Release duration	Clinical Trial / NDA
Vitrasert®	1996	PVA, EVA	Intravitreal	Ganciclovir	AIDS-related cytomegalovirus retinitis	5-8 months	20569
Retisert®	2004	PVA, silicone	Intravitreal	Flucinolone acetonide	Noninfectious uveitis	2.5 years	21737
Ozurdex®	2009	PLGA	Intravitreal	Dexamethosone	DME, posterior uveitis	6 months	22315
Iluvien®	2014	Polyimide	Intravitreal	Flucinolone acetonide	DME	3 years	201923
Yutiq®	2018	Polyimide	Intravitreal	Flucinolone acetonide	Chronic noninfectious uveitis	3 years	210331
DEXYCU®	2018	Acetyl triethyl citrate	Posterior chamber	Dexamethasone	Postoperative inflammation	2-3 weeks	208912

implant that is injected intravitreally and achieves sustained release of FA for over three years. It was approved in 2014 for the treatment of DME in patients who have been previously treated with a course of corticosteroids and did not have a clinically significant rise in intraocular pressure. Similarly, Yutiq® (EyePoint Pharmaceuticals, Watertown, MA), is a polyimide non-bioerodible intravitreal micro-insert releasing FA over 36 months. It received FDA approval in October 2018 for treatment of chronic noninfectious uveitis affecting the posterior segment of the eye.

Biodegradable implants offer some advantages over reservoir systems. In addition to the ability to be tuned to change release rates based on drug properties, they eliminate the need for extraction and thereby decrease the risk associated with surgery.

The first sustained-release biodegradable steroid implant, Ozurdex®, was developed by Allergan and approved in 2009 for treatment of macular edema following vein occlusion and noninfectious posterior uveitis. The intravitreal implant is made of PLGA co-extruded with dexamethasone. It is placed in the vitreous through the pars plana by needle injection and releases peak doses of dexamethasone for 2 months followed by a lower dose for an additional 4 months. Since its approval, many studies have investigated the efficacy of Ozurdex® for treatment of other indications such as uveitis and diabetic macular edema [51], [52] as well as trying to find ways to mitigate adverse effects of the implant such as elevated IOP [53].

Another recently approved intraocular drug delivery system uses the EyePoint Pharmaceuticals (previously Icon Biosciences, Inc) Verisome technology, an injectable suspension that allows sustained release of small molecules. DEXYCU® (Icon Biosciences, Inc) is dexamethasone suspension in acetyl triethyl citrate, and was approved in 2018 for treatment of postoperative inflammation. The suspension is injected into the posterior chamber of the eye,

where gel settles into a small sphere and slowly degrades [54]. The release duration of dexamethasone is between 2-3 weeks (NDA 208912). In clinical trial controlled by placebo, DEXYCU® led to a 2- to 3-fold increase in the proportion of patients with clearing of anterior chamber cells, and a lower proportion of patients requiring rescue medications (NCT02006888).

3.6.2 Implants in the Pipeline

Intraocular drug delivery implants that are currently in clinical trials are summarized in Table 3.3. Allergan is currently working on the development of a brimonidine tartrate intravitreal implant (Brimo PS DDS®) in patients with geographic atrophy due to age-related macular degeneration. The implant is currently in phase II clinical trials (NCT01080209). Allergan reported functional recovery after implantation of the Brimo PS DDS® system in a rabbit model of retinal ganglion cell degeneration [55]. Additionally, the implant enhanced spatial acuity in a non-human primate model of chronic glaucoma [56]. However, it remains to be seen whether inflammation due to PLGA degradation products, which may be masked in Ozurdex® as it delivers an anti-inflammatory agent, would become an issue in the brimonidine implant.

The Genentech/ForSight Vision4 Port Delivery System (PDS), as mentioned above, is a non-biodegradable, refillable reservoir device designed to deliver ranibizumab for treatment of wAMD. The refillable port is designed to extend the effective lifetime of the reservoir by delivering additional therapeutic doses when drug in the reservoir depletes. Phase II results showed that 80% of PDS patients who received a 100 mg/mL dose can go at least six months between refills, while achieving similar visual acuity outcomes as monthly ranibizumab injections [38]. Genentech is currently planning Phase III clinical trials.

Table 3.3 Investigational intraocular drug delivery implants in clinical trials

Implant	Phase	Material	Delivery method	Drug	Indication	Release duration	Clinical Trial / NDA number
OTX-TKI/IVT	Phase I	Hydrogel	Intravitreal	Tyrosine kinase inhibitors; anti-VEGF	AMD	12 months/4-6 months	NCT03630315
Port Delivery System	Phase II	Undisclosed polymer	Intravitreal	Ranibizumab	Wet AMD	~6 months before first refill	NCT02510794, NCT03677934
Brimo PS DDS®	Phase I, II	PLGA	Intravitreal	Brimonidine tartrate	Pars plana vitrectomy, AMD, retinal detachment, Geographic atrophy MD	3 to 6 months *	NCT01080209, NCT00972374

Ocular Therapeutix uses a hydrogel-based formulation technology for treating various eye diseases. OTX-TIC is a bioresorbable intracameral implant containing micronized travoprost with a target delivery duration of four to six months and is intended for patients with glaucoma. A study in beagle dogs showed that the implant was well-tolerated and released travoprost with zero-order release kinetics for 4 months [57]. Additionally, a sustained-release tyrosine kinase inhibitor (TKI) implant is under development in Phase I trials [53]. The implant is ad bioresorbable hydrogel that contains TKI particles in an injectable fiber, designed for intravitreal injection for a release duration of up to 12 months. Ocular Therapeutix is also collaborating with Regeneron Pharmaceuticals to developing a sustained-release implant for aflibercept (EYLEA®). The device, OTX-IVT is intended to reduce the frequency of injections to once every 4-6 months (ocutx.com) and is in preclinical development.

3.7 Conclusion

To date, the only successfully marketed implantable devices release small molecules, either an antiviral or a corticosteroid, and have focused on implantation in the vitreous. With increased acceptance of stent/shunt deployment for glaucoma treatment, the field will likely see new devices enter the anterior segment. The majority of existing devices are non-degradable, but their use is limited by the device therapeutic duration and requires retrieval or abandonment of depleted devices. For biodegradable devices, PLGA has been successfully employed in Ozurdex®; however, the inflammatory nature of PLGA may limit wide-spread tolerability of PLGA in intraocular applications beyond delivery of anti-inflammatory drugs.

A significant need exists to deliver protein therapeutics for treating back-of-the-eye diseases. The Port Delivery System (PDS) is poised to be the first protein delivery system within

the eye, and early trial results indicate significantly extended duration between drug administration. However, there are substantial potential complications, and the required surgical device placement may not be suitable for all patients. An injectable device that only requires administration 2-3 times per year would be a notable advance in ocular drug delivery devices, particularly if constructed from biodegradable materials. A self-coiling device is compelling as it can be injected and subsequently occupy limited space within the vitreous. An in-situ gel-based depot or reservoir-based thin film device are other promising approaches for an injectable biodegradable system for protein delivery, which may expand the competitive landscape in the coming years. While drug delivery to the eye will continue to be a difficult therapeutic area, intraocular device development has remained a source of continued innovation, and ongoing commercial successes are expected to open the field to further acceptance and adoption of novel drug delivery technologies.

3.8 References

[1] N. Congdon, B. O'Colmain, C. C. W. Klaver, R. Klein, B. Muñoz, D. S. Friedman, J. Kempen, H. R. Taylor, P. Mitchell, and Eye Diseases Prevalence Research Group, "Causes and prevalence of visual impairment among adults in the United States.," *Arch. Ophthalmol. (Chicago, Ill. 1960)*, vol. 122, no. 4, pp. 477–85, Apr. 2004.

[2] S. R. Flaxman, R. R. A. Bourne, S. Resnikoff, P. Ackland, T. Braithwaite, M. V Cicinelli, A. Das, J. B. Jonas, J. Keeffe, J. H. Kempen, J. Leasher, H. Limburg, K. Naidoo, K. Pesudovs, A. Silvester, G. A. Stevens, N. Tahhan, T. Y. Wong, H. R. Taylor, R. Vision Loss Expert Group of the Global Burden of Disease Study, P. Ackland, A. Arditi, Y. Barkana, B. Bozkurt, T. Braithwaite, A. Bron, D. Budenz, F. Cai, R. Casson, U. Chakravarthy, J. Choi, M. V. Cicinelli, N. Congdon, R. Dana, R. Dandona, L. Dandona, A. Das, I. Dekaris, M. Del Monte, J. deva, L. Dreer, L. Ellwein, M. Frazier, K. Frick, D. Friedman, J. Furtado, H. Gao, G. Gazzard, R. George, S. Gichuhi, V. Gonzalez, B. Hammond, M. E. Hartnett, M. He, J. Hejtmancik, F. Hirai, J. Huang, A. Ingram, J. Javitt, J. Jonas, C. Joslin, J. Keeffe, J. Kempen, M. Khairallah, R. Khanna, J. Kim, G. Lambrou, V. C. Lansingh, P. Lanzetta, J. Leasher, J. Lim, H. LIMBURG, K. Mansouri, A. Mathew, A. Morse, B. Munoz, D. Musch, K. Naidoo, V. Nangia, M. Palaiou, M. B. Parodi, F. Y. Pena, K. Pesudovs, T. Peto, H. Quigley, M. Raju, P. Ramulu, Z. Rankin, S. Resnikoff, D. Reza, A. Robin, L. Rossetti, J. Saaddine, M. Sandar, J. Serle, T. Shen, R. Shetty, P. Sieving, J. C. Silva, A. Silvester, R. S. Sitorus, D. Stambolian, G. Stevens, H. Taylor, J. Tejedor, J. Tielsch, M. Tsilimbaris, J. van Meurs, R. Varma, G. Virgili, Y. X. Wang, N.-L. Wang, S. West, P. Wiedemann, T. Wong, R. Wormald, and Y. Zheng, "Global causes of blindness and distance vision impairment 1990-2020: a systematic review and meta-

analysis.," *Lancet. Glob. Heal.*, vol. 5, no. 12, pp. e1221–e1234, Dec. 2017.

[3] A. Gordois, H. Cutler, L. Pezzullo, K. Gordon, A. Cruess, S. Winyard, W. Hamilton, and K. Chua, "An estimation of the worldwide economic and health burden of visual impairment," *Glob. Public Health*, vol. 7, no. 5, pp. 465–481, May 2012.

[4] G. Reardon, S. Kotak, and G. Schwartz, "Objective assessment of compliance and persistence among patients treated for glaucoma and ocular hypertension: a systematic review," *Patient Prefer. Adherence*, vol. 5, p. 441, Sep. 2011.

[5] S. Rofagha, R. B. Bhisitkul, D. S. Boyer, S. R. Sadda, and K. Zhang, "Seven-Year Outcomes in Ranibizumab-Treated Patients in ANCHOR, MARINA, and HORIZON: A Multicenter Cohort Study (SEVEN-UP)," *Ophthalmology*, vol. 120, no. 11, pp. 2292–2299, Nov. 2013.

[6] D. F. Martin, D. J. Parks, S. D. Mellow, F. L. Ferris, R. C. Walton, N. A. Remaley, E. Y. Chew, P. Ashton, M. D. Davis, and R. B. Nussenblatt, "Treatment of Cytomegalovirus Retinitis With an Intraocular Sustained-Release Ganciclovir Implant," *Arch. Ophthalmol.*, vol. 112, no. 12, p. 1531, Dec. 1994.

[7] G. J. Jaffe, D. Martin, D. Callanan, P. A. Pearson, B. Levy, T. Comstock, and Fluocinolone Acetonide Uveitis Study Group, "Fluocinolone acetonide implant (Retisert) for noninfectious posterior uveitis: thirty-four-week results of a multicenter randomized clinical study.," *Ophthalmology*, vol. 113, no. 6, pp. 1020–7, Jun. 2006.

[8] J. A. Haller, F. Bandello, R. Belfort, M. S. Blumenkranz, M. Gillies, J. Heier, A. Loewenstein, Y.-H. Yoon, M.-L. Jacques, J. Jiao, X.-Y. Li, and S. M. Whitcup, "Randomized, Sham-Controlled Trial of Dexamethasone Intravitreal Implant in Patients with Macular Edema Due to Retinal Vein Occlusion," *Ophthalmology*, vol. 117, no. 6, p.

1134–1146.e3, Jun. 2010.

[9] D. G. Callanan, G. J. Jaffe, D. F. Martin, P. A. Pearson, and T. L. Comstock, “Treatment of Posterior Uveitis With a Fluocinolone Acetonide Implant,” *Arch. Ophthalmol.*, vol. 126, no. 9, p. 1191, Sep. 2008.

[10] C. J. F. Bertens, M. Gijs, F. J. H. M. van den Biggelaar, and R. M. M. A. Nuijts, “Topical drug delivery devices: A review,” *Exp. Eye Res.*, vol. 168, pp. 149–160, Mar. 2018.

[11] J. C. Imperiale, G. B. Acosta, and A. Sosnik, “Polymer-based carriers for ophthalmic drug delivery,” *J. Control. Release*, vol. 285, pp. 106–141, Sep. 2018.

[12] M. A. Kamaleddin, “Nano-ophthalmology: Applications and considerations,” *Nanomedicine Nanotechnology, Biol. Med.*, vol. 13, no. 4, pp. 1459–1472, May 2017.

[13] K. McAvoy, D. Jones, and R. R. S. Thakur, “Synthesis and Characterisation of Photocrosslinked poly(ethylene glycol) diacrylate Implants for Sustained Ocular Drug Delivery,” *Pharm. Res.*, vol. 35, no. 2, p. 36, Feb. 2018.

[14] T. J. Smith, P. A. Pearson, D. L. Blandford, J. D. Brown, K. A. Goins, J. L. Hollins, E. T. Schmeisser, P. Glavinos, L. B. Baldwin, and P. Ashton, “Intravitreal Sustained-Release Ganciclovir,” *Arch. Ophthalmol.*, vol. 110, no. 2, p. 255, Feb. 1992.

[15] D. C. F. Soares, D. C. de Paula Oliveira, L. S. Barcelos, A. S. Barbosa, L. C. Vieira, D. M. Townsend, D. Rubello, A. L. B. de Barros, L. P. Duarte, and A. Silva-Cunha, “Antiangiogenic activity of PLGA-Lupeol implants for potential intravitreal applications,” *Biomed. Pharmacother.*, vol. 92, pp. 394–402, 2017.

[16] A. G. R. Solano, A. de Fátima Pereira, L. G. A. de Faria, S. L. Fialho, P. S. de Oliveira Patricio, A. da Silva-Cunha, G. O. Fulgêncio, G. R. da Silva, and G. A. Pianetti, “Etoposide-Loaded Poly(Lactic-co-Glycolic Acid) Intravitreal Implants: In Vitro and In

Vivo Evaluation," *AAPS PharmSciTech*, vol. 19, no. 4, pp. 1652–1661, May 2018.

[17] G. M. Fernandes-Cunha, S. L. Fialho, G. R. da Silva, A. Silva-Cunha, M. Zhao, and F. Behar-Cohen, "Ocular safety of Intravitreal Clindamycin Hydrochloride Released by PLGA Implants," *Pharm. Res.*, vol. 34, no. 5, pp. 1083–1092, May 2017.

[18] B. S. Zolnik and D. J. Burgess, "Effect of acidic pH on PLGA microsphere degradation and release," *J. Control. Release*, vol. 122, no. 3, pp. 338–344, Oct. 2007.

[19] M. S. Kim, H. H. Ahn, Y. N. Shin, M. H. Cho, G. Khang, and H. B. Lee, "An in vivo study of the host tissue response to subcutaneous implantation of PLGA- and/or porcine small intestinal submucosa-based scaffolds," *Biomaterials*, vol. 28, no. 34, pp. 5137–5143, Dec. 2007.

[20] K. D. Lance, S. D. Good, T. S. Mendes, M. Ishikiriyama, P. Chew, L. S. Estes, K. Yamada, S. Mudumba, R. B. Bhisitkul, and T. A. Desai, "In Vitro and In Vivo Sustained Zero-Order Delivery of Rapamycin (Sirolimus) From a Biodegradable Intraocular Device," *Investig. Opthalmology Vis. Sci.*, vol. 56, no. 12, p. 7331, Nov. 2015.

[21] J. Kim, M. Kudisch, N. R. K. da Silva, H. Asada, E. Aya-Shibuya, M. M. Bloomer, S. Mudumba, R. B. Bhisitkul, and T. A. Desai, "Long-term intraocular pressure reduction with intracameral polycaprolactone glaucoma devices that deliver a novel anti-glaucoma agent," *J. Control. Release*, vol. 269, pp. 45–51, Jan. 2018.

[22] D. A. Bernards, R. B. Bhisitkul, P. Wynn, M. R. Steedman, O.-T. Lee, F. Wong, S. Thoongsuwan, and T. A. Desai, "Ocular biocompatibility and structural integrity of micro- and nanostructured poly(caprolactone) films.," *J. Ocul. Pharmacol. Ther.*, vol. 29, no. 2, pp. 249–57, 2013.

[23] C. G. Pitt, F. I. Chasalow, Y. M. Hibionada, D. M. Klimas, and A. Schindler, "Aliphatic

polyesters. I. The degradation of poly(ϵ-caprolactone) *in vivo*," *J. Appl. Polym. Sci.*, vol. 26, no. 11, pp. 3779–3787, Nov. 1981.

[24] C. G. Pitt, M. M. Gratzl, G. L. Kimmel, J. Surles, and K. Schindler, "Aliphatic polyesters II. The degradation of poly (DL-lace), poly (E-caprolactone), and their copolymers in viva."

[25] E. Schlesinger, N. Ciaccio, and T. A. Desai, "Polycaprolactone thin-film drug delivery systems: Empirical and predictive models for device design.," *Mater. Sci. Eng. C. Mater. Biol. Appl.*, vol. 57, pp. 232–9, Dec. 2015.

[26] K. D. Lance, D. A. Bernards, N. A. Ciaccio, S. D. Good, T. S. Mendes, M. Kudisch, E. Chan, M. Ishikiriyama, R. B. Bhisitkul, and T. A. Desai, "In vivo and in vitro sustained release of ranibizumab from a nanoporous thin-film device," *Drug Deliv. Transl. Res.*, vol. 6, no. 6, pp. 771–780, 2016.

[27] J. Kim, M. Kudisch, S. Mudumba, H. Asada, E. Aya-Shibuya, R. B. Bhisitkul, and T. A. Desai, "Biocompatibility and Pharmacokinetic Analysis of an Intracameral Polycaprolactone Drug Delivery Implant for Glaucoma.," *Invest. Ophthalmol. Vis. Sci.*, vol. 57, no. 10, pp. 4341–6, 2016.

[28] R. Sheshala, G. C. Hong, W. P. Yee, V. S. Meka, and R. R. S. Thakur, "In situ forming phase-inversion implants for sustained ocular delivery of triamcinolone acetonide," *Drug Deliv. Transl. Res.*, pp. 1–9, Feb. 2018.

[29] C. Bode, H. Kranz, F. Siepmann, and J. Siepmann, "In-situ forming PLGA implants for intraocular dexamethasone delivery," *Int. J. Pharm.*, vol. 548, no. 1, pp. 337–348, Sep. 2018.

[30] J. Kim, M. Kudisch, N. R. K. da Silva, H. Asada, E. Aya-Shibuya, M. M. Bloomer, S.

Mudumba, R. B. Bhisitkul, and T. A. Desai, “Long-term intraocular pressure reduction with intracameral polycaprolactone glaucoma devices that deliver a novel anti-glaucoma agent,” *J. Control. Release*, vol. 269, pp. 45–51, Jan. 2018.

[31] O. Polat, S. İnan, S. Özcan, M. Doğan, T. Küsbeci, G. F. Yavaş, and Ü. Ü. İnan, “Factors affecting compliance to intravitreal anti-vascular endothelial growth factor therapy in patients with age-related macular degeneration,” *Turk Oftalmoloiji Derg.*, vol. 47, no. 4, pp. 205–210, 2017.

[32] A. Mandal, D. Pal, V. Agrahari, H. M. Trinh, M. Joseph, and A. K. Mitra, “Ocular delivery of proteins and peptides: Challenges and novel formulation approaches,” *Advanced Drug Delivery Reviews*, vol. 126. pp. 67–95, 2018.

[33] R. Vaishya, V. Khurana, S. Patel, and A. K. Mitra, “Long-term delivery of protein therapeutics,” *Expert Opin. Drug Deliv.*, vol. 12, no. 3, pp. 415–440, 2015.

[34] P. Badiee, R. Varshochian, M. Rafiee-Tehrani, F. Abedin Dorkoosh, M. R. Khoshayand, and R. Dinarvand, “Ocular implant containing bevacizumab-loaded chitosan nanoparticles intended for choroidal neovascularization treatment,” *J. Biomed. Mater. Res. Part A*, vol. 106, no. 8, pp. 2261–2271, Aug. 2018.

[35] C. Zhou, M. C. Robert, V. Kapoulea, F. Lei, A. M. Stagner, F. A. Jakobiec, C. H. Dohlman, and E. I. Paschalis, “Sustained subconjunctival delivery of infliximab protects the cornea and retina following alkali burn to the eye,” *Investig. Ophthalmol. Vis. Sci.*, vol. 58, no. 1, pp. 96–105, 2017.

[36] D. A. Bernards, K. D. Lance, N. A. Ciaccio, and T. A. Desai, “Nanostructured thin film polymer devices for constant-rate protein delivery.,” *Nano Lett.*, vol. 12, no. 10, pp. 5355–61, Oct. 2012.

[37] E. B. Schlesinger, D. A. Bernards, H. H. Chen, J. Feindt, J. Cao, D. Dix, C. Romano, R. B. Bhisitkul, and T. A. Desai, “Device design methodology and formulation of a protein therapeutic for sustained release intraocular delivery,” *Bioeng. Transl. Med.*, Dec. 2018.

[38] C. Awh, “LADDER trial of the Port Delivery System for ranibizumab: Initial study results.,” 2018.

[39] A. L. Daugherty and R. J. Mrsny, “Formulation and delivery issues for monoclonal antibody therapeutics,” *Adv. Drug Deliv. Rev.*, vol. 58, no. 5–6, pp. 686–706, Aug. 2006.

[40] D. G. Birch, R. G. Weleber, J. L. Duncan, G. J. Jaffe, and W. Tao, “Randomized trial of ciliary neurotrophic factor delivered by encapsulated cell intraocular implants for retinitis pigmentosa,” *Am. J. Ophthalmol.*, vol. 156, no. 2, 2013.

[41] D. G. Birch, L. D. Bennett, J. L. Duncan, R. G. Weleber, and M. E. Pennesi, “Long-term Follow-up of Patients With Retinitis Pigmentosa Receiving Intraocular Ciliary Neurotrophic Factor Implants,” *Am. J. Ophthalmol.*, vol. 170, pp. 10–14, 2016.

[42] J. Zhang, H. Sun, N. Zhou, B. Zhang, and J. Ma, “Preparation and Evaluation of Biodegradable Scleral Plug Containing Curcumin in Rabbit Eye,” *Curr. Eye Res.*, vol. 42, no. 12, pp. 1597–1603, 2017.

[43] E. Y. Chew, T. E. Clemons, T. Peto, F. B. Sallo, A. Ingerman, W. Tao, L. Singerman, S. D. Schwartz, N. S. Peachey, and A. C. Bird, “Ciliary neurotrophic factor for macular telangiectasia type 2: Results from a phase 1 safety trial,” *Am. J. Ophthalmol.*, vol. 159, no. 4, pp. 659–666, 2015.

[44] H. Tawfik-Schlieper, “Pharmacokinetics of Ophthalmic Drugs Anatomical Conditions.”

[45] R. S. Verhoeven, A. Garcia, R. Robeson, B. C. Gilger, D. Culp, C. Struble, L. Hamm, T. Navratil, and B. Yerxa, “Nonclinical Development of ENV905 (Difluprednate)

Ophthalmic Implant for the Treatment of Inflammation and Pain Associated with Ocular Surgery."

[46] U. B. Kompella, R. S. Kadam, and V. H. L. Lee, "Recent advances in ophthalmic drug delivery.," *Ther. Deliv.*, vol. 1, no. 3, pp. 435–56, Sep. 2010.

[47] J. I. Lim, R. A. Wolitz, A. H. Dowling, H. R. Bloom, A. R. Irvine, and D. M. Schwartz, "Visual and anatomic outcomes associated with posterior segment complications after ganciclovir implant procedures in patients with AIDS and cytomegalovirus retinitis," *Am. J. Ophthalmol.*, vol. 127, no. 3, pp. 288–293, Mar. 1999.

[48] C. Furino, F. Boscia, M. V. Cicinelli, A. Sborgia, and G. Alessio, "Subconjunctival sustained-release dexamethasone implant as an adjunct to trabeculectomy for primary open angle glaucoma.," *Indian J. Ophthalmol.*, vol. 64, no. 3, pp. 251–2, Mar. 2016.

[49] E. Moisseiev, M. Regenbogen, T. Rabinovitch, A. Barak, A. Loewenstein, and M. Goldstein, "Evaluation of pain during intravitreal Ozurdex injections vs intravitreal bevacizumab injections," *Eye*, vol. 28, no. 8, pp. 980–985, Aug. 2014.

[50] C. H. Meyer, Z. Liu, C. K. Brinkmann, E. B. Rodrigues, and T. Bertelmann, "Penetration Force, Geometry, and Cutting Profile of the Novel and Old Ozurdex Needle: The MONO Study," *J. Ocul. Pharmacol. Ther.*, vol. 30, no. 5, pp. 387–391, Jun. 2014.

[51] F. Pacella, A. F. Ferraresi, P. Turchetti, T. Lenzi, R. Giustolisi, A. Bottone, V. Fameli, M. R. Romano, and E. Pacella, "Intravitreal Injection of Ozurdex(®) Implant in Patients with Persistent Diabetic Macular Edema, with Six-Month Follow-Up.," *Ophthalmol. Eye Dis.*, vol. 8, pp. 11–6, 2016.

[52] A. Adán, L. Pelegrín, A. Rey, V. Llorenç, M. Mesquida, B. Molins, J. Ríos, and J. Keller, "Dexamethasone intravitreal implant for treatment of uveitic persistent cystoid macular

edema in vitrectomized patients," *Retina*, vol. 33, no. 7, pp. 1435–1440, 2013.

[53] S. S. Bollinger KE, "Prevalence and management of elevated intraocular pressure after placement of an intravitreal sustained-release steroid implant.," *Curr. Opin. Ophthalmol.*, vol. 20, no. 2, pp. 99–103, 2009.

[54] N. Haghjou, M. Soheilian, and M. J. Abdekhodaie, "Sustained release intraocular drug delivery devices for treatment of uveitis," *Journal of Ophthalmic and Vision Research*, vol. 6, no. 4. pp. 317–319, 2011.

[55] J. A. B. Corine Ghosn, "fMRI shows Functional Recovery by Intravitreal Brimonidine Drug Delivery System (Brimo DDS Generation 1) in a Rabbit Model of Retinal Ganglion Cell (RGC) Degeneration," *Investig. Opthalmology Vis. Sci.*, no. ARVO E-Abstract 6127-C0246, 2018.

[56] J. A. Burke, K. Zhang, W. Orilla, C. Ghosn, and L. A. Wheeler, "Intravitreal Brimonidine Drug Delivery System (Brimo DDS Generation 1) Enhances Spatial Sweep Visual Evoked Potential (sVEP) in a Non-human Primate Model of Chronic Glaucoma," *Investig. Opthalmology Vis. Sci.*, no. ARVO E-Abstract 1246-A0087, 2018.

[57] A. D. Charles D. Blizzard, Ankita Desai, Shelby D'Abbraccio, Jessica Mangano, Jennifer Langh, Noah Buff, Jamie Lynne Metzinger, Michael H. Goldstein, Ann Gelormini, "Efficacy and Pharmacokinetics of a Sustained Release Travoprost Intracameral Hydrogel Implant in Beagle Dogs," *Investig. Ophthalmol. Vis. Sci.*, no. ARVO E-Abstract 1245-A0086, 2018.

Co-delivery of Timolol and Brimonidine with a Polymer Thin-film Intraocular Device

4.1 Abstract

PURPOSE. We developed a polycaprolactone (PCL) co-delivery implant that achieves zero-order release of two ocular hypotensive agents, timolol maleate and brimonidine tartrate. We also demonstrate IOP-lowering effects of the implant for three months in vivo.

METHODS. Two PCL thin-film compartments were attached to form a V-shaped co-delivery device using film thicknesses of approximately 40 μm and 20 μm for timolol and brimonidine compartments, respectively. In vitro release kinetics were measured in pH- and temperature-controlled fluid chambers. Empty or drug-loaded devices were implanted intracamerally in normotensive rabbits for up to 13 weeks with weekly measurements of intraocular pressure (IOP). For ocular concentrations, rabbits were euthanized at 4, 8, or 13 weeks, aqueous fluid was collected and ocular tissues dissected. Drug concentrations were measured by liquid chromatography-tandem mass spectrometry (LC-MS/MS).

RESULTS. In vitro studies show zero-order release kinetics for both timolol (1.75 μg/day) and brimonidine (0.48 μg/day) for up to 60 days. In rabbit eyes, the device achieved an average aqueous fluid concentration of 98.1 {plus minus} 68.3 ng/mL for timolol and 5.5 {plus minus} 3.6 ng/mL for brimonidine. Over 13 weeks, the drug-loaded co-delivery device resulted in a statistically significant cumulative reduction in IOP compared to untreated eyes ($p<0.05$) and empty-device eyes ($p<0.05$).

CONCLUSIONS. The co-delivery device demonstrated a zero-order release profile in vitro for two hypotensive agents over 60 days. In vivo, the device led to significant cumulative IOP

reduction of 3.4 {plus minus} 1.6 mmHg over 13 weeks. Acceptable ocular tolerance was seen, and systemic drug levels were unmeasurable.

4.2 Introduction

Glaucoma is one of the leading causes of irreversible blindness worldwide[1]. While glaucoma is most commonly treated with hypotensive eye drops to control intraocular pressure (IOP), the barriers to patient compliance are well-documented [2], [3], [4] with non-adherence to prescribed eye drops among glaucoma patients of 20-60% [2], [5]–[7].

To circumvent problems with topical eye drop therapies, there has been substantial effort in developing a sustained release formulation for glaucoma therapy. For example, delivery of timolol maleate or brimonidine tartrate has been explored in the forms of microspheres [8], [9], [10], nanovesicles [11], ocular inserts [12], contact lenses [13], and others. Furthermore, a recent study demonstrated that sustained release of dorzolamide via biodegradable microparticles not only reduced IOP in normotensive rabbits [14], but also decreased glaucomatous retinal ganglion cell loss in a rat disease model of glaucoma [15]. We also have previously demonstrated that biodegradable polycaprolactone (PCL) intracameral devices delivering a prostaglandin analog [16], [17] attained over 5 months of IOP reduction in normotensive rabbits[16].

Simultaneous long-term delivery of multiple glaucoma agents would offer an advance in patient treatment. Managing glaucoma with two or more agents for additive or synergistic IOP reduction is common practice, for which a number of topical drug combination formulations have been developed, such as Combigan® (Allergan, Dublin, Ireland) combining timolol maleate and brimonidine tartrate, and CosoptPF- (Akorn, Lake Forest, IL), combining dorzolamide HCl and timolol maleate. For sustained release devices, effectively delivering

multiple agents can be challenging, because different drugs often require tailored release rates. We optimized the thickness of diffusion-limiting PCL films to achieve customized controlled release rates of timolol maleate and brimonidine tartrate using a single device. Here, we report the design and characterization of a co-delivery implant, demonstrating customizable zero-order release kinetics of both drugs. We also show pharmacokinetic profiles of co-delivery devices *in vivo* and cumulative reduction in IOP using a normotensive rabbit model.

4.3 Materials and Methods

4.3.1 Materials

All chemicals were obtained from Sigma-Aldrich Corp. (St. Louis, MO) unless noted otherwise. Brimonidine tartrate was obtained from Cayman Chemical (Ann Arbor, MI).

4.3.2 Device Fabrication

Devices were fabricated as previously described [17]. Briefly, PCL (M_n = 80 kDa) was dissolved in 2,2,2-trifluoroethanol at a concentration of 150 mg/mL, and spin-casted on a silicon wafer at 1000 RPM, then annealed at 110°C. To achieve the desired drug release rate of timolol and brimonidine, respectively, the film thickness was tuned for each drug compartment. Film thickness was measured using a film micrometer (iGaging, San Clemente, CA, USA). The casting process resulted in an approximately 20 μm thick film, which was used for fabricating the brimonidine compartment. The casting process was repeated to achieve a double layer of approximately 40 μm thickness, which was used to fabricate the timolol compartment.

To make each compartment, spun-cast PCL thin films with the desired thickness were folded in half and heat sealed by applying current to a nichrome wire, selectively heating the edges (Figure 4.1, dotted lines) to form a pocket. Lyophilized timolol or brimonidine powder

was loaded into the pocket and heat sealed, creating a closed compartment. Each compartment is approximately 2 mm in width by 4 mm in length. To form the attached co-delivery device, the

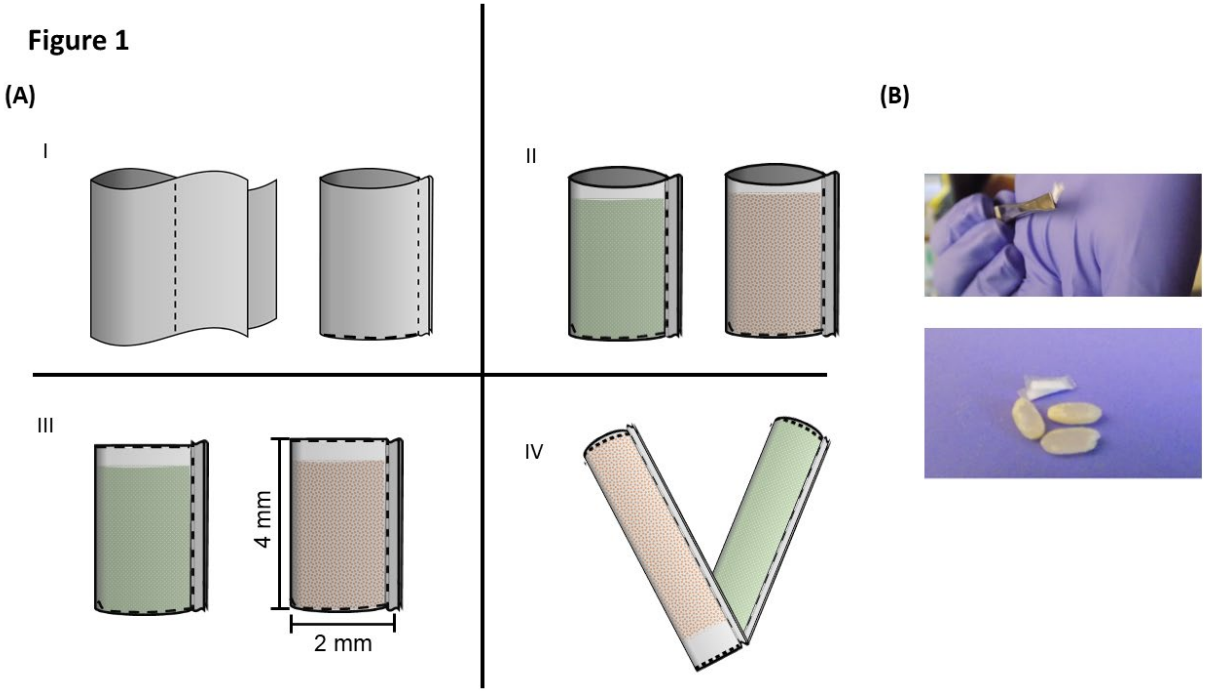

Figure 4.1 Schematic diagram of two-compartment device fabrication (A). To make each compartment, spun-cast PCL thin films were heat sealed along the edges (I) shown as dotted lines, and filled with either timolol maleate (orange) or brimonidine tartrate (green) (II). The drug-loaded compartments were sealed closed (III) and the two compartments were attached at a sealed edge (IV). Each compartment is about 2 mm in width by 4 mm in length. The attached device is shown with grains of rice for scale (B).

two compartments, each containing either timolol or brimonidine, were stacked together, and heat-sealed along one edge (Figure 4.1).

4.3.3 In Vitro Drug Release

The release rate of each drug-containing compartment was tested individually. The compartment was submerged in 0.5 mL of phosphate buffered saline (PBS) at 37°C on an orbital shaker. Elution medium was replaced with fresh PBS at each time point. Drug concentration was quantified by UV-Vis spectrometry (absorption wavelengths of timolol = 294nm and

brimonidine = 254nm). The release rate was calculated by dividing the amount of drug released at each time point by the time passed since the previous time point.

To verify that the process of attaching the drug compartments did not lead to defects in the device, drug release rate of the attached compartments was also tested as described above. Drug concentrations were measured using liquid chromatography with tandem mass spectrometry (LC-MS/MS) to separate each drug from the mixed drug solution.

4.3.4 In Vivo Device Implantation

Co-delivery devices were washed with 70% ethanol for 10 seconds in a sterile hood and subsequently dried in ambient conditions. Implantation of PCL devices in the eyes of adult male and female New Zealand rabbits was approved by the institutional review board and was performed in accordance with the ARVO Statement for the Use of Animals in Ophthalmic and Vision Research. Using ophthalmic microsurgical techniques under sterile conditions in anesthetized rabbits, the devices were implanted in normotensive rabbit eyes as previously described [16], [17] with minor adjustments. A clear corneal incision was performed using a 2.4 or 2.6mm slit knife (Alcon Laboratories, Ft. Worth, TX, USA) through which the device was implanted into the anterior chamber of the left eyes. An 8-0 nylon suture (Alcon Laboratories, Ft. Worth, TX, USA) was used to close the incision.

Sixteen rabbits underwent surgery: 4 rabbits with drug-loaded devices at 3 time points (euthanized after 4, 8, and 13 weeks for analysis) and 4 rabbits with empty devices at the final 13-week time point. Contralateral eyes were untreated and served as controls. Photos were taken after implantation as well as prior to euthanasia with the Canon camera body and a SLR camera-microscope adapter (Carl Zeiss Meditec, Inc., Dublin, CA, USA). 1% prednisolone (Sandoz, Holzkirchen, Germany) was administered to all rabbits twice a day for 5 days and once a day for

5 additional days after surgery to minimize post-surgical inflammation. IOP was measured weekly using a handheld tonometer (TonoVet®, Icare, Vantaa, Finland). All IOP measurements were performed between 12 pm and 6 pm to control for high diurnal IOP fluctuations. The area under the curve (AUC) of baseline-subtracted IOP values was calculated using the trapezoidal rule over 13 weeks. The AUC of drug-loaded device treated eyes was compared to the AUC of untreated contralateral eyes and empty device treated eyes using a one-way ANOVA followed by Tukey's multiple comparisons test to evaluate statistically significant differences among the AUC of the three groups. Data is presented as mean ± standard deviation.

4.3.5 Pharmacokinetic Analysis in Rabbit Ocular Tissue

At each endpoint, rabbits were anesthetized and 1 ml of blood was collected in lithium-heparin tubes (BD Vacutainer®, BD, Franklin Lakes, NJ) and kept on ice until centrifugation. Whole blood was centrifuged at 1300 x g for 15 minutes in a refrigerated centrifuge to remove red blood cells from the sample. Before euthanasia, aqueous humor was withdrawn by limbal paracentesis using a 30-gauge needle on a 1-mL syringe. The rabbits were then euthanized by injecting 2 mmol/kg potassium chloride into the marginal ear vein. The ocular globe was enucleated immediately after euthanasia. Cornea, iris-ciliary body, vitreous and retina-choroid were dissected, placed in microcentrifuge tubes and frozen at -80°C until LC-MS/MS analysis.

4.3.6 LC-MS/MS

Brimonidine and timolol were dissolved in DMSO, mixed and further diluted in 50% methanol to prepare spiking solutions. The internal standard (IS) mix (brimonidine-d4 and timolol-d5) was prepared in the same way. Plasma, aqueous humor and vitreous samples were prepared using spiked standards. Analyte extraction was performed in a bullet blender (Next Advance, Troy, NY) at 4°C. After centrifugation at 10,000 rpm for 5 min, 75 µl of supernatant

was diluted with 150 µl water + 0.1% formic acid. The LC-MS/MS system consists of a Shimadzu LC-20AB HPLC system interfaced with QTRAP 4000 mass spectrometer (AB SCIEX, Redwood City, CA). LC separation was carried out on an Agilent ZORBAX SB-Phenyl column (50 mm × 4.6 mm, 3.5 µm) with the following mobile phase: A, LCMS grade water + 0.1% formic acid; B, LCMS grade acetonitrile + 0.1% of formic acid. The flow rate was set at 0.6 ml/min. Column temperature was 25ºC. The injection volume was 20 µl. Data acquisition and analyses were performed using the Analyst 1.6.1 software (AB SCIEX, Redwood City, CA).

4.3.7 Histological Analysis

For histologic studies, the empty device-implanted eyes and contralateral control eyes were enucleated immediately after euthanasia and submerged in 50-60 mL of Hartman's Fixative, and incubated for 1 day. The eyes were then transferred to 70% ethanol until histological analysis. Histological preparation was performed by the Gladstone Histology and Light Microscopy Core (San Francisco, CA, USA). Eyes were hemisected in the sagittal plane. Each half was paraffin-embedded, sectioned, and stained with hematoxylin and eosin (H&E).

4.4 Results

4.4.1 In Vitro Drug Release

The average *in vitro* release rate of drug from the device was determined by linear regression on the cumulative drug released versus time. Data is presented as mean ± standard deviation. *In vitro* drug release results in Figure 4.3 show that timolol was released at a rate of 1.75 ± 0.15 µg/day (n=3, linear regression, R^2= 0.99), and brimonidine was released at a rate of 0.48 ± 0.03µg/day (n=3, linear regression, R^2= 0.98) and demonstrate zero-order release kinetics from each drug compartment. The drug released before the first time point is likely due to excess

drug powder adsorbed to the outside of the devices during fabrication. Attached compartments led to a measured drug release of 1.57 ± 0.55 μg/day and 0.27 ± 0.17 μg/day (n=3), respectively (Figure 4.2). The difference in brimonidine release rate in a single-drug compartment (Figure 4.3) as compared to the released rate as part of attached devices (Figure 4.2) can be partly due to variations in device surface areas during fabrication. Since the devices are small and handmade, a slight variation of 0.25 mm in length and width can result in an approximately 18-20% difference in device surface area. The variations in release rate may also be attributed to the differences in measurement method (UV-vis and LC-MS/MS, respectively).

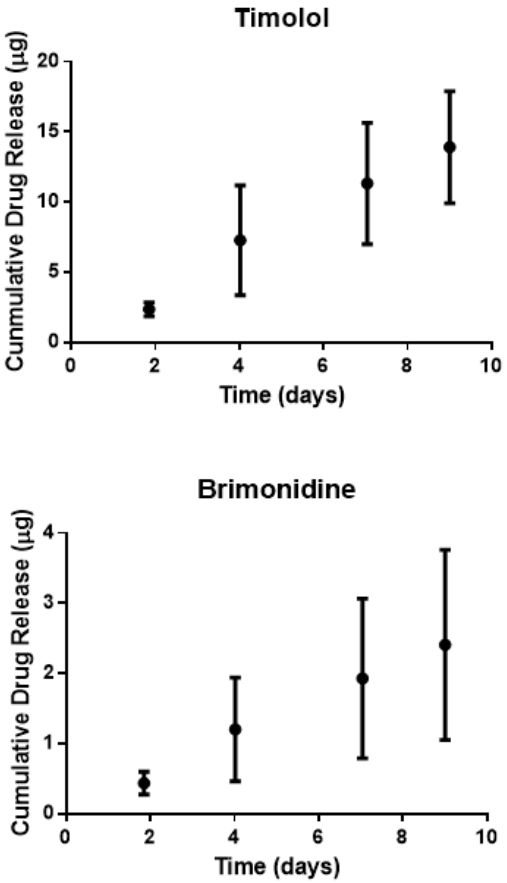

Figure 4.2 Cumulative drug release of timolol maleate (A) and brimonidine tartrate (B) from attached devices (n=3). Drug concentrations were measured using LC-MS/MS. Release rates were calculated to be 1.57 μg/day for timolol and 0.27 μg/day for brimonidine.

However, the release rates of attached devices and single compartments were on the same order of magnitude and both demonstrated a zero-order release profile.

4.4.2 In Vivo Ocular Concentrations

Polymer co-delivery devices were successfully impl anted and tolerated in the anterior chamber of rabbit eyes (Figure 4.4). No signs of cataracts or ocular inflammation were observed in our study. However, some complications occurred due to the surgical procedure and device shape, as well as other unrelated medical issues. Two 8-week rabbits with drug-loaded devices experienced hyphema during the study period. The rabbits were prescribed 1% prednisolone twice a day for 3-5 days after which the condition was relieved. Three cases of anterior synechia

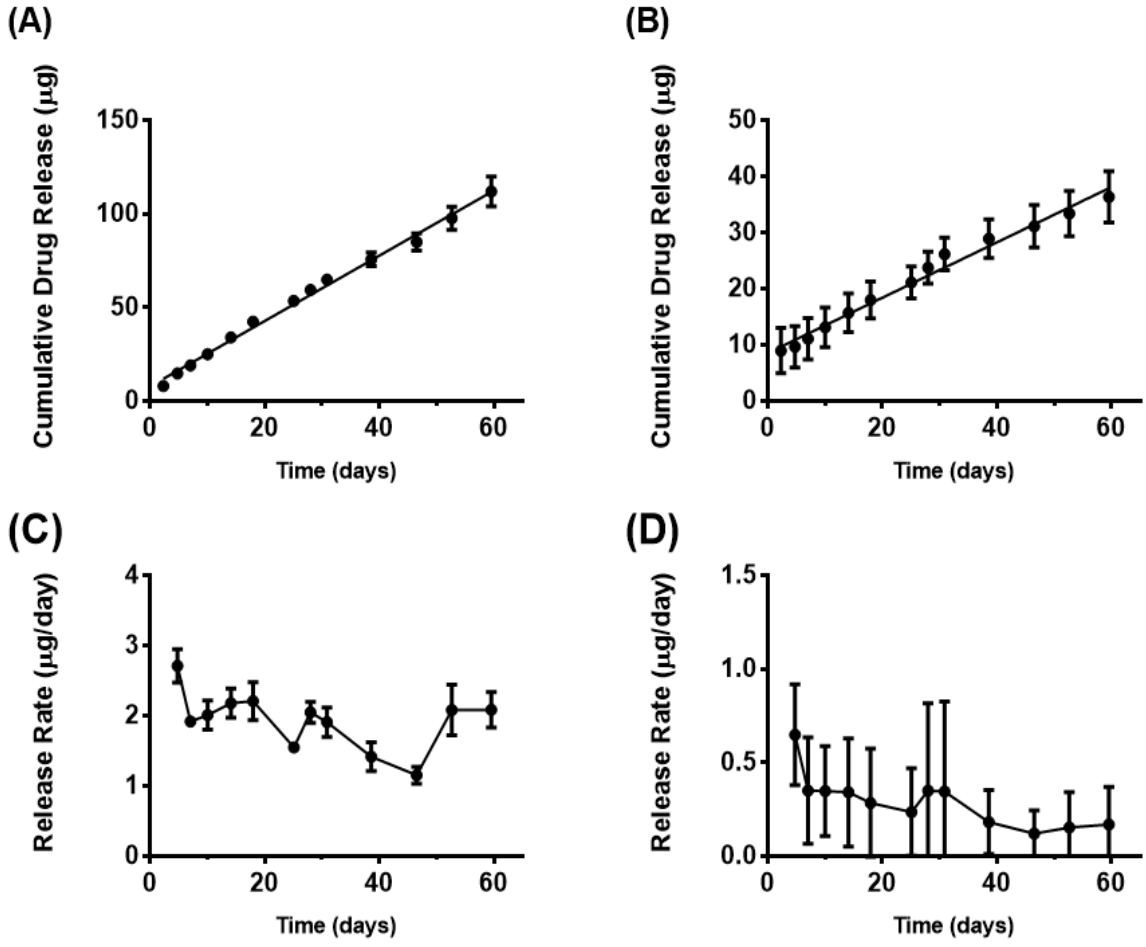

Figure 4.3 Cumulative drug release (A, B) and release rates (C, D) of timolol maleate (A, C) and brimonidine tartrate (B, D). Linear regression fit of cumulative drug release versus time demonstrated zero-order release for both timolol and brimonidine.

were observed in two 13-week rabbits and one 8-week rabbit. Four cases of corneal neovascularization were observed in two 13-week rabbits an d two 8-week rabbits including one case of corneal edema. One 8-week drug-loaded device rabbit had very low IOP caused by the device not being fully enclosed in the anterior chamber. The rabbit was sacrificed early as the surgery was incomplete and the data was not used for analysis. An additional 8-week rabbit was added to the study. LC-MS/MS analysis of ocular tissues of eyes collected at different time points (week 4, 8, and 13) indicated sustained release of both drugs in the anterior chamber over 13 weeks. Timolol maintained a relatively steady concentration of 98.1 ± 68.3 ng/ml in the aqueous humor (Figure 4.5A) with no statistically significant difference in measured concentrations at the three timepoints (p=0.16). Timolol concentrations in the ICB also indicated sustained release (Figure 4.5A). One of the 13-week rabbits showed an ICB concentration more than six times that of the three other rabbits, which resulted in a large standard deviation in the 13-week group. The average measured aqueous humor concentration for brimonidine was 5.5 ± 3.6 ng/ml. There was no significant difference in average aqueous humor concentrations measured at different

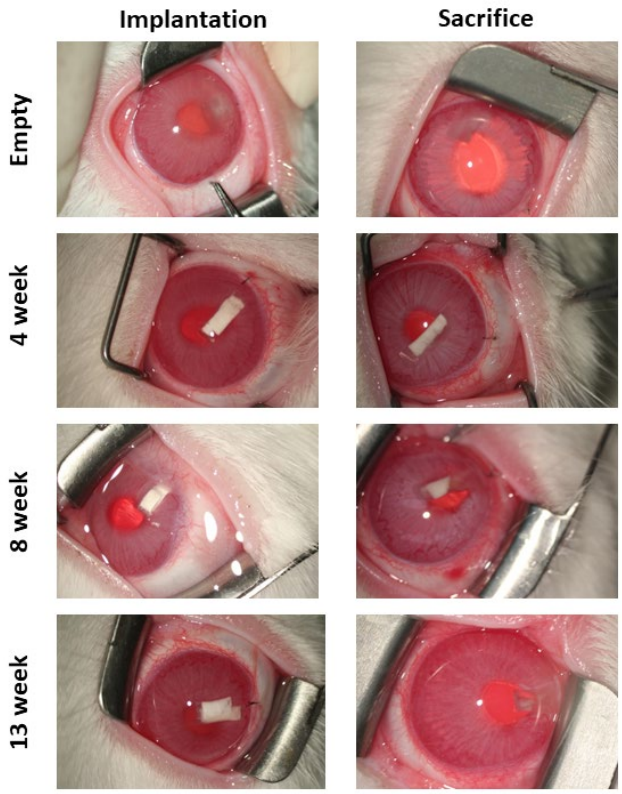

Figure 4.4 Representative photos of rabbit eyes immediately after implantation (left column) and before sacrifice (right column) of empty or drug loaded co-delivery devices in the anterior chamber of the OS eyes.

timepoints (p=0.1). However, two of the four 13-week rabbits had non-detectable brimonidine concentrations in the aqueous humor (Figure 4.5B). Brimonidine ICB concentrations were low at all time points with an average of 0.9 ± 0.5 ng/ml. Retina choroid concentrations were below or close to the quantification limit for both drugs (Figure 4.5C, D). Additionally, concentrations of both drugs in the blood were below the limit of detection indicating that systemic levels of both drugs are very low. The aqueous humor concentrations in the untreated contralateral eyes were below quantification limit indicating no crossover effect.

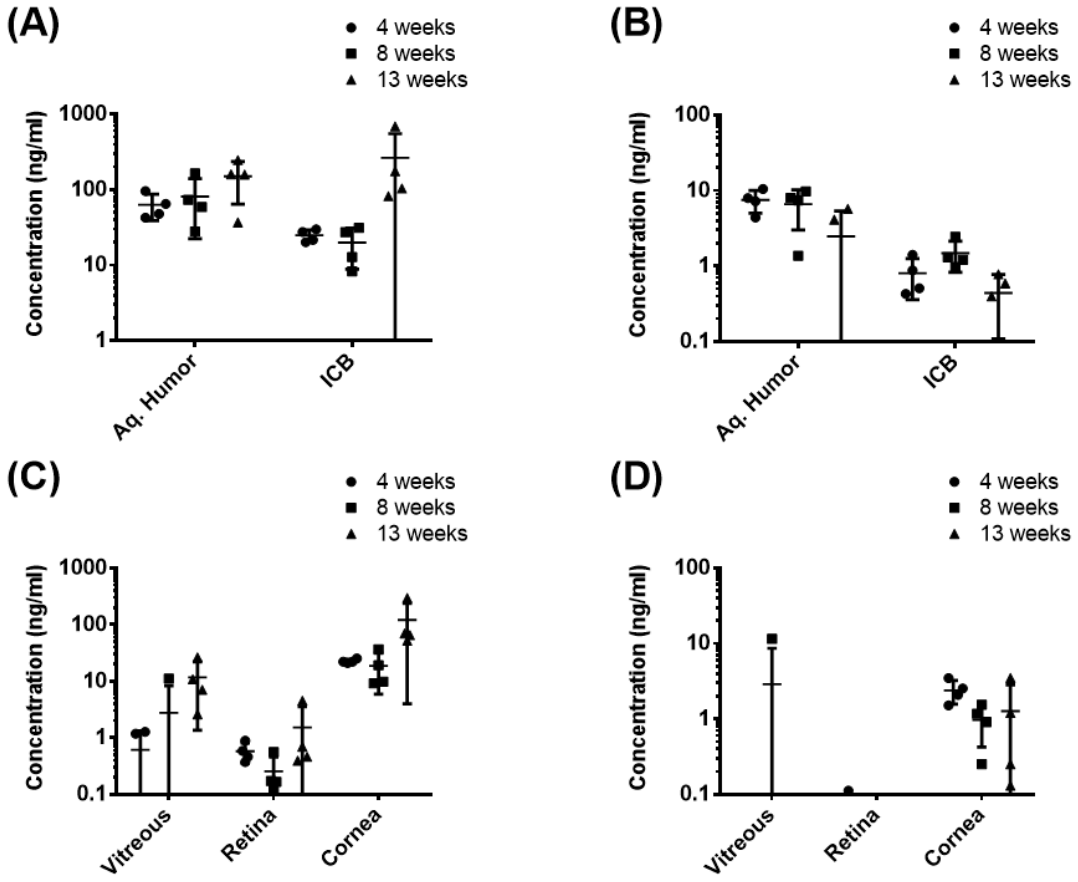

Figure 4.5 Concentrations of timolol maleate (A) and brimonidine tartrate (B) in relevant ocular tissues after 4 weeks, 8 weeks, and 13 weeks of device implantation and concentrations in the aqueous humor (C) and the ICB (D) of both drugs.

4.4.3 IOP

IOP measurements of the device implanted eyes were compared to those of untreated, contralateral eyes for approximately 13 weeks after device implantation (Figure 4.6). Pre-surgery baseline IOP of device-implanted and contralateral eyes were 11 ± 2.1 mmHg and 9.4 ± 1.8 mmHg, respectively. Within 7 days, the IOP of the drug-loaded device treated eyes dropped by 4.4 ± 2.9 mmHg, while the IOP for the untreated contralateral eyes increased by 1.3 ± 2.3 mmHg. This corresponds to an average relative drop of 37% (normalized to each rabbit's baseline IOP). Over 13 weeks, the IOP of the drug-loaded device eyes decreased by 3.4 ± 1.6 mmHg on average, whereas the IOP of the control eyes increased on average by 0.54 ± 0.97 mmHg. Cumulative IOP reduction was evaluated by comparing the AUC of baseline-subtracted IOP measurements of the three groups (Figure 4.7). The drug-loaded device treated eyes resulted in a statistically significant cumulative reduction in IOP compared to untreated contralateral eyes (ANOVA with Tukey post-hoc test, $p<0.01$) and empty device treated eyes ($p<0.05$). There was no significant difference in cumulative IOP reduction between empty-device treated eyes and untreated contralateral eyes.

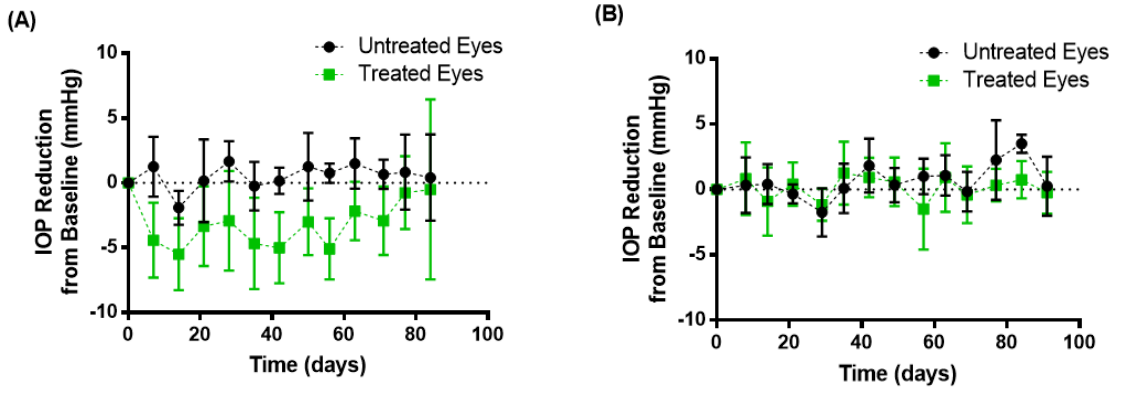

Figure 4.6 Mean ± standard deviation of IOP change from baseline for drug-loaded eyes (A) and empty device eyes (B) compared to their contralateral control eyes over 91 days.

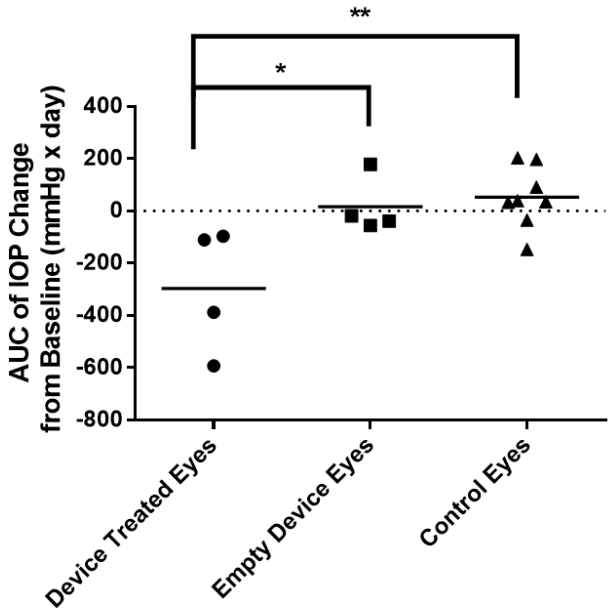

Figure 4.7 Cumulative IOP reduction represented as the area under the curve (AUC) of baseline subtracted IOP values of drug-loaded device treated eyes (n=4), empty-device treated eyes (n=4), and their contralateral control eyes (n=8) over 91 days.

4.4.4 Histological Analysis after 13 weeks of Device Implantation

Granulation tissue with a chronic inflammatory infiltrate was present at the site of incision in the cornea, consistent with a surgical wound. In two cases, there was corneal neovascularization associated with the wound (Figure 4.8C). At the site of device implantation, there is evidence of local mechanical disruption to the anterior iris and posterior cornea. There were two cases of anterior synechia (Figure 4.8E), and three cases of fibrous metaplasia due to the device touching the iris and corneal endothelium (Figure 4.8D). There was one case of iris neovascularization. The disruptions and some inflammation are seen at the implantation site (Figure 4.8F), and no effect on the tissue is observed in the distal half of the eye (Figure 4.8A, B). No global inflammatory response was observed, which agrees with previous studies using PCL devices in the eye [17].

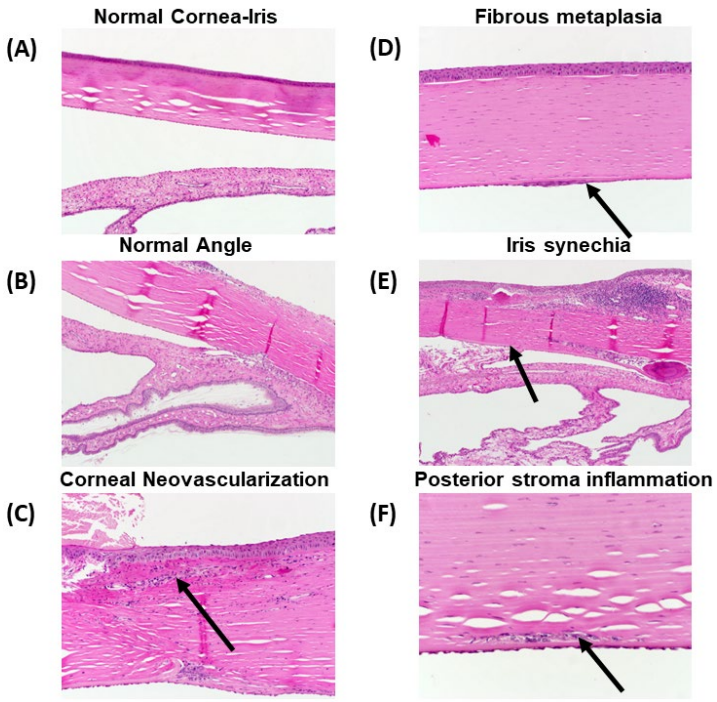

Figure 4.8 Histological images of the rabbit normal cornea (A) and normal angle (B) in the anterior segment of the OS eye. Images of the anterior segment showing examples of corneal neovascularization (C), fibrous metaplasia shown by thickening of the endothelium (D) iris synechia (E) and lymphocytes in the posterior stroma signaling focal inflammation (F).

4.5 Discussion

Poor patient compliance is a well-documented problem with topical glaucoma therapies. Sustained-delivery formulations of glaucoma medication represent an unmet need in the field, particularly the simultaneous delivery of multiple hypotensive agents. Here, we report the development of a polymeric intracameral ocular implant for simultaneous sustained delivery of both timolol maleate and brimonidine tartrate.

According to pharmacokinetics analysis, the amount of drug in the contralateral eye and the plasma is below quantifiable limits of LC-MS/MS (<1 ng/mL). This is expected because the

implantation site in the anterior chamber is not connected to the nasolacrimal duct, the typical route for systemic drug absorption. This allows our device to avoid systemic toxicities associated with topical beta blocker application [18]. Assuming a simple one-compartment model with a fixed release source and one route of elimination, the steady state concentration $\boldsymbol{C_{SS}}$ of each drug can be estimated from the half-life of each drug using the following two equations

$$\boldsymbol{k_e = \frac{ln(2)}{t_{half-life}}, C_{SS} = \frac{R_{in}}{k_e V}}$$

where $\boldsymbol{k_e}$ is the elimination rate constant, $\boldsymbol{R_{in}}$ is the release rate from the device, $\boldsymbol{t_{half-life}}$ is the half-life of each drug in the aqueous humor and V is the volume of the aqueous humor assuming the drug is distributed across the entire volume. The steady state concentration of timolol concentration in the aqueous humor was calculated to be 323.8 ng/ml based on its half-life of 60 min [19] and assuming a fixed release source at the measured *in vitro* release rate of 1.75 µg/ml and an aqueous humor volume of 0.325 ml [20]. Our measured aqueous humor concentration is on the same order of magnitude, but is approximately 3-fold lower, suggesting that the *in vivo* release rate of timolol from the device might be slightly slower than *in vitro*. However, this concentration is consistent with the aqueous humor concentration measured after 18 h of administering a single dose of topical 0.5% timolol to human patients which was reported to be 105.5 ± 60.9 ng/ml [21]**.** Based on a study of beta receptor binding activity of timolol in the aqueous humor, the measured timolol concentration of approximately 100 ng/ml in the aqueous humor would result in 99% beta1 receptor occupancy [21].

Based on the half-life of brimonidine in the aqueous humor of 34 min [22], and the *in vitro* release rate of 0.48 μg/day, the expected *in vivo* steady state concentration in the aqueous humor is 50.2 ng/ml. The measured concentrations in the aqueous humor and ICB are an order of magnitude lower than anticipated based on the *in vitro* release rate. Upon examining the devices at week 13 we noticed that little to no brimonidine powder was visible in the devices. Based on the amount loaded (approximately 1 mg) and their release rate pre-implantation, we anticipated the drug release from the devices to last for a substantially longer period of time. This suggests that 1) the *in vivo* release rate of brimonidine may be higher than the measured rate *in vitro*, leading to faster depletion of the device reservoir, and 2) there are modes of clearance in addition to the outflow of aqueous humor, such as degradation, that might be contributing to the low tissue concentrations

The return to baseline IOP starting at day 56 may be due to the lowered brimonidine concentrations measured in the tissues. However, even with the low brimonidine concentrations (under 10 ng/mL) in the aqueous humor and ICB, we were able to achieve statistically significant cumulative IOP reductions at earlier time points. We achieved a maximum IOP drop of 5.5 ± 2.8 mmHg at day 14, which corresponds to a 47% reduction from baseline. According to the FDA approval letter [22], brimonidine tartrate ophthalmic solution 0.1% resulted in a maximum of 29% reduction in IOP after 3 hours in male albino New Zealand rabbits. It is important to note that there is less room for IOP reduction in normotensive rabbits compared to rabbits with congenitally elevated IOP.

The histological analysis shows that there was no global inflammation in the eye. All abnormalities observed are local to the device implantation site. Given the small dimensions of the rabbit eye relative to the human eye (25% relative volume) [23] the device size was

associated with iris and corneal contact in the confines of the small anterior chamber. However, the current device geometry can be redesigned to further improve biocompatibility. One aspect of the geometry was the two-armed, V-shaped design. We observed that the two arms of the device did not remain folded, and instead opened up within the eye into a wider V-shape, pushing against the corneal epithelium and the iris. This created mechanical pressure that explains the observed damage in those tissues. Future goals include reconfiguring and further miniaturizing the co-delivery devices to further improve biocompatibility.

Taken together, we have demonstrated that our polymer thin-film intracameral implant device can achieve controlled release of two different hypotensive agents at different release rates. The device achieved a statistically significant reduction of cumulative IOP over 13-weeks in normotensive rabbits. Timolol maleate concentration in the target tissue was maintained for 13 weeks. While the *in vivo* release rate of brimonidine was lower than expected, the low concentrations still achieved significant IOP drop. Further optimization of brimonidine formulation and/or device size can increase the *in vivo* release rate and duration of brimonidine through the thin-film device. This study demonstrates that the prototype device has the potential to achieve sustained-release of two hypotensive agents for glaucoma therapy.

4.6 Acknowledgments and Author Disclosure Statement

Supported by That Man May See Foundation, NIH-NEI EY002162 - Core Grant for Vision Research, Research to Prevent Blindness Unrestricted Grant, and National Institutes of Health (NIH) R01EY021574

Author Disclosure Statement

Tejal A. Desai is a co-founder of Zordera; is on the advisory board for Santen.

Robert B. Bhisitkul receives a research grant from Genentech; receives consulting fees from Ribomic, Inc. and AntriaBio; is a co-founder of Zordera; is on the advisory board for Santen; is on the advisory board for Sandoz, Biotime and Quark.

4.7 References

[1] Y. C. Tham, X. Li, T. Y. Wong, H. a. Quigley, T. Aung, and C. Y. Cheng, "Global prevalence of glaucoma and projections of glaucoma burden through 2040: A systematic review and meta-analysis," *Ophthalmology*, vol. 121, no. 11, pp. 2081–2090, 2014.

[2] C. Y. Kim *et al.*, "Treatment patterns and medication adherence of patients with glaucoma in South Korea.," *Br. J. Ophthalmol.*, vol. 101, no. 6, pp. 801–807, Jun. 2017.

[3] S. Frech, D. Kreft, R. F. Guthoff, and G. Doblhammer, "Pharmacoepidemiological assessment of adherence and influencing co-factors among primary open-angle glaucoma patients — An observational cohort study," pp. 1–14, 2018.

[4] T. Naito *et al.*, "Factors affecting eye drop instillation in glaucoma patients with visual field defect," *PLoS One*, vol. 12, no. 10, pp. 1–11, 2017.

[5] C. M. G. Olthoff, J. S. A. G. Schouten, B. W. Van De Borne, and C. A. B. Webers, "Noncompliance with ocular hypotensive treatment in patients with glaucoma or ocular hypertension: An evidence-based review," *Ophthalmology*, vol. 112, no. 6. pp. 953–961, 2005.

[6] G. Reardon, G. F. Schwartz, and E. Mozaffari, "Patient persistency with topical ocular hypotensive therapy in a managed care population," *Am. J. Ophthalmol.*, vol. 137, no. SUPPL., 2004.

[7] J. D. Gatwood, J. Johnson, and B. Jerkins, "Comparisons of Self-reported Glaucoma Medication Adherence with a New Wireless Device: A Pilot Study," *J. Glaucoma*, vol. 26, no. 11, pp. 1056–1061, 2017.

[8] E. Lavik, M. H. Kuehn, A. J. Shoffstall, K. Atkins, A. V. Dumitrescu, and Y. H. Kwon, "Sustained Delivery of Timolol Maleate for Over 90 Days by Subconjunctival Injection,"

J. Ocul. Pharmacol. Ther., vol. 32, no. 10, pp. 642–649, 2016.

[9] M. V. Fedorchak, I. P. Conner, C. A. Medina, J. B. Wingard, J. S. Schuman, and S. R. Little, "28-day intraocular pressure reduction with a single dose of brimonidine tartrate-loaded microspheres," *Exp. Eye Res.*, vol. 125, pp. 210–216, 2014.

[10] Y. S. Pek, H. Wu, S. T. Mohamed, and J. Y. Ying, "Long-Term Subconjunctival Delivery of Brimonidine Tartrate for Glaucoma Treatment Using a Microspheres/Carrier System," *Adv. Healthc. Mater.*, vol. 5, no. 21, pp. 2823–2831, 2016.

[11] S. Maiti, S. Paul, R. Mondol, S. Ray, and B. Sa, "Nanovesicular Formulation of Brimonidine Tartrate for the Management of Glaucoma: In Vitro and In Vivo Evaluation," *AAPS PharmSciTech*, vol. 12, no. 2, pp. 755–763, 2011.

[12] J. E. Mealy, M. V. Fedorchak, and S. R. Little, "In vitro characterization of a controlled-release ocular insert for delivery of brimonidine tartrate," *Acta Biomater.*, vol. 10, no. 1, pp. 87–93, 2014.

[13] C. C. Peng, M. T. Burke, B. E. Carbia, C. Plummer, and A. Chauhan, "Extended drug delivery by contact lenses for glaucoma therapy," *J. Control. Release*, vol. 162, no. 1, pp. 152–158, 2012.

[14] J. Fu *et al.*, "Subconjunctival delivery of dorzolamide-loaded poly(ether-anhydride) microparticles produces sustained lowering of intraocular pressure in rabbits," *Mol. Pharm.*, vol. 13, no. 9, pp. 2987–2995, 2016.

[15] I. Pitha *et al.*, "Sustained Dorzolamide Release Prevents Axonal and Retinal Ganglion Cell Loss in a Rat Model of IOP – Glaucoma," vol. 7, no. 2, pp. 1–12, 2018.

[16] J. Kim *et al.*, "Long-term intraocular pressure reduction with intracameral polycaprolactone glaucoma devices that deliver a novel anti-glaucoma agent," *J. Control.*

Release, vol. 269, pp. 45–51, Jan. 2018.

[17] J. Kim *et al.*, "Biocompatibility and pharmacokinetic analysis of an intracameral polycaprolactone drug delivery implant for glaucoma," *Investig. Ophthalmol. Vis. Sci.*, vol. 57, no. 10, pp. 4341–4346, 2016.

[18] J. Mäenpää and O. Pelkonen, "Cardiac safety of ophthalmic timolol," *Expert Opin. Drug Saf.*, vol. 15, no. 11, pp. 1549–1561, 2016.

[19] A. A. Acheampong, A. Breau, M. Shackleton, W. Luo, S. Lam, and D. D. Tang-Liu, "Comparison of concentration-time profiles of levobunolol and timolol in anterior and posterior ocular tissues of albino rabbits," *J Ocul Pharmacol Ther*, vol. 11, no. 4, pp. 489–502, 1995.

[20] P. J. Missel, "Simulating intravitreal injections in anatomically accurate models for rabbit, monkey, and human eyes," *Pharm. Res.*, vol. 29, no. 12, pp. 3251–3272, 2012.

[21] K. M. Saari, T. Ali-Melkkilä, M.-L. Vuori, T. Kaila, and E. Lisalo, "Absorption of ocular timolol: drug concentrations and β-receptor binding activity in the aqueous humour of the treated and contralateral eye," *Acta Ophthalmol.*, vol. 71, no. 5, pp. 671–676, 1993.

[22] "U.S. Food and Drug Administration, Center for Drug Evaluation and Research," 2004.

[23] G. Bozkir, M. Bozkir, H. Dogan, K. Aycan, and B. Güler, "Measurements of Axial Length and Radius of Corneal Curvature in the Rabbit Eye," *Acta Med. Okayama*, vol. 51, no. 1, pp. 9–11, 1997.

Conclusions and Outlook

The work presented in this dissertation illustrates the diversity of research in the interdisciplinary field of biomaterials. Drawing upon techniques in polymer chemistry, electrochemistry, drug delivery, and tissue engineering, many engineering and biological approaches were involved in the design of two distinct biomaterials for eliciting desired therapeutic responses. The results and opportunities provided by these studies have the potential to benefit researchers, clinicians, and patients.

5.1 Titania nanotube coatings

Titania nanotube topography has several advantages as an approach for attenuating restenosis. The anodization process is scalable and compatible with metallic substrates, the surface modification does not affect bulk mechanical properties, and it avoids the use of the toxic drugs commonly used in DES. By better understanding the interactions between titania nanotubes and vascular cells, this study can contribute to the further development of an anti-restenotic surface coating for bare metal stents This study elucidated the effects of nanotube topography on a cellular level. The results of this study illustrated that titania nanotube topography decreases SMC surface coverage and decreases both EC and SMC response to inflammation as compared to flat titania surfaces. Further, 90 nm diameter nanotube geometry led to a greater extent cellular response compared to 30 nm or 50 nm diameter nanotubes.

This work contributes to the understanding of the interactions between titania nanotubes and vascular cells on a cellular level, and setting the stage for further mechanistic investigation on a molecular level. For example, it would be interesting to further probe the pathways that are downstream from FAK, including Rho/ROCK/MLCK, and YAP/Taz, to dissect how the

topographical cues of the titania nanotube is transduced as cellular signals that lead to the observed phenotype changes. It would be especially interesting to probe how the interactions with titania nanotubes affects integrin binding and clustering, and any crosstalk with growth factor and cytokine receptor signaling.

5.2 Ocular drug delivery

This study demonstrated proof-of-concept for a PCL thin-film device for the sustained delivery of hypotensive agents without the need for patient input. PCL film-thickness was tuned independently for each compartment to achieve desired release rates of for timolol maleate and brimonidine tartrate respectively. The device also achieved sustained drug concentrations locally in ocular tissues *in vivo*, with undetectable drug concentrations in systemic circulation. We also observed a decrease in intraocular pressure in a normotensive rabbit model, demonstrating that the device can achieve a therapeutic response.

The device design and results also provide opportunities for further optimization and refinement. First, the v-shaped design caused the device to open, which sometimes led to mechanical disruption of the corneal epithelium and the iris. An alternative design can be considered to further improve device biocompatibility, such as by annealing the open ends of the device to form a seal and lessen device movement. Another strategy to avoid device contact with the delicate structures in the front of the eye is to consider an alternative implantation site in the posterior chamber of the eye. In addition, optimization of manufacturing methods has the opportunity to lead to increased consistency and further miniaturization of the device. All in all, this study demonstrated that film thickness can be tuned to achieve distinct desired release rates for two different hypotensive agents. Similar strategies can be applied to other drugs for

alternative mono- or combination therapies for the long-term treatment of glaucoma or other intraocular diseases.

Scientists working on the development of biomaterials have the opportunity to draw from a diverse array of engineering, biological, and clinical tools to develop technologies that have therapeutic potential. The work presented in this dissertation demonstrate the application of biomaterials science for addressing persisting clinical needs in the ocular and cardiovascular field. The interdisciplinary and creative nature of this field is exciting and enabling. It is my hope that this work can contribute to advancing the development of biomaterials for medical applications.

Publishing Agreement

It is the policy of the University to encourage the distribution of all theses, dissertations, and manuscripts. Copies of all UCSF theses, dissertations, and manuscripts will be routed to the library via the Graduate Division. The library will make all theses, dissertations, and manuscripts accessible to the public and will preserve these to the best of their abilities, in perpetuity.

I hereby grant permission to the Graduate Division of the University of California, San Francisco to release copies of my thesis, dissertation, or manuscript to the Campus Library to provide access and preservation, in whole or in part, in perpetuity.

Author Signature Gigi Cao Date 12/09/2019